

Modern meson spectroscopy: the fundamental role of unitarity

E. van Beveren¹ and G. Rupp²

¹Centro de Física da UC, Departamento de Física
Universidade de Coimbra, P-3004-516 Coimbra, Portugal

²Centro de Física e Engenharia de Materiais Avançados, Instituto Superior Técnico
Universidade de Lisboa, P-1049-001 Lisbon, Portugal

June 9, 2022

Abstract

The importance of S -matrix unitarity in realistic meson spectroscopy is reviewed, both its historical development and more recent applications. First the effects of imposing S -matrix unitarity on meson resonances are demonstrated in both the elastic and the inelastic case. Then, the static quark model is revisited and its theoretical as well as phenomenological shortcomings are highlighted. A detailed account is presented of the mesons in the tables of the Particle Data Group that cannot be explained at all or only poorly in models describing mesons as pure quark-antiquark bound states. Next the earliest unitarised and coupled-channel models are revisited, followed by several examples of puzzling meson resonances and their understanding in a modern unitarised framework. Also, recent and fully unquenched lattice descriptions of such mesons are summarised. Finally, attention is paid to production processes, which require an unconventional yet related unitary approach. Proposals for further improvement are discussed.

1 Introduction

Knowledge of low-energy QCD is encoded in the observable properties of hadrons, that is, mesons and baryons. Most importantly, hadronic mass spectra should provide detailed information on the forces that keep the quarks and/or antiquarks in such systems permanently confined, inhibiting their observation as free particles. However, since QCD is not tractable through perturbative calculations at low energies, owing to a large running coupling in that regime, quark confinement is usually dealt with employing a confining potential in the context of some phenomenological quark model. The shape of this potential is largely empirical, though its short-distance behaviour can be reasonably determined from one-gluon exchange, resulting in a Coulomb-like interaction, usually endowed with an r -dependent coupling constant in order to simulate asymptotic freedom. At large distances, the potential is mostly supposed to grow linearly, on the basis of flux-tube considerations, which have been observed [1] in lattice simulations of string formation for static quarks. The most cited quark model of mesons with such a Coulomb-plus-linear confining potential, sometimes also called “funnel potential”, is due to Godfrey & Isgur (GI) [2], which also accounts for kinematically relativistic effects. The

enormous popularity of the model is understandable, in view of its exhaustive description of practically all imaginable $q\bar{q}$ systems, including those with one or two top quarks, which had not yet even been discovered then. Experimentalists as well as model builders often invoke GI predictions as a touchstone for their observations or results. However, the GI model does not reproduce the excitation spectra of mesons made of light quarks, as already analysed in Ref. [3]. Its principal shortcoming is the prediction of much too large radial splittings for mesons in the range of roughly 1–2 GeV, resulting in several experimentally observed states that do not fit in the GI level scheme. Also the lowest-lying scalar mesons, below 1 GeV, are not at all reproduced in the GI model. In Sec. 3 we shall come back to this particular case in much more detail.

Logically, there can be two reasons for the problems of the GI model in the mentioned energy region, namely possible deficiencies of the employed confining potential and/or certain approximations inherent in the model. Let us first consider the employed funnel-type confining potential

$$V_{\text{conf}} = -\frac{\alpha_s(r)}{r} + \lambda r, \quad (1)$$

where the constant parameter λ is the so-called string tension and $\alpha_s(r)$ a configuration-space parametrisation of the running strong coupling. Ignoring for the moment the r -dependence of α_s , we see that V_{conf} is independent of (quark) mass and therefore also flavour-independent, in accordance with the QCD Lagrangian. Consequently, the mass spectrum of a Schrödinger or related relativistic equation with such a potential will inexorably be mass-dependent, that is, radial splittings will increase according as the quark mass decreases. This had already been realised by the Cornell group when developing their potential model of charmonium [4], in which the strength κ of the Coulombic part was fitted to the few then known charmonium observables (quote):

“The recent discovery of the $\mu^+\mu^-$ enhancement Υ probably implies the existence of another $Q\bar{Q}$ family, where Q is a quark carrying a new flavor and having a mass of 4–5 GeV. The variation of the spectrum with quark mass m_Q is very sensitive to the form of $V(r)$, and present indications are that our ansatz (1.1) may not pass this test.”

Two years later, with more data available, the same authors [5] adjusted their model parameters so as to try to accommodate charmonium as well as bottomonium states, both in the static and the coupled-channel version of the model, though resulting in a clearly too heavy 3^3S_1 state in the latter case. Also, one of the authors [6] used a slightly smaller value of κ when applying the coupled-channel model only to bottomonium states, by indeed arguing on the basis of a running coupling in the Coulombic part. We shall come back to unitarisation effects in the Cornell model in Sec. 4. An empirical way to account for a running strong coupling $\alpha_s(r)$ in the context of the static quark model simultaneously applied to charmonium and bottomonium states was presented in Ref. [7].

Now, the mechanism that allows to reproduce the approximate equal radial spacings in charmonium and bottomonium for the funnel potential, despite the quark-mass independence of its confining part, is a very delicate balance between the Coulombic behaviour and running coupling at short distances, as well as the linear rising at larger distances. However, this is impossible to sustain for light quarkonia, resulting in considerably increased spacings in the energy region of 1–2 GeV, in conflict with experiment. A model proposed by us almost four decades ago [8,9] does reproduce the observed radial spacings for light, charm, and bottom quarks, being based on a flavour-dependent harmonic-oscillator confining potential, while also accounting for non-perturbative coupled-channel effects in a manifestly unitary S -matrix formalism. In Sec. 4 the model will be described in detail.

The other possible reason why the GI and related quark models often fail in light-meson spectroscopy is the usual neglect of unitarisation effects. By this we mean that, as most mesons are resonances and not stable or quasi-stable $q\bar{q}$ states, they must strictly speaking be described as poles in some unitary S -matrix, and not as bound states in a static potential. This becomes all the more true if one realises

that many mesonic resonances are broad or very broad, some of which having widths of the same order of magnitude as the observed radial spacings. Picking just one typical example from the PDG [10] Meson Summary Tables, we see that the mass difference between the ground-state $s\bar{s}$ tensor meson $f_2'(1525)$ and its first radial excitation $f_2(1950)$ is about 420 MeV, while the full width of the latter resonance is (464 ± 24) MeV [10]. So it is clear that a reliable determination of radial splittings that originate exclusively in the underlying confining potential demands to account for unitarisation effects, which inevitably will give rise to both the observed decay widths and real mass shifts hidden in the spectrum. Note that the size of such a mass shift may very well depend on the specific radial (or angular) quantum number and/or the vicinity of some decay threshold. This will be comprehensively discussed in Sec. 4.

Before outlining the organisation of the present review, we should stress that this is not intended to be an exhaustive overview of research on meson spectroscopy. We rather aim at showing where the traditional static quark model fails to reproduce the observed mass spectra and how unitarisation can explain several discrepancies. For a not very recent yet highly insightful review of mesons from an experimentalist's point of view, we recommend Ref. [11]. A detailed review of truly exotic charmonium- and bottomonium-like candidate states, not treated here, can be found in Ref. [12]. For reviews on glueballs and baryons, we recommend Refs. [13, 14] and [15], respectively.

Coming back to our work, in Sec. 2 a simple unitary ansatz for the S -matrix in the elastic case is shown to lead to significant deviations from common Breit-Wigner (BW) parametrisations, when applied to some light resonances. Section 3 revisits the static quark model, in which the dynamical effects of strong decay are neglected. Several serious weaknesses will be highlighted. In Sec. 4 we briefly review a number of unitarised or coupled-channel quark models of mesons with their respective predictions for mass shifts, discussing some of the differences. This includes the original model developed by the present authors, in collaboration with others at the University of Nijmegen, as well as its more recent formulation in momentum space. The latter ‘‘Resonance Spectrum Expansion’’ (RSE) formalism is presented in Sec. 5, both in its simplest form and the fully unitary multichannel version, with several applications to controversial meson resonances. The charmed axial-vector mesons and the puzzling charmonium-like state $\chi_{c1}(3872)$ are described in detail in Sec. 6 as typical examples of employing momentum-space and coordinate-space formulations of the RSE model. Section 7 presents selected results of fully unquenched lattice-QCD computations of some mesons that are often modelled as tetraquarks. These show that standard quark-antiquark configurations are adequate provided that two-meson interpolators are included in the simulations as well. In Sec. 8 the issue of resonances produced in production processes instead of elastic scattering is discussed. An unconventional production formalism strongly related to the RSE model is shown to lead to non-resonant threshold enhancements that may be mistaken for genuine resonances. Finally, Sec. 9 summarises the main results and outlines avenues of possible future research.

2 Unitarity and Breit-Wigner amplitudes

The most fundamental cornerstone of the PDG tables is the uniqueness of S -matrix pole positions of unstable particles, as a consequence of quantum-field-theory principles. Therefore, the unitarity property of the S -matrix should ideally be respected in whatever description of mesonic resonances in experiment, quark models, and lattice-QCD simulations. In this section we use a minimal yet manifestly unitary S -matrix ansatz to compare pole and BW masses in the case of three broad to very broad mesons. Simplistic BW parametrisations continue to be widely used in data analyses of mesonic processes, in spite of often not satisfying unitarity, as e.g. in the isobar model for overlapping resonances. Moreover, even for an isolated resonance and so unitary BW parametrisation of the amplitude, the BW mass will be different from the real part of the complex-energy pole in an S -matrix parametrisation, as

demonstrated below. Thus, as an illustration (also see Refs. [16,17]), we study the resulting discrepancies for the meson resonances $\rho(770)$, $f_0(500)$ (alias σ), and $K_0^*(700)$ (alias κ). Let us consider the simplest possible parametrisation of an elastic resonance that respects S -matrix unitarity. The regularity of the independent wave-function solutions at the origin and infinity, respectively, leads to a 1×1 partial-wave S -matrix as a function of the on-shell relative momentum k expressed as [18]

$$S_l(k) = \frac{J_l(-k)}{J_l(k)}, \quad (2)$$

where $J_l(k)$ is the so-called Jost function. A resonance then corresponds to a simple pole in $S_l(k)$ for complex k with positive real part and negative imaginary part, that is, a pole lying in the fourth quadrant of the complex- k plane. So the simplest ansatz for the S -matrix and thus for the Jost function is to write

$$J_l(k) = k - k_{\text{pole}} = k - (c - id), \quad \text{with } c > 0, d > 0. \quad (3)$$

Note that Eq. (2) requires $S_l(k)$ to have a zero in the second quadrant, viz. for $k = -c + id$. However, then the S -matrix cannot be unitary, for real k , i.e.,

$$S_l^*(k) \neq S_l^{-1}(k) \Leftrightarrow J_l^*(k) J_l(k) \neq J_l^*(-k) J_l(-k). \quad (4)$$

Thus, $S_l(k)$ will only satisfy unitarity if [18], for real k ,

$$J_l^*(k) = J_l(-k). \quad (5)$$

Consequently, instead of Eq. (3), the Jost function should read

$$J_l(k) = (k - k_{\text{pole}})(k + k_{\text{pole}}^*) = (k - c + id)(k + c + id). \quad (6)$$

So $S_l(k)$ has a symmetric pair of poles in the 3rd and 4th quadrants, corresponding to an equally symmetric pair of zeros in the 1st and 2nd quadrants. Note that in the corresponding complex-energy plane, given by

$$E = 2\sqrt{k^2 + m^2} \quad (7)$$

in the case of two equal-mass particles, this amounts to one pole and one zero lying symmetrically in the 4th and 1st quadrants, respectively. Since a 1×1 S -matrix can generally be written as

$$S_l(k) = \exp 2i\delta_l(k) = \frac{1 + i \tan \delta_l(k)}{1 - i \tan \delta_l(k)}, \quad (8)$$

and from Eqs. (2,6) also as

$$S_l(k) = \frac{(-k - k_{\text{pole}})(-k + k_{\text{pole}}^*)}{(k - k_{\text{pole}})(k + k_{\text{pole}}^*)} = \frac{1 + \frac{2ik \operatorname{Im}(k_{\text{pole}})}{k^2 - |k_{\text{pole}}|^2}}{1 - \frac{2ik \operatorname{Im}(k_{\text{pole}})}{k^2 - |k_{\text{pole}}|^2}}, \quad (9)$$

we get, using $k_{\text{pole}} = c - id$ from Eq. (3),

$$\tan \delta_l(k) = \frac{2k \operatorname{Im}(k_{\text{pole}})}{k^2 - |k_{\text{pole}}|^2} = \frac{2dk}{c^2 + d^2 - k^2}. \quad (10)$$

With the partial-wave amplitude given by $T_l(k) = e^{i\delta_l(k)} \sin \delta_l(k)$, we thus obtain

$$|T_l(k)|^2 = \sin^2 \delta_l(k) = \frac{\tan^2 \delta_l(k)}{1 + \tan^2 \delta_l(k)} = \frac{4d^2 k^2}{(k^2 - c^2 + d^2)^2 + 4c^2 d^2}. \quad (11)$$

So we see that the modulus of the amplitude is maximum, i.e., equal to 1, for

$$k_{\max}^2 = c^2 + d^2, \quad (12)$$

where the phase shift passes through 90° . Note that the corresponding energy

$$E_{\max} = 2\sqrt{k_{\max}^2 + m^2} = 2\sqrt{c^2 + d^2 + m^2} \quad (13)$$

usually corresponds to the mass M_{BW} in a typical Breit-Wigner (BW) amplitude

$$T_l(E) \propto \frac{1}{E - M_{\text{BW}} + i\Gamma_{\text{BW}}/2}, \quad (14)$$

at least in the elastic case. So we take the (unitary) BW mass as

$$M_{\text{BW}} = 2\sqrt{k_{\max}^2 + m^2} = 2\sqrt{c^2 + d^2 + m^2}. \quad (15)$$

Next we compare this BW mass with the pole mass in the complex-energy plane for several cases.

2.1 $\rho(770)$

Now we illustrate the consequences of these considerations in the simple case of the very well-known meson $\rho(770)$ [10], which is an elastic P -wave resonance in $\pi\pi$ scattering. The PDG lists its mass and total width as [10]

$$M_{\rho^0} = (775.26 \pm 0.25) \text{ MeV}, \quad \Gamma_{\rho^0} = (147.8 \pm 0.9) \text{ MeV}, \quad (16)$$

where the width follows almost exclusively ($\approx 100\%$) from the decay mode $\rho^0 \rightarrow \pi^+\pi^-$, with $m_{\pi^\pm} = 139.57$ MeV. The PDG makes the following remark ahead of the listed ρ^0 masses, from which the average value given in Eq. (16) is determined:

“We no longer list S -wave Breit-Wigner fits, or data with high combinatorial background.”

However, for several of these analyses it remains unclear whether unitarity is respected.

In the following and as mentioned above, we shall refer to BW mass (M_{BW}) for the energy where the resonance's phase shift passes through 90° and so the modulus of the amplitude is maximum (cf. Eqs. (11,13)). This indeed also holds for the standard BW amplitude in Eq. (14). Here, we want to determine for the $\rho(770)$ the discrepancy between pole mass and BW mass (cf. Eq. (15))

$$M_{\text{BW}} = 2\sqrt{c^2 + d^2 + m^2}. \quad (17)$$

In order to find the corresponding pole mass, we write

$$E_{\text{pole}} = 2\sqrt{k_{\text{pole}}^2 + m^2} = 2\sqrt{c^2 - d^2 + m^2 - 2icd} = M_{\text{pole}} - i\Gamma_{\text{pole}}/2. \quad (18)$$

Thus,

$$\text{Re}(E_{\text{pole}}^2) = 4(c^2 - d^2 + m^2) = M_{\text{pole}}^2 - \Gamma_{\text{pole}}^2/4 \quad (19)$$

and

$$\text{Im}(E_{\text{pole}}^2) = -8cd = -M_{\text{pole}}\Gamma_{\text{pole}}. \quad (20)$$

So combining Eqs. (17) and (19) we get

$$M_{\text{BW}}^2 + \text{Re}(E_{\text{pole}}^2) = 8(c^2 + m^2) = M_{\text{BW}}^2 + M_{\text{pole}}^2 - \Gamma_{\text{pole}}^2/4 \quad (21)$$

and

$$M_{\text{BW}}^2 - \text{Re}(E_{\text{pole}}^2) = 8d^2 = M_{\text{BW}}^2 - M_{\text{pole}}^2 + \Gamma_{\text{pole}}^2/4. \quad (22)$$

From Eqs. (21) and (22), c and d follow straightforwardly, viz.

$$c = \sqrt{M_{\text{BW}}^2 + M_{\text{pole}}^2 - \Gamma_{\text{pole}}^2/4 - 8m^2}/\sqrt{8} \quad (23)$$

and

$$d = \sqrt{M_{\text{BW}}^2 - M_{\text{pole}}^2 + \Gamma_{\text{pole}}^2/4}/\sqrt{8}, \quad (24)$$

respectively. Combining Eqs. (23) and (24) with Eq. (20), we arrive, after some basic algebra, at the final expression

$$M_{\text{pole}} = \sqrt{\sqrt{(M_{\text{BW}}^2 - 4m^2)^2 - 4m^2 \Gamma_{\text{pole}}^2} + 4m^2 - \Gamma_{\text{pole}}^2/4}. \quad (25)$$

Note that it is not possible to write M_{pole} as a simple closed-form expression in terms of both M_{BW} and Γ_{BW} . Nevertheless, assuming for the moment that $\Gamma_{\text{pole}} \simeq \Gamma_{\text{BW}}$, we substitute in Eq. (25) the PDG values given in Eq. (16) for M_{BW} and Γ_{pole} , which yields

$$M_{\text{pole}} = 770.67 \text{ MeV}. \quad (26)$$

Thus, we see that even in the case of the very well-known $\rho(770)$ resonance, whose mass is given with 5 significant digits in the PDG tables, the difference between the (unitary) BW mass and the pole mass is as large as 4.5 MeV! Now we check whether indeed $\Gamma_{\text{pole}} \simeq \Gamma_{\text{BW}}$, by calculating the half-width of the $\rho(770)$ peak from the modulus-squared of the amplitude $T_l(k)$. Using Eq. (11) we have

$$\frac{1}{2} = |T_l(k_{\pm})|^2 = \frac{4d^2 k_{\pm}^2}{(k_{\pm}^2 - c^2 + d^2)^2 + 4c^2 d^2}, \quad (27)$$

yielding

$$k_{\pm}^2 = c^2 + 3d^2 \pm \sqrt{8d^4 + 4c^2 d^2}. \quad (28)$$

Taking now the expressions for c and d in Eqs. (23) and (24), respectively, we can evaluate Γ_{BW} as

$$\Gamma_{\text{BW}} = E_+ - E_- = 2\sqrt{k_+^2 + m^2} - 2\sqrt{k_-^2 + m^2}, \quad (29)$$

with $M_{\text{pole}} = 770.67 \text{ MeV}$ and $\Gamma_{\text{pole}} = 147.8 \text{ MeV}$, resulting in

$$\Gamma_{\text{BW}} = 147.83 \text{ MeV}. \quad (30)$$

So indeed, in this case Γ_{BW} is an excellent approximation for Γ_{pole} , to be contrasted with the significant difference between M_{BW} and M_{pole} .

At this point we should return to the peak amplitude given by Eqs. (11) and (12). As a matter of fact, the maximum in the partial-wave cross section [18]

$$\sigma_l(k) \equiv \frac{4\pi}{k^2} (2l+1) \sin^2 \delta_l(k) = \frac{16\pi(2l+1)d^2}{(k^2 - c^2 + d^2)^2 + 4c^2 d^2} \quad (31)$$

does not occur at the same k value as in $|T_l(k)|^2$, but rather at $k^2 = c^2 - d^2$ instead of $k^2 = c^2 + d^2$. Accordingly, the cross-section half-width follows from

$$k_{\pm}^2 = c^2 - d^2 \pm 2cd \quad (32)$$

instead of Eq. (28). As a result, for the PDG $\rho(770)$ mass of 775.26 MeV and width of 147.8 MeV, the cross-section peak comes out at 767.13 MeV, with a half-width of 149.19 MeV, which values are

8.13 MeV lower and 1.39 MeV higher than the PDG ones, respectively. This further reinforces the need for a consistent unitary approach.

A final remark is due, as $\rho(770)$ is an elastic resonance and so suitable for our simple study here. However, its first radial excitation, listed as $\rho(1450)$ [10] in the PDG tables, is highly inelastic and also considerably broader. So one naturally expects potentially larger effects due to unitarity. Yet a discrepancy of 170 MeV between a unitary and a non-unitary analysis of the very same resonance, as found in Ref. [19], may still come as a shock to some, because it could wreak havoc with mainstream meson spectroscopy, in particular the $\rho(1450)$ PDG assignment. As a matter of fact, a very recent reanalysis [20] of P -wave $\pi\pi$ phase shifts and inelasticities employing a manifestly unitary multichannel S -matrix parametrisation of resonance poles, with crossing-symmetry constraints, shows strong evidence of a $\rho(1250)$ instead of $\rho(1450)$ as the first radial excitation of $\rho(770)$. We shall come back to this controversy in Sec. 3. Let us just mention here the inevitability of resorting to a coupled-channel S -matrix description, if one insists not only on a fully unitary description of the data, but also on proper analyticity.

2.2 $f_0(500)$ and $K_0^*(700)$

Next we focus our attention on two resonances that have much larger widths than $\rho(770)$, namely the scalar mesons $f_0(500)$ (alias σ) and $K_0^*(700)$ (alias κ). These two states have been very controversial over the years [21,22], but are now included as established resonances in the 2020 PDG Meson Summary Tables [10]. For extensive reviews of the σ and κ meson, see Refs. [23] and [24], respectively. In order to be able to deal with $K_0^*(700)$, we must consider the unequal-mass case, as its (only) hadronic decay mode is $K\pi$. Of course, the unequal-mass formulae can also be applied to $f_0(500) \rightarrow \pi\pi$, possibly with a negligibly small correction so as to avoid numerical problems.

The relativistic relative momentum of two unequal-mass particles reads

$$k = \frac{E}{2} \sqrt{\left\{1 - \frac{(m_1 + m_2)^2}{E^2}\right\} \left\{1 - \frac{(m_1 - m_2)^2}{E^2}\right\}}, \quad (33)$$

with the total energy

$$E = \sqrt{k^2 + m_1^2} + \sqrt{k^2 + m_2^2}. \quad (34)$$

Now it is not feasible anymore to derive a simple closed-form expression for the pole mass as in Eq. (25). Instead, we shall derive M_{BW} and Γ_{BW} for a given M_{pole} and Γ_{pole} , though not in an explicit form. Thus, we write

$$c = \text{Re}(k_{\text{pole}}) = \text{Re} \left[\frac{E_{\text{pole}}}{2} \sqrt{\left\{1 - \frac{(m_1 + m_2)^2}{E_{\text{pole}}^2}\right\} \left\{1 - \frac{(m_1 - m_2)^2}{E_{\text{pole}}^2}\right\}} \right] \quad (35)$$

and similarly for the corresponding imaginary part

$$d = -\text{Im}(k_{\text{pole}}). \quad (36)$$

Using

$$E_{\text{pole}} = M_{\text{pole}} - i\Gamma_{\text{pole}}/2 \quad (37)$$

and

$$M_{\text{BW}} = \sqrt{k_{\text{BW}}^2 + m_1^2} + \sqrt{k_{\text{BW}}^2 + m_2^2}, \quad \text{with } k_{\text{BW}} = \sqrt{c^2 + d^2}, \quad (38)$$

we can numerically compute M_{BW} as a function of M_{pole} and Γ_{pole} with Eqs. (35,36). In the same way, Γ_{BW} can be calculated employing Eqs. (28,29).

Let us now check what this means for the very broad scalar mesons $f_0(500)$ and $K_0^*(700)$. Their pole positions as well as BW masses and widths are listed in the PDG Meson Tables as [10]

$$f_0(500) : \begin{cases} E_{\text{pole}} = \{(400-550) - i(200-350)\} \text{ MeV} , \\ M_{\text{BW}} = (475 \pm 75) \text{ MeV} , \quad \Gamma_{\text{BW}} = (550 \pm 150) \text{ MeV} \end{cases} \quad (39)$$

and

$$K_0^*(700) : \begin{cases} E_{\text{pole}} = \{(630-730) - i(260-340)\} \text{ MeV} , \\ M_{\text{BW}} = (824 \pm 30) \text{ MeV} , \quad \Gamma_{\text{BW}} = (478 \pm 50) \text{ MeV} . \end{cases} \quad (40)$$

If on the other hand we use our Eqs. (28,29) and (33-38), we obtain

$$\begin{aligned} f_0(500) : \quad M_{\text{BW}} &= (591 \pm 70) \text{ MeV} , \quad \Gamma_{\text{BW}} = (560 \pm 153) \text{ MeV} ; \\ K_0^*(700) : \quad M_{\text{BW}} &= (906 \pm 37) \text{ MeV} , \quad \Gamma_{\text{BW}} = (707 \pm 97) \text{ MeV} . \end{aligned} \quad (41)$$

The errors in Eq. (41) are determined with the variance formula, given the data spreading for the real and imaginary parts of the pole positions shown in Eqs. (39,40), instead of simply [17] from those PDG limits. The conclusion is that the PDG seems to underestimate the BW masses of both $f_0(500)$ and $K_0^*(700)$, as well as the BW width of $K_0^*(700)$. As a word of caution, we repeat that our label ‘BW’ refers to the energy where the phase shift passes through 90° , in the context of the present simple pole model. Note that reality is more complicated, as the $f_0(500)$ resonance overlaps with $f_0(980)$ and $K_0^*(700)$ overlaps with $K_0^*(1430)$, apart from the influence of Adler zeros on the amplitudes [25]. We also recall our alternative definition of M_{BW} and Γ_{BW} based on the cross-section peak and its half-width (cf. Eqs. (31) and (32)). When applied to the light scalars, we find an $f_0(500)$ BW mass below the pole mass, while no BW width can be consistently computed. In the $K_0^*(700)$ case, not even a BW mass can be defined in part of the PDG’s range of pole values, while a BW width is again not possible to calculate. This lends further support to the generally accepted non-BW nature of the $f_0(500)$ and $K_0^*(700)$ resonances, making the use of BW ansatzes in their description highly questionable.

3 Shortcomings of the Static Quark Model

Traditional quark models treat hadrons as $q\bar{q}$ or qqq bound states, in spite of the fact that the vast majority of mesons and baryons are resonances, many of which have large to very large decay widths. In some cases these are of the same order of magnitude as average level spacings (see e.g. the example of excited f_2 mesons above). The rationale behind these models is essentially a poor man’s approach, since one cannot convincingly argue that decay processes giving rise to hadronic widths of hundreds of MeV will not also normally lead to comparably large real mass shifts. Such effects are always governed by analyticity of some S -matrix in which those resonances show up as simple poles. Since the couplings that produce strong-decay widths are large, the resulting complex mass shifts are generally non-perturbative and non-linear and so there is no reason to believe that unitarisation effects will keep real mass splittings in the bare spectrum intact. To make things worse, even states lying below their respective lowest OZI-allowed decay threshold may undergo sizeable mass shifts due to virtual meson loops, which in this case are always real and negative. A famous example is the $D_{s_0}^*(2317)$ [10] charmed-strange scalar meson, whose bare state was found on the lattice [26] to shift from above the DK threshold to clearly below it owing to the inclusion of meson-meson interpolators in the simulation, besides the usual $c\bar{s}$ ones. This result was confirmed very recently in the independent lattice computation of Ref. [27]. We shall extensively revisit this meson in Secs. 5 and 7.

Nevertheless, the success of the Cornell model in reasonably reproducing the then known $c\bar{c}$ [4, 5] and $b\bar{b}$ [6] states in the model’s static as well as the coupled-channel version, seemed to indicate that unitarisation could be accommodated through a modest change of parameters. In the following we shall

try to make clear that this is not the case at least in the light-meson spectra, on the basis of the GI model [2]. Note that this choice is exclusively motivated by the exhaustiveness of the GI predictions of meson spectra for all flavours and is in no way intended to downplay the importance of this pioneering work.

3.1 Observed meson spectrum and Godfrey-Isgur [2] model

The GI [2] quark model of mesons is still referred to very frequently for comparison when new mesons are observed in experiment or other models make predictions. This is understandable in view of the GI model's completeness in predicting meson spectra for almost any desired flavour combination and quantum numbers, besides the employment of the widely accepted funnel potential, with a running coupling constant in the colour-Coulombic part similarly to the approach in Ref. [7]. Also, the model employs relativistic kinematics, which should make its predictions for light meson more reliable. Other typical ingredients are colour spin-spin and spin-orbit interactions, as well as the use of constituent quark masses. Note that this makes the model's application to especially the pion somewhat questionable, in view of the neglect of dynamical chiral-symmetry breaking [28, 29], which may account for even more than half of the $\rho(770)$ - π mass splitting [28]. In spite of this, the pion mass is reproduced in the GI parameter fit, which is possible owing to the small non-strange constituent quark mass of 220 MeV, usually of the order of 350 MeV in non-relativistic models.

In the following, we compare the predictions of the GI model for meson masses with those of the latest PDG tables [10], focusing especially on radial meson spectra for light and strange quarks. A similar analysis was already carried out in Ref. [3], on the basis of the 2012 PDG tables [30].

3.1.1 Light-quark isoscalar mesons [2] (Fig. 1)

- $0^{++}/^3P_0$:
 Lowest GI scalar ~ 600 MeV heavier than $\mathbf{f_0(500)}$ ¹ (alias σ);
 GI $s\bar{s}$ scalar almost 400 MeV heavier than $\mathbf{f_0(980)}$.
 Note: we shall come back to these light scalar mesons in much more detail in Secs. 4 and 5.
- $2^{++}/^3P_2$ - 3F_2 :
 PDG listings report 6 likely $n\bar{n}$ ($n = u, d$) states up to ≈ 2.15 GeV, viz. $\mathbf{f_2(1270)}$, $f_2(1565)$, $f_2(1640)$, $f_2(1810)$, $f_2(1910)$, and $f_2(2150)$, whereas GI only predict 3. In the probably dominant $s\bar{s}$ sector, PDG also lists 6 states up to ≈ 2.35 GeV: $f_2(1430)$, $\mathbf{f'_2(1525)}$, $\mathbf{f_2(1950)}$, $\mathbf{f_2(2010)}$, $\mathbf{f_2(2300)}$, and $\mathbf{f_2(2340)}$, while GI again only predict 3.
 Note: some PDG f_2 states may not be resonances [11], but $f_2(1565)$ looks reliable. Also, PDG: $m(2^3P_2) - m(1^3P_2) \approx 300$ MeV; GI: $m(2^3P_2) - m(1^3P_2) = 540$ MeV.
 For unclear reasons, the PDG has been omitting $f_2(1565)$ from the Summary Tables.
- $1^{+-}/^1P_1$:
 PDG $n\bar{n}$ entries: $\mathbf{h_1(1170)}$, $h_1(1595)$;
 GI predict: $h_1(1220)$ (1^1P_1), $h_1(1780)$ (2^1P_1).

3.1.2 Light-quark isovector mesons [2] (Fig. 2)

- $0^{++}/^3P_0$:
 PDG entries: $\mathbf{a_0(980)}$, $\mathbf{a_0(1450)}$;
 GI: $a_0(1090)$ (1^3P_0), $a_0(1780)$ (2^3P_0).

¹Henceforth, we shall print the states included in the PDG Summary Tables [10] in boldface.

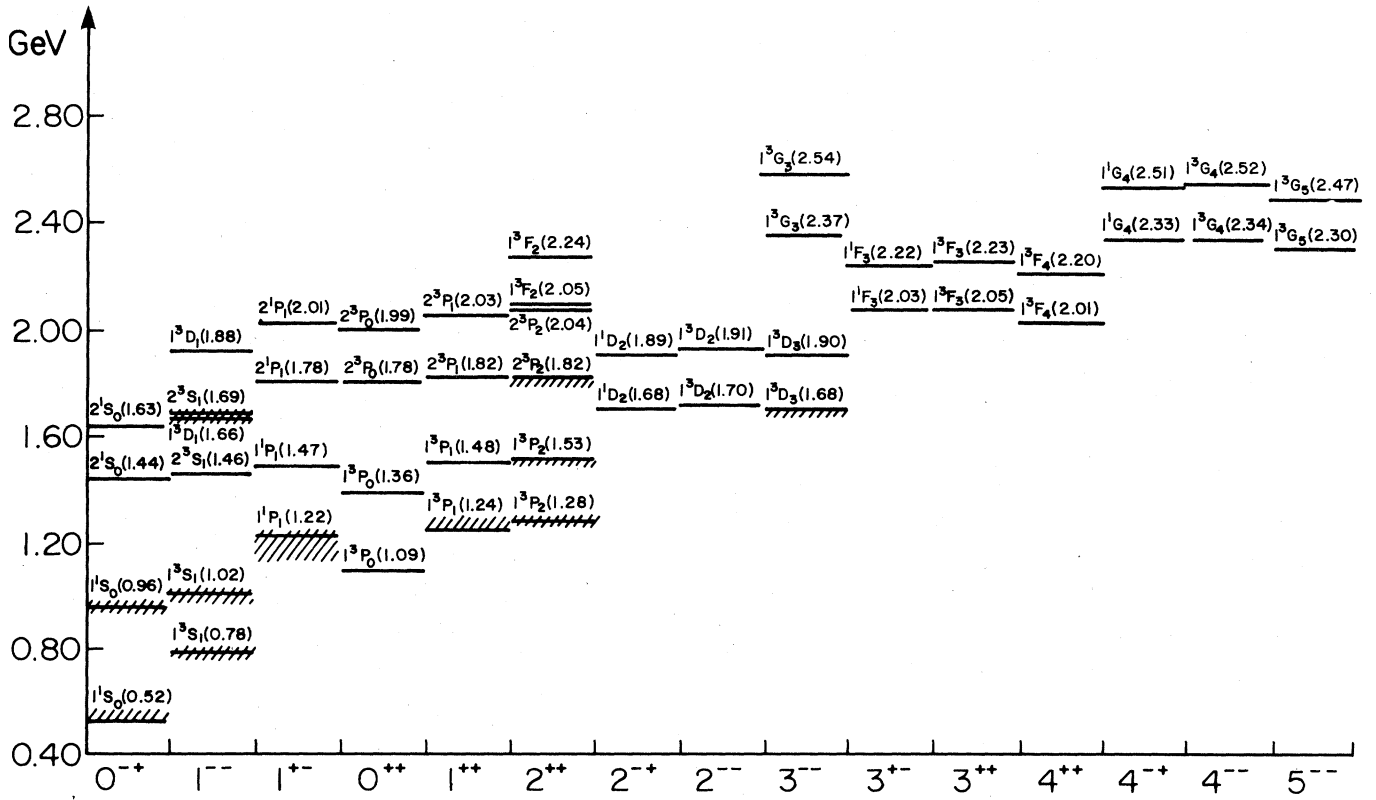


Figure 1: Light-quark isoscalar mesons as predicted in the GI model [2].

- $1^{++}/^3P_1$:
 PDG entries: $a_1(1260)$, $a_1(1640)$;
 GI: $a_1(1240)$ (1^3P_1), $a_1(1820)$ (2^3P_1).
- $2^{++}/^3P_2$:
 PDG entries: $a_2(1320)$, $a_2(1700)$;
 GI: $a_2(1310)$ (1^3P_2), $a_2(1820)$ (2^3P_2).
- $1^{--}/^3S_1$ - 3D_1 :
 PDG entries: $\rho(1450)$, $\rho(1570)$, $\rho(1700)$, $\rho(1900)$;
 GI: $\rho(1450)$ (2^3S_1), $\rho(1660)$ (1^3D_1), $\rho(2000)$ (3^3S_1), $\rho(2150)$ (2^3D_1).
 Note: as already mentioned above, a very recent [20] multichannel unitary S -matrix reanalysis of P -wave $\pi\pi$ phase shifts and inelasticities has confirmed $\rho(1250)$, besides finding evidence of the further resonances $\rho(1450)$, $\rho(1600)$, and $\rho(1800)$.

3.1.3 Strange mesons [2] (Fig. 3)

- $0^-/^1S_0$:
 PDG entries: $K(1460)$, $K(1830)$;
 GI: $K(1450)$ (2^1S_0), $K(2020)$ (3^1S_0).
- $0^+/^3P_0$:
 PDG entries: $K_0^*(700)$, $K_0^*(1430)$, $K_0^*(1950)$;
 GI: $K_0^*(1240)$ (1^3P_1), $K_0^*(1890)$ (2^3P_1).

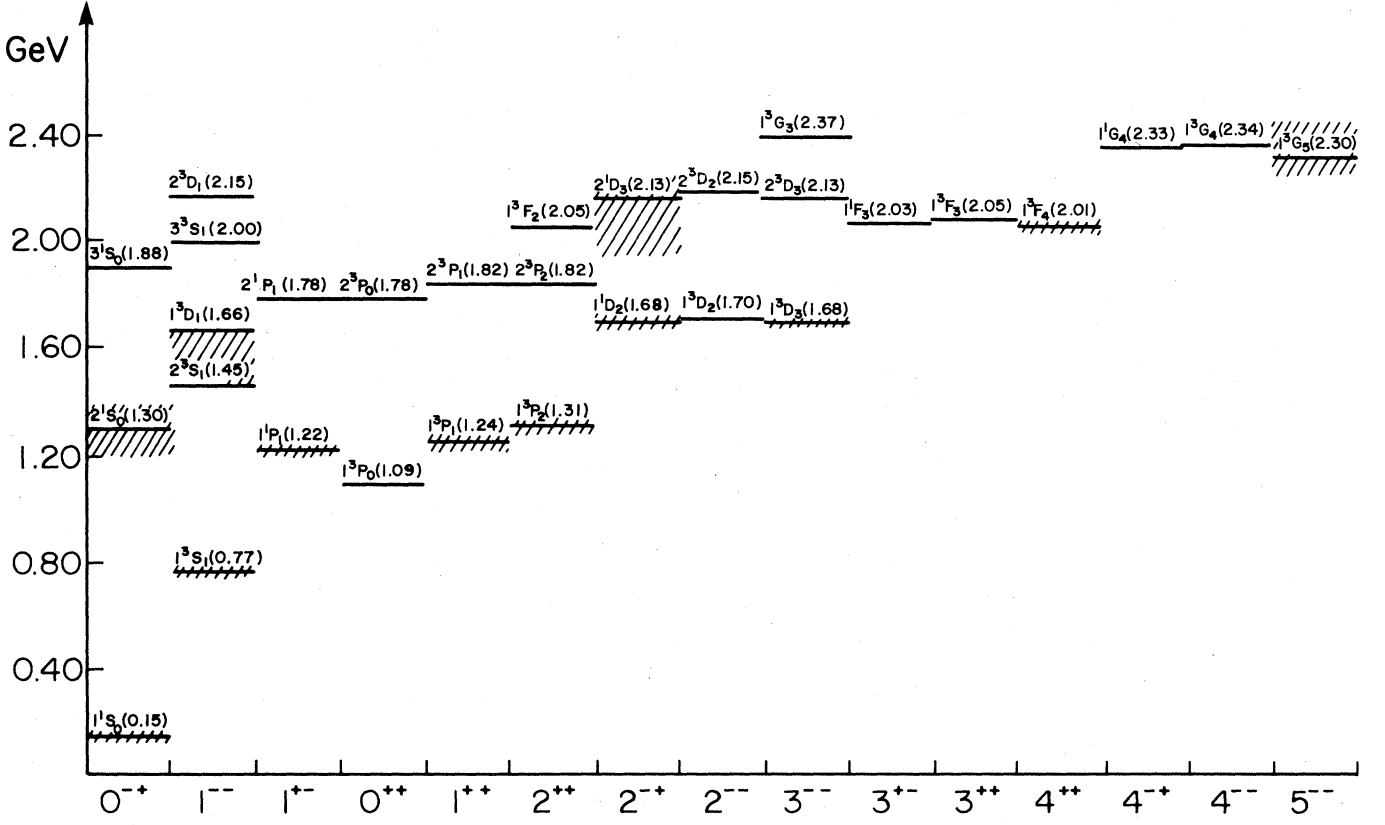


Figure 2: Light-quark isovector mesons as predicted in the GI model [2].

For $K_0^*(700)$, also see Secs. 4 and 5.

- $1^- / ^3S_1 - ^3D_1$: PDG entries: $K^*(1410)$, $K^*(1680)$;
GI: $K^*(1580)$ (2^3S_1), $K^*(1780)$ (1^3D_1).
- $1^+ / ^3P_1 - ^1P_1$:
PDG entries: $K_1(1270)$, $K_1(1400)$, $K_1(1650)$;
GI: $K_1(1340)$ (1^1P_1), $K_1(1380)$ (1^3P_1), $K_1(1900)$ (2^1P_1), $K_1(1930)$ (2^3P_1).
- $2^- / ^1D_2 - ^3D_2$:
PDG entries: $K_2(1580)$, $K_2(1770)$, $K_2(1820)$, $K_2(2250)$;
GI: $K_2(1780)$ (1^1D_2), $K_2(1810)$ (1^3D_2), $K_2(2230)$ (2^1D_2), $K_2(2260)$ (2^3D_2).

3.1.4 Summary of light mesons [2]

As we have seen above, The GI model predicts radial level splittings in the light and strange meson sectors that are considerably larger than the listed [10] ones. Lattice QCD simulations that ignore the dynamical effects of strong decay predict radial splittings that are even larger [31] (also see Sec. 7 below). Moreover, there is no indication that some of the observed resonances might be crypto-exotics, i.e., states with non-exotic quantum numbers yet not having the standard $q\bar{q}$ configuration, like tetraquarks ($qq\bar{q}\bar{q}$) and hybrids ($q\bar{q}g$). Therefore, no excess of regular mesons can be claimed on the basis of the experimental data [32]. On the other hand, several missing states in e.g. the strange and vector ϕ sectors further complicate the picture. Nevertheless, there can be no doubt that this part of meson spectroscopy poses a huge challenge to the usual quark model.

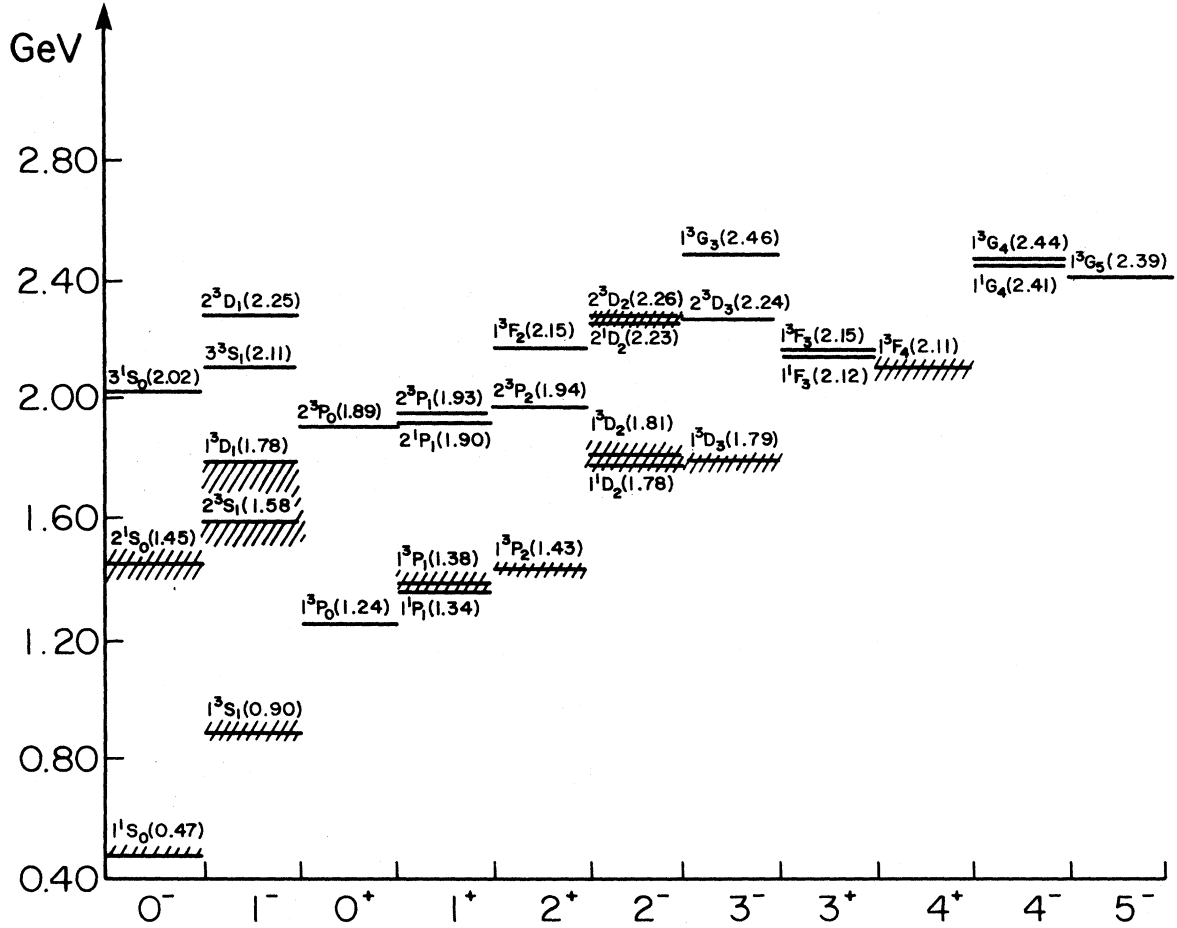


Figure 3: Strange mesons as predicted in the GI model [2].

3.1.5 Charm and bottom mesons

Especially the scalar D_{s0}^* (2317) but also the axial-vector D_{s1} (2460) come out too heavy [2] in the GI model. However, this may be strongly related to the failure of the static quark model in describing the light scalar mesons as $q\bar{q}$, as demonstrated in Ref. [33] (also see Sec. 5 below). Apart from these clear discrepancies, there are insufficient data on radial excitations of open-charm and open-bottom mesons for any definite conclusions.

3.1.6 Charmonium and bottomonium

Up to the 2002 PDG edition [34], the list of charmonia and bottomonia had remained largely unaltered, with all states more or less compatible [2] with the GI model and similar ones. Things changed dramatically in 2003 with the discovery [35] of the charmonium-like state $X(3872)$, which by now has been firmly established as a 3P_1 state and is therefore called [10] χ_{c1} (3872). Its mass is about 80 MeV below the one predicted [2] in the GI model, which is a lot when compared with the accuracy of the model in reproducing the masses of the 1^3P_1 $c\bar{c}$ states. Moreover, at 3872 MeV, χ_{c1} (3872) lies on top of the lowest strong decay threshold, viz. $D^0\bar{D}^{*0}$, within a hundredth of an MeV when considering the central values of the 2020 fitted PDG masses of the D^0 and D^{*0} charmed mesons. Therefore, χ_{c1} (3872) is often considered a kind of very weakly bound $D^0\bar{D}^{*0}$ molecule. However, in Refs. [36–38] it was shown that this state can be successfully described as a strongly unitarised 2^3P_1 $c\bar{c}$ meson, with a naturally very

large $D^0\bar{D}^{*0}$ component in its wave function [37, 38]. For more details, see Sec. 5 below.

Starting in 2005, many more enhancements have been found in the charmonium spectrum and included in the PDG listings, besides a few new ones for bottomonium, too. As for charmonium-like states, several have only been observed in OZI-violating strong-decay modes like $J/\psi\pi\pi$, most notably the vector $X(4260)$, now called [10] $\psi(4260)$. This state has a very long list of open-charm decay modes listed in the PDG tables as “not observed” [10], which has led to a plethora of suggestions involving different crypto-exotic configurations for $\psi(4260)$, viz. a hybrid, tetraquark, charm-baryonium molecule, For more details, see e.g. the review on hidden-charm pentaquarks and tetraquarks in Ref. [12]. An alternative explanation [39] of the $\psi(4260)$ peak in $e^+e^- \rightarrow J/\psi\pi\pi$ data amounts to a non-resonant, merely apparent enhancement owing to strong inelasticities from competing OZI-allowed channels and true ψ vector resonances. We shall come back to this modelling [39] in Sec. 8 below.

Even several charged hidden-charm and hidden-bottom states have been observed [10] in recent years. Clearly, if these indeed correspond to genuine resonances, they must be of an exotic non- $q\bar{q}$ nature, but there are alternative explanations in terms of purely kinematical “triangle” singularities. Discussion of such models lies outside the scope of the present review, so let us again refer to Ref. [12] for a detailed discussion of all these exotic candidates. For an overview of the rapidly expanding and changing PDG listings of hidden-charm and hidden-bottom states between 2002 and 2018, see Ref. [40].

3.2 Other relativistic static quark models

In order to show that problems foremostly in the light-meson spectrum are not unique to the GI model, we now briefly resume the formalisms and predictions of two static quark models that treat relativity in a more complete fashion. The first model [41] concerns a relativistically covariant quasipotential calculation in configuration space, applied to most light, heavy-light, and heavy mesons, It excludes light isoscalars as e.g. the scalars $f_0(500)$, $f_0(980)$, and the several $J^{PC} = 2^{++}$ f_2 states, owing to the difficulty of dealing with the inevitable $n\bar{n} \leftrightarrow s\bar{s}$ mixing. Although the starting point is the fully relativistic four-dimensional (4D) Bethe-Salpeter [42] equation (BSE) with the complete Dirac spin structure, the enormous complexity of properly dealing with all singularities involved in the Wick rotation and the confining potential [43], a three-dimensional (3D) reduction of the BSE is carried out, by integrating out the relative-energy variable. This can be done in many different ways, but special care is required in order to preserve relativistic covariance. In Ref. [41], two different approaches are tested empirically in fits to the meson spectrum. The first 3D approximation is the Blankenbecler-Sugar-Logunov-Tavkhelidze [44] (BSLT) formalism, which basically uses delta functions to put the two particles equally off mass shell in the intermediate state when they have the same mass, while correctly reducing to the Dirac equation if one of the two becomes infinitely heavy [45]. The other approach employed in Ref. [41] is the so-called equal-time (ET) equation [46], which is based on the assumption that the potential does not depend on the relative energy in the centre-of-mass system. This facilitates integrating out this variable, thus reducing the equation from 4D to 3D. However, in order to ensure that it reduces to the Dirac equation for the lighter particle if the other mass goes to infinity, an extra term is added to the two-body propagator in the intermediate state which stands for propagation inside the crossed-box diagram. This is also guarantees to approximately account for all crossed diagrams when iterating the equation. For further details, see Ref. [46]. In both 3D approaches [41], the $q\bar{q}$ potential in r -space consists of a Coulombic part from one-gluon exchange, similarly to Ref. [7], plus a linearly rising confining part with a constant term as well. The former part has a natural Dirac vector structure, while the confining piece is taken as dominantly scalar with a small vector admixture. The resulting coupled integro-differential equations for the bound-state wave functions in coordinate space, including both positive- and negative-energy components, are solved numerically using an expansion in terms of cubic Hermite spline functions [41]. Finally, the solutions of the equations are gauge dependent as far as the vector parts in the potential are concerned, due to the 3D nature of the formalism and the fixing of the

relative energy. Therefore, two different gauges are chosen in order to test the corresponding sensitivity of the results, viz. the Feynman gauge and the Coulomb gauge, but only in the BSLT approximation, since the ET formalism does not allow a satisfactory fit to the spectra at all.

Coming now to the fit results in Ref. [41], our first observation is that the constituent quark masses $m_{u,d}$, m_s , m_c , and m_b are close to those found in the GI model, especially $m_{u,d}$ and m_s . As for the thus computed spectra, the radial spacings are clearly much too large, both in the light-quark sector and for the heavy quarkonia $c\bar{c}$, $b\bar{b}$ (see Table III in Ref. [41]). Therefore, the discrepancies are even worse than in the GI model. This may not have been so evident back in 1994, but is now undeniable when comparing the predictions [41] to PDG [10] mass values. A typical example: $m_{\rho'''}(3^3S_1) - m_{\rho''}(2^3S_1) \simeq 600\text{--}700$ MeV, depending mildly on the BSLT or ET approach and also on the chosen gauge (for BSLT), to be compared to 300–350 MeV in the very recent analysis of Ref. [20]. Note that the $(n+1)^3S_1$ states lie above the corresponding n^3D_1 states in the light-quark sector, as opposed to the GI and non-relativistic models, but not for charmonium and bottomonium. Another light-quark example: $m_{\pi''}(3^1S_0) - m_{\pi'}(2^1S_0) \simeq 600\text{--}800$ MeV [41], cf. 510 MeV according to the PDG. The radial splittings also come out much too large for $c\bar{c}$ and $b\bar{b}$ states, giving rise to mass predictions for the 4^3S_1 bottomonium and charmonium² states that are 300–400 MeV too high.

The other [47] relativistic model calculation of meson spectra is of a completely different nature, though the employed interaction is very similar to the one used in Ref. [41]. The so-called RdG formalism [48] is not derived from the BSE. Its principal characteristic is that all particles are always kept on their mass shells, even in the intermediate state, where total three-velocity is conserved and not total four-momentum. Nevertheless, in asymptotic states total four-momentum is naturally conserved. Also, since there is no relative-energy variable, the resulting equations are automatically of a 3D type. Furthermore, as the RdG approach is not derived from quantum field theory but rather from ordinary quantum mechanics, no negative-energy states occur in the equations, despite the use of Dirac spinors for the individual quark and antiquark composing a meson. Finally, Lorentz invariance of the formalism is guaranteed, as the potential is a function of scalars constructed from the quark and antiquark four-momenta. The RdG equations are solved numerically in momentum space, again with cubic Hermite splines, after regularising the potential's singularities in both the Coulombic part with running strong coupling and the linear-plus-constant part. Also, different Dirac structures in the confining potential are tested in the fits, namely as purely scalar or with a sizeable vector admixture. For further details, see Ref. [47].

The results of this RdG model of mesons are better than those of the previous quasipotential approach when focusing on the radial excitations in charmonium and bottomonium. In the light-quark sector, this aspect is more difficult to evaluate, in view of the scarcity of reported higher radial excitations in Table III of Ref. [47]. Nevertheless, the radial spacings for the excited ρ states, though considerably smaller than in Ref. [41], still seem to be somewhat on the large side when compared with the analysis of Ref. [20], albeit agreeing on interpreting $\rho(1450)$ as the 1^3D_1 state instead of the 2^3S_1 favoured by the PDG. However, these good fit results come at a high price, namely much too large constituent quark masses, in all 4 flavour sectors (see Table II [47]), when compared to other quark models. The values $m_{u/d} = 512\text{--}966$ MeV, $m_s = 766\text{--}1072$ MeV, $m_c = 2066\text{--}2249$ MeV, and $m_b = 5474\text{--}5593$ MeV, depending on the specific fit, are very unusual and quite worrying, notwithstanding the fact that quark masses are not directly observable. As the author explains [47], these very heavy constituent quarks are a consequence of the large negative constant $C \sim -1$ GeV in the confining potential needed to obtain reasonable radial and angular splittings for light and strange quarks. The author also adds that the quality of the fits in charmonium and bottomonium depends only weakly on C , but that a large negative value is absolutely required for good results in the lighter sectors. Now, it seems obvious to ask why a negative constant c of the same order of magnitude ($c \sim -1$ GeV) in the confining potential as

²Note that there is a typographical error in Table III of Ref. [41]: 3^3S_1 for ψ^v should read 4^3S_1 .

employed in Ref. [41] does not give rise to such huge quark masses. However, one must realise that the quasipotential equations in the latter work are time-reversal invariant, so that for each positive-energy solution there is also a negative-energy solution with equal mass modulus. A further lowering of c would eventually lead to two equal massless solutions, beyond which point the equations do not support a bound-state solution for the ground state anymore and only for excitations. This is to be contrasted with the RdG equations in Ref. [47], which do not have negative-energy solutions. So the role that the constant term in the confining potential plays is very different in the two approaches.

The purpose of discussing these two different relativistic models of mesons in quite some detail was to show that a much more complete treatment of relativity than in the GI model does not necessarily lead to better or even unambiguous predictions. In particular, either the radial spacings in all meson spectra become much too large, as is the case of the quasipotential model of Ref. [41], or one ends up with unrealistically heavy constituent quarks, with possibly still somewhat too large radial splittings in the light sector. Thus, it appears safe to conclude that either the commonly used static $q\bar{q}$ potential must be reconsidered or other mechanisms lead to very significant deformations of the static meson spectrum, which might allow to bridge the gap with experiment. In the remainder of this review, we shall explore the latter hypothesis.

4 Unitarity and coupled-channel mass shifts in quark models

As mentioned in Sec. 1, even nowadays many experimentalists still confront any enhancement in their meson data with predictions of the GI model [2] in order to arrive at a $q\bar{q}$ assignment or otherwise claim to have found evidence of some exotic state. Yet, models going beyond the static quark model have been around for more than four decades, the pioneering ones dating back to several years before the GI model. These were the already mentioned Cornell model for charmonium [4, 5] and bottomonium [6], the Helsinki model for light pseudoscalars and vectors [49, 50], and the also referred Nijmegen model for heavy quarkonia [8] and all pseudoscalar as well as vector mesons [9]. Despite the at times huge mass shifts predicted by these models, for many years the effects of decay, also called coupled-channel contributions or unitarisation, were largely ignored. The success of the Cornell model for heavy quarkonia and the vast scope of the GI model no doubt contributed to this state of affairs.

Quark models that try to account for the effects of $q\bar{q}$ pair creation and/or hadronic decay are often called “unquenched” [38, 51–55]. Now, this is actually a very sloppy name, as the term “unquenched” originates in lattice calculations with dynamical instead of static quarks, via a fermion determinant. We shall nevertheless use this inaccurate name when generically referring to such quark models, because the various approaches are very different. For instance, Refs. [53] and [55] evaluate real mass shifts from lowest-order hadronic loops. Now, Ref. [53] introduced an unquenched quark model for baryons (also see Ref. [56]), based on the flux-tube-breaking model of Ref. [57], but the authors and their collaborators later applied it to mesons as well, as e.g. $\chi_{c1}(3872)$ [58] and bottomonium states [59]. In Ref. [57] it was claimed, on the basis of overlap integrals of (real) harmonic-oscillator wave functions, that cancellations among different sets of hadronic loops will lead to violations of the OZI rule that are much smaller than typical widths of meson resonances. In the same spirit, Ref. [55] argued that the hyperfine spin-orbit splittings among P -wave states remain surprisingly small, in spite of often large mass shifts. In particular, the ordering of these states remains unaltered. These features were shown to be a consequence of negative real mass shifts of comparable size for the different states, depending critically on Clebsch-Gordan coefficients and on the created 3P_0 light $q\bar{q}$ pair having spin 1. However, the conclusions of both Refs. [57] and [55] do not necessarily hold above the physical decay thresholds. Indeed, as we shall see below, in the case of genuine decay and complex meson-meson loops, resonance pole positions are also strongly influenced by unitarity, analyticity, phase space, and possibly the proximity of other thresholds as well as poles. This makes any predictions about the real parts of

mass shifts highly unreliable without a full-fledged S -matrix approach.

An alternative method to simulate effects from $q\bar{q}$ pair creation is via a screened confining potential (see e.g. Refs. [54, 60]), which is in fact not confining anymore above a certain energy. The problem with this approach is that thereabove it will give rise to spurious free quarks instead of physical free mesons. Moreover, the threshold for e.g. charmonium decay to open-charm mesons lies far below this “deconfinement” energy, so that the method will not naturally account for hadronic widths, let alone unitarity.

Finally, the unquenched quark model of Ref. [38] for different stable charmonium states is formulated as a multichannel problem in coordinate space, with a confining potential in the $c\bar{c}$ sector and several open-charm meson-meson channels. Despite the fact that this calculation is limited to states below all open-charm thresholds, the formalism is based on a fully unitary S -matrix, analytically continued below threshold and so including meson loops to all orders. Applications of a simpler version of this r -space model yet also in the scattering region can be found in Ref. [37] (for both versions, see Subsecs. 6.5 and 6.4 below, respectively). Also the original models of Refs. [4, 8, 9] were truly unitarised, but there are enormous differences as well in the computed mass shifts from unquenching, even among in principle similar models. In Table 1 (also see Refs. [61, 62]) we show the corresponding predictions of

Table 1: Negative mass shifts from unquenching. Abbreviations: BT = bootstrap, χ = chiral, QM = quark model, RGM = Resonating Group Method, RSE = Resonance Spectrum Expansion, CC = coupled channels, HO = harmonic oscillator, WF = wave function, PT = perturbation theory, q = light quark; P, V, S = pseudoscalar, vector, scalar meson, respectively.

Refs.	Approach	Mesons	$-\Delta M$ (MeV)
[4]	S -matrix, r -space	charmonium	48–180
[49, 50, 65]	one-loop BT	$q\bar{q}, c\bar{c}, b\bar{b}; P, V$	23–1300, 11–500
[8, 9]	S -matrix, r -space	$q\bar{q}, c\bar{q}, c\bar{s}, c\bar{c}, b\bar{b}; P, V$	180–700, 3–350
[63]	S -matrix, r -space	light, intermediate S	510–830, ~ 0
[66]	χ QM, RGM	$\rho(770), \phi(1020)$	328, 94
[33]	RSE, p -space	$D_{s_0}^*(2317), D_0^*(2300)$	260, 410
[67]	CC, χ Lagrangian	$D_{s_0}^*(2317), D_s^*(2632)$	173, 51
[68]	CC, PT	charmonium	165–228
[69]	CC, HO WF	charmonium	416–521
[36]	RSE, p -space	$X(3872)$	≈ 100
[64]	RSE, p -space	$c\bar{q}, c\bar{s}; J^P = 1^+$	4–13, 5–93

a number of unquenched quark models for mesons, including the Nijmegen model and its more recent momentum-space version (RSE), to be dealt with comprehensively in Sec. 5. Note that the mass shifts in Refs. [8, 9, 33, 36, 63, 64] are in general complex, in some cases [33, 63, 64] with huge imaginary parts, corresponding to pole positions in an exactly solved S -matrix. As for the disparate shifts among the various approaches, they are due to differences in the assumed decay mechanism, included channels, and possibly drastic approximations. Another crucial point should be to properly account for the nodal structure of the bare $q\bar{q}$ wave functions.

Let us now look in more detail at some results shown in Table 1. First of all, we emphasise again that mass shifts for resonances must be complex, amounting to pole positions in the complex-energy plane with respect to the inherently bound states in a quenched model calculation. These poles may show up in a fully unitary and non-perturbative S -matrix, or just correspond to the real and imaginary parts of complex mass shifts computed perturbatively. In Table 1 we only specify the real parts of such

mass shifts, both for bound states and resonances. Concerning the charmonium results, we see large differences among the different models referred in Table 1, both in size and pattern of the obtained mass shifts. Starting with the two earliest approaches, namely by the Cornell [4, 5] and Nijmegen [8, 9] groups, we observe negative mass shifts that on average are of the same order of magnitude. However, in the Nijmegen model the shift is largest for the 1^3S_1 state ($J/\psi(3097)$) and in the Cornell model for the 1^3D_1 ($\psi(3770)$). This can at least qualitatively be understood by noting that in the Cornell model the decay process is thought to be directly linked to the confining potential, whereas in the Nijmegen model it is supposed to be governed by the empirically successful 3P_0 model [70, 71]. Since the Cornell potential is instantaneous, the created $q\bar{q}$ pair in the decay process is then necessarily in a 1S_0 state, which implies that the transition potential between the confined charm-anticharm sector and the final state with two free open-charm mesons essentially probes the $c\bar{c}$ wave function's inner region. In contrast, the 3P_0 model assumes that a new $q\bar{q}$ pair is created with vacuum quantum numbers, that is, $J^{PC} = 0^{++}$, which necessarily implies $S = L = 1$ for the created pair, being in a 3P_0 spectroscopic state. The corresponding transition potential has necessarily a peaked structure at some interquark distance, as it must vanish both at the origin, for being in a P -wave, and at large separations because of quark confinement. Such a peaked behaviour, resulting from string breaking at a certain distance and confirmed [72] in lattice-QCD calculations, was represented phenomenologically in the Nijmegen model by a spherical delta-shell [8] or a Gaussian-type peaked function [9]. As a consequence, in this approach it is the ground state that shifts most, because its wave function has no nodes. Since the Cornell and Nijmegen models do not use the same confining potential and so predict disparate bare spectra, both models are capable of fitting the physical spectra, despite the significant differences in the pattern of mass shifts due to unitarisation. This emphasises the need to apply unitarised models to a wide range of mesons, in order to allow to disentangle confinement and decay effects on mass spectra. Note that in Ref. [9] the model parameters were fitted to the vector and pseudoscalar spectra, with good results for the vector mesons in the light, charmonium, and bottomonium sectors, both for masses and hadronic widths. Moreover, exactly the same parameters and Gaussian-like transition potential were employed in Ref. [63], predicting a complete nonet of light scalar mesons, besides the regular 3P_0 $q\bar{q}$ resonances in the energy region of 1.3–1.5 GeV (also see Subsec. 4.1).

The other two papers in Table 1 on coupled-channel mass shifts in charmonium, viz. Refs. [68] and [69], both show little sensitivity to the radial or angular excitation of the bare $c\bar{c}$ state. So this roughly amounts to an overall downward mass shift of the spectra, which could be compensated for by accordingly increasing the charm quark mass [69]. However, in view of the enormous quantitative discrepancy between the mass shifts in these two works, namely 165–228 MeV vs. 416–521 MeV, these results should be interpreted with a lot of caution.

Next we compare the predictions of the Helsinki [49, 50, 65] and Nijmegen [8, 9] models for light as well as heavy pseudoscalar and vector mesons (cf. second and third line in Table 1). *Grosso modo*, the results are quite comparable. This is not surprising, since both models employ the 3P_0 mechanism for decay and satisfy multichannel unitarity. However, there are two significant differences. First of all, the Helsinki model, based on a Cornell-type potential for the bare spectra, predicts much smaller mass shifts for bottomonium than for charmonium, whereas in the Nijmegen model these shifts are comparable. Note, though, that the Nijmegen model was intentionally formulated in a universal way, with the same confinement and decay parameters for light, medium-heavy, and heavy mesons. Anyhow, both models manage to describe the spectra reasonably well without resorting to many adjustable parameters. This is a reminder that just looking at the observed resonance spectra does not allow to draw straightforward conclusions on the kind of confining potential. Another difference concerns the 3S_1 and 3D_1 states in charmonium and bottomonium. In the Helsinki model, these levels are generally well separated and undergo comparable shifts. On the other hand, in the Nijmegen model, based on HO confinement, the $(n+1)^3S_1$ and n^3D_1 bare states are degenerate. Now, upon unitarisation, the degeneracy is lifted, with the 3S_1 level becoming an S -matrix pole that shifts much more than the 3D_1 partner pole. A similar

phenomenon occurs through unitarisation of the degenerate 3P_1 and 1P_1 bare $c\bar{q}$ or $c\bar{s}$ state, when describing the open-charm axial-vector mesons in the momentum-space formulation of the Nijmegen model [64] (eleventh line in Table 1). Since such mesons have no definite C -parity, the physical states are linear combinations of 3P_1 and 1P_1 . One combination then results in a strongly shifted pole, whereas the other combination almost decouples from the decay channel(s), giving rise to a quasi-bound state in the continuum [64].

Other very intriguing results in Table 1 concern the already mentioned scalar mesons, as described in the Nijmegen model [63] (fourth line in Table 1). Here, we see some enormous mass shifts, but also others that are close to zero, which clearly requires further explanation. The point is that one is not actually dealing with mass-shifted states here, but rather with emergence of extra states, of a more dynamical origin and not present in the unquenched spectrum. The real parts of the latter resonances indeed lie many hundreds of MeV below the bare 3P_0 $q\bar{q}$ states. However, the latter ones also shift, but mostly in the imaginary direction upon unquenching, thus acquiring significant decay widths yet with their masses changed much less. So it is more correct to refer to this phenomenon as duplication instead of mass shift of states, since two complete $SU(3)_{\text{flavour}}$ nonets result from this doubling. The unusual mass pattern in the lightest nonet reflects the very strong influence of hadronic decay thresholds and is not an indication of a non- $q\bar{q}$ substructure as postulated in Ref. [73] (see Subsec. 4.1 for more details).

To conclude this section, let us look in more detail at the light pseudoscalar mesons, in particular the pion. Checking again Table 1, second and third line, we see huge mass shifts of up to 700 MeV in the Nijmegen model and even about 1300 MeV in the Helsinki model. However, one should realise that a significant fraction of these shifts is due to a coupling constant made proportional to the lowest-order hyperfine interaction in QCD, due to one-gluon exchange. In the Helsinki model this was done as a fundamental ingredient of the approach, whereas in the Nijmegen model it was a numerical procedure of making this interaction proportional to the unitarised wave function at the origin. Anyhow, in both models the result is that pseudoscalar mesons shift roughly three times as much as vectors, because of the eigenvalues of the colour-spin operator $\vec{F}_q \cdot \vec{F}_{\bar{q}} \vec{S}_q \cdot \vec{S}_{\bar{q}}$, which are -1 for 1S_0 and +1/3 for 3S_1 . The same is done in traditional static quark models of mesons. However, it must be noted that the very low mass of the pion is not only due to one-gluon exchange, but equally or even dominantly to dynamical chiral-symmetry breaking. The Helsinki and Nijmegen models, which use effective, constituent quark masses, are not well-suited to describe the pion, as it is much lighter than such constituent quarks. Instead, starting from massless current quarks and a chirally symmetric confining interaction with the appropriate Dirac spin structure, the models of Refs. [28, 29] indeed obtain a massless pion in the chiral limit, via a gap equation describing dynamical chiral-symmetry breaking. Moreover, in the approach of [29] and by modelling the vector-meson resonances $\rho(770)$ and $\phi(1020)$ via Salpeter [74] and Resonating-Group-Method (RGM) [66] equations with the very same interaction, reasonable masses and widths are found for these mesons. Also note that the real mass shift thus obtained [66] for $\rho(770)$ is -328 MeV, so very near the value found in the Nijmegen model [9].

Summarising, we have seen that unitarised and other coupled-channel models of mesons can give rise to enormous real mass shifts, which may completely obfuscate the underlying bound-state spectrum resulting from the confining potential only and so the very nature of this potential. The challenge then is to determine the most realistic approach, in view of the quantitatively very different predictions of the here described models. For a minireview on unquenching hadrons and some more references, see Ref. [75]. Next we shall revisit the special case of the light scalar mesons in the Nijmegen model [9].

4.1 Light scalar mesons in the Nijmegen model

Now we look in more detail at the predictions of the Nijmegen model for light and heavy pseudoscalar and vector mesons [9], as applied [63] to the light scalar mesons. It must be emphasised that this did not involve any fit, as the parameters determined in Ref. [9] were left completely unaltered. Recapitulating,

the resulting modelling of light isoscalar, isovector, and strange scalar mesons amounts to coupling a confined quark-antiquark pair with 3P_0 quantum numbers to all OZI-allowed decay channels with pairs of ground-state pseudoscalar or vector mesons, in relative S -waves or D -waves (only for vector-meson pairs with intrinsic spin 2). The isoscalar $q\bar{q}$ states require two channels, namely $n\bar{n}$ and $s\bar{s}$, owing to their unavoidable mixing through the common KK and K^*K^* channels. All included two-meson channels can be found in Table 1 of Ref. [63], together with the corresponding channel couplings derived in Ref. [76] employing a microscopic formalism of wave-function overlaps in a harmonic-oscillator basis.

The kinematically relativistic coupled-channel Schrödinger equations in coordinate space are solved numerically for the S -matrix as in Ref. [9], using an increasing number of delta functions to approximate the transition potential between the $q\bar{q}$ and meson-meson sectors. Thus, regular scalar resonances show up in the energy region of about 1.3–1.5 GeV, through S -matrix poles with real parts not far from the discrete energy levels of 3P_0 $q\bar{q}$ bound states and imaginary parts that are also roughly compatible with the observed widths of the PDG [10] states $f_0(1370)$, $a_0(1450)$, $K_0^*(1430)$, and $f_0(1500)$. Note that these experimentally determined masses are about 200–300 MeV higher than those found in the GI [2] model. However, the big surprise — as it certainly was almost four decades ago when the phenomenon was first observed [77] — is the appearance of additional S -matrix poles, viz. at much lower energies and larger imaginary parts. The nature of these extra poles is clearly different from the ones above 1 GeV, as they do not approach the corresponding $q\bar{q}$ bound states on the real energy axis when the overall coupling constant is reduced to zero. In contrast, these poles disappear in the scattering continuum with ever increasing negative imaginary part. So they are clearly of a dynamical origin, as opposed to the other, “intrinsic” [78] mesons, which can be simply linked to the bare 3P_0 quark-antiquark spectrum.

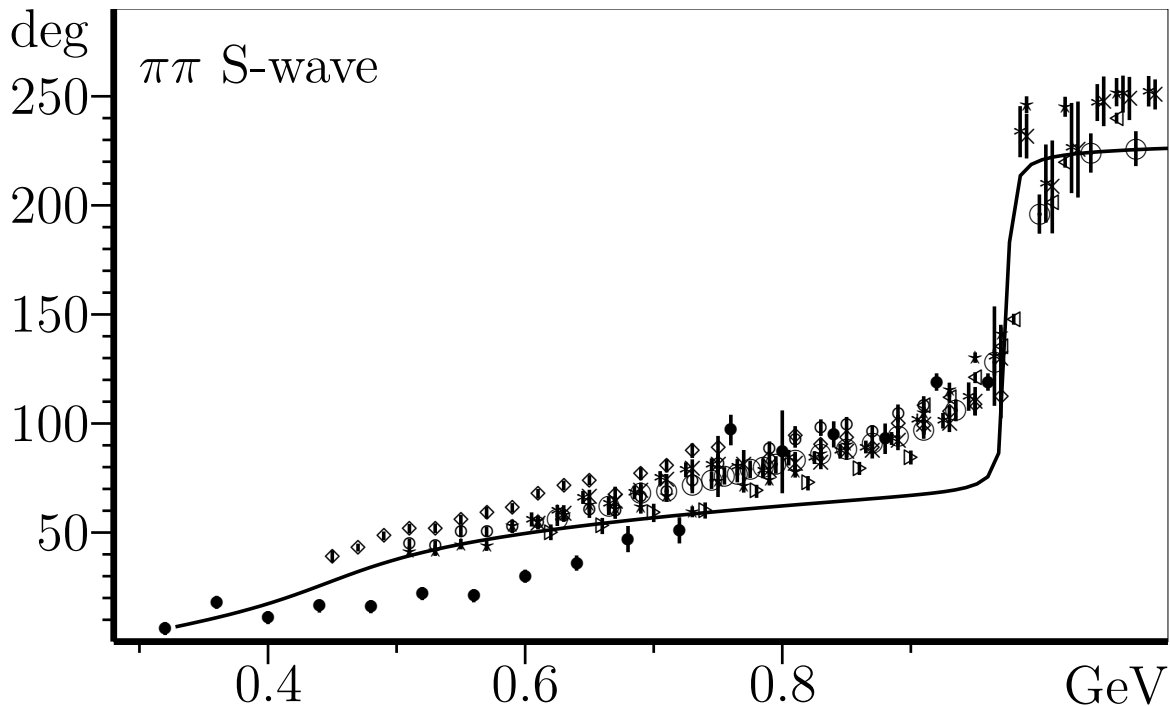


Figure 4: S -wave $\pi\pi$ phases predicted in Ref. [63] (see this reference for the different data).

Coming now to the actual findings of light scalar-meson resonances as published in Ref. [63], the lowest-lying isoscalar, isodoublet, and isovector poles are, with the old names ϵ for $f_0(500)$, S for $f_0(980)$, κ for $K_0^*(700)$, and δ for $a_0(980)$:

$$\epsilon(470 - i208) \text{ MeV}, S(994 - i20) \text{ MeV}, {}^3\kappa(727 - i263) \text{ MeV}, \delta(968 - i28) \text{ MeV}. \quad (42)$$

³Note that there is a typographical error in Ref. [63], with the imaginary part of the S resonance pole given as $-2i$ MeV

It is worthwhile noting that the corresponding masses and widths are still compatible with present-day PDG [10] limits.

Since the Nijmegen model allows to obtain a closed-form expression for the full multichannel S -matrix, it is straightforward to predict a variety of observables, as e.g. partial-wave phase shifts for any of the included meson-meson channels. Thus, in Ref. [63] S -wave $\pi\pi$ phase shifts were computed up to 1.2 GeV, shown in Fig. 4 with the then available data. Considering that no fit was carried out, with the theoretical phase shifts being *bona fide* predictions, the global agreement with experiment was and is still remarkable.

In conclusion, we must stress that the pole doubling discovered in Refs. [63, 77] does not depend on details of the confining potential, only on the existence of bare $q\bar{q}$ states that couple strongly to S -wave meson-meson channels. As a matter of fact, the same phenomenon was observed [21] about a decade later, in the context of the already mentioned Helsinki [49, 50, 65] model. However, in Ref. [21] no pole doubling⁴ was found for the isodoublet scalar meson (“ κ ”) and it was even argued why in this case the doubling mechanism should not occur. Thus, no $K_0^*(700)$ was predicted and merely a $K_0^*(1430)$. This failure was explained as possibly due to the use of channel couplings that are not fully flavour symmetric [22] or the inclusion of an *ad hoc* negative Adler zero in $K\pi$ S -wave scattering [80]. In much more recent work, the pole-doubling phenomenon for one $q\bar{q}$ seed in the scalar-meson sector was also observed in an effective-Lagrangian model to one-loop order, namely for the isovector pair $a_0(980)$, $a_0(1450)$ [81] and the isodoublet pair $K_0^*(800)$ (cf. $K_0^*(700)$), $K_0^*(1430)$ [82].

5 Resonance Spectrum Expansion and Applications

5.1 Simple unitarised momentum-space model

Despite the surprising results for the light scalar mesons in Ref. [63], this work was largely ignored for 15 years. Things changed in 2001, when we received an email [83] from a co-spokesperson of the E791 Collaboration at Fermilab, informing us about preliminary evidence [84] of a light strange scalar meson (K_0^* , “ κ ”). He also mentioned that our Comment [22] on Ref. [21], in which we insisted on the existence of a light K_0^* meson, had been encouraging to E791 and motivated his sending us the email [83]. The final E791 result was eventually published in Ref. [85], confirming a light K_0^* with mass $(797 \pm 19 \pm 43)$ MeV and width $(410 \pm 43 \pm 87)$ MeV, i.e., values fully compatible with our pole position of $(727 - i263)$ MeV predicted [63] in 1986 (cf. Eq. (42)).

In the ensuing email exchange [83] with the same E791 co-spokesperson, he encouraged us to provide easy-to-use formulae to fit the light scalars to data, as these mesons had been awkward not only to model builders but also to experimentalists. Indeed, our original work predicting [63] a complete light scalar nonet was based on a very complicated multichannel quark model in coordinate space [9] and impracticable for experimental analysis. Thus, we immediately developed [86] an exactly solvable yet fully unitary and analytic general ansatz in momentum space for non-exotic meson resonances. The only assumption here is that, like in Ref. [8], transitions between the confined $q\bar{q}$ and free meson-meson sectors are governed by string breaking at a sharp distance, modelled with a spherical delta function. In the case of only one confined quark-antiquark channel and only one free meson-meson channel, which is appropriate to describe e.g. S -wave $K\pi$ scattering in the elastic region, the resulting expression for the phase shift takes the simple form [86]

$$\cotg(\delta_\ell(p)) = \frac{n_\ell(pa)}{j_\ell(pa)} - \left[2\lambda^2 \mu pa j_\ell^2(pa) \sum_{n=0}^{\infty} \frac{|\mathcal{F}_{n\ell_c}(a)|^2}{E - E_{n\ell_c}} \right]^{-1}, \quad (43)$$

instead of the value $-20i$ MeV as corrected in the posterior arXiv version 0710.4067v1 [hep-ph].

⁴In an earlier [79] application of the Helsinki model to the light scalar mesons, not even an $f_0(500)$ (“ σ ”) was found.

where j_ℓ and n_ℓ are spherical Bessel and Neumann functions, respectively, with ℓ the orbital angular momentum in the meson-meson channel, p and μ are the relativistically defined momentum and reduced mass in the latter channel, a is the string-breaking radius, λ is an overall coupling constant, ℓ_c is the orbital angular momentum in the $q\bar{q}$ sector, $\mathcal{F}_{n\ell_c}(a)$ is the n -th radial solution of whatever confining potential is employed in the $q\bar{q}$ channel, $E_{n\ell_c}$ is the corresponding bare radial spectrum, and E is the total energy of the system, which becomes complex for physical meson resonances. For a detailed derivation of Eq. (43) in momentum space via a step-wise solution of the Lippmann-Schwinger Born series, see Ref. [87]. Furthermore, by solving the same Hamiltonian directly in coordinate space, a spectral representation of the bare $q\bar{q}$ Green's function was derived, viz.

$$\sum_{n=0}^{\infty} \frac{|\mathcal{F}_{n\ell_c}(a)|^2}{E - E_{n\ell_c}} = \frac{2\mu}{a^4} \frac{F_{c,\ell_c}(E, a)G_{c,\ell_c}(E, a)}{W(F_{c,\ell_c}(E, a), G_{c,\ell_c}(E, a))}, \quad (44)$$

where F_{c,ℓ_c} and G_{c,ℓ_c} are the two solutions of the Schrödinger equation with the unspecified confining potential that are regular at the origin and at infinity, respectively. The identity in Eq. (44) gave rise to the designation *Resonance Spectrum Expansion* (RSE) for the formalism developed in Refs. [86, 87].

Now, contrary to BW-type expressions, Eq. (43) does not exhibit resonance pole positions explicitly. Nevertheless, the complex resonance energies can be easily found by solving the equation numerically for $\cotg(\delta_\ell(p)) = i$. Moreover, the $|\mathcal{F}_{n\ell_c}(a)|^2$ are just a set of real numbers for different n , which makes Eq. (43) extremely flexible. Namely, theorists can use their favourite model and corresponding bare spectrum for the confining potential, being left with only two free parameters (λ , a) to show the predictive power of that model. On the other hand, experimentalists may just consider those real numbers and energies fit parameters when analysing their data, while restricting the infinite sum to merely a few terms, with the argument that much higher energies will hardly influence the fit in a certain region. In the following we shall demonstrate the potentiality of either approach.

5.1.1 $K_0^*(700)$ from a fit to S -wave $K\pi$ phase shifts

In Ref. [86], Eq. (43) serves as the basis to fit elastic $K\pi$ scattering in P - and S -waves, by taking only a few terms in the infinite sum and fit the real constants to the data, together with the parameters λ and a . In the P -wave case, two terms and one bare energy are sufficient to obtain a good fit and a very reasonable value for the $K^*(892)$ pole position, whose real part comes out about 60 MeV below the fitted bare $K^*(892)$ mass. Note that this relatively small negative mass shift from unitarisation when compared to those found in Refs. [8, 9] is easy to understand, as in this simple model only one meson-meson channel is coupled. All the other, kinematically closed channels, which are not considered here, will contribute with extra negative yet purely real mass shifts and so not affect in principle the imaginary part of the pole. Inclusion of such channels will lead to a significantly higher bare ground-state mass, though, of the order of 1.2 GeV in the case of $K^*(892)$, as found in the model of Ref. [9].

The more complicated S -wave case requires an additional term and two instead of one bare energies when truncating Eq. (43), in order to be able to extract resonance information above 1 GeV as well. Moreover, the different experimental S -wave $K\pi$ data are rather conflicting with each other below 1 GeV (see Fig. 5). In the fit to the S -wave phase shifts, the λ value found for the P -wave at $0.75 \text{ GeV}^{-3/2}$ is kept fixed, whereas the decay radius a is reduced from 5 GeV^{-1} to 3.2 GeV^{-1} . This is related to the different behaviour of spherical Bessel functions for small argument in the $\ell = 1$ and the $\ell = 0$ case. The results of the fit are shown in Fig. 5, both for the phase shift and the extracted cross section. The broad cross-section peak below 1 GeV must be due to a pole with a relatively large imaginary part in the corresponding energy region, despite the fact that the phase shift only reaches 90° above 1.3 GeV. As already mentioned above, this is due to the presence of an Adler zero in the S -wave $K\pi$ amplitude [25, 80] below yet very close to threshold, which slows down the phase-shift's rise at low energies, and the overlapping of the $K_0^*(700)$ and $K_0^*(1430)$ resonances [25]. Searching

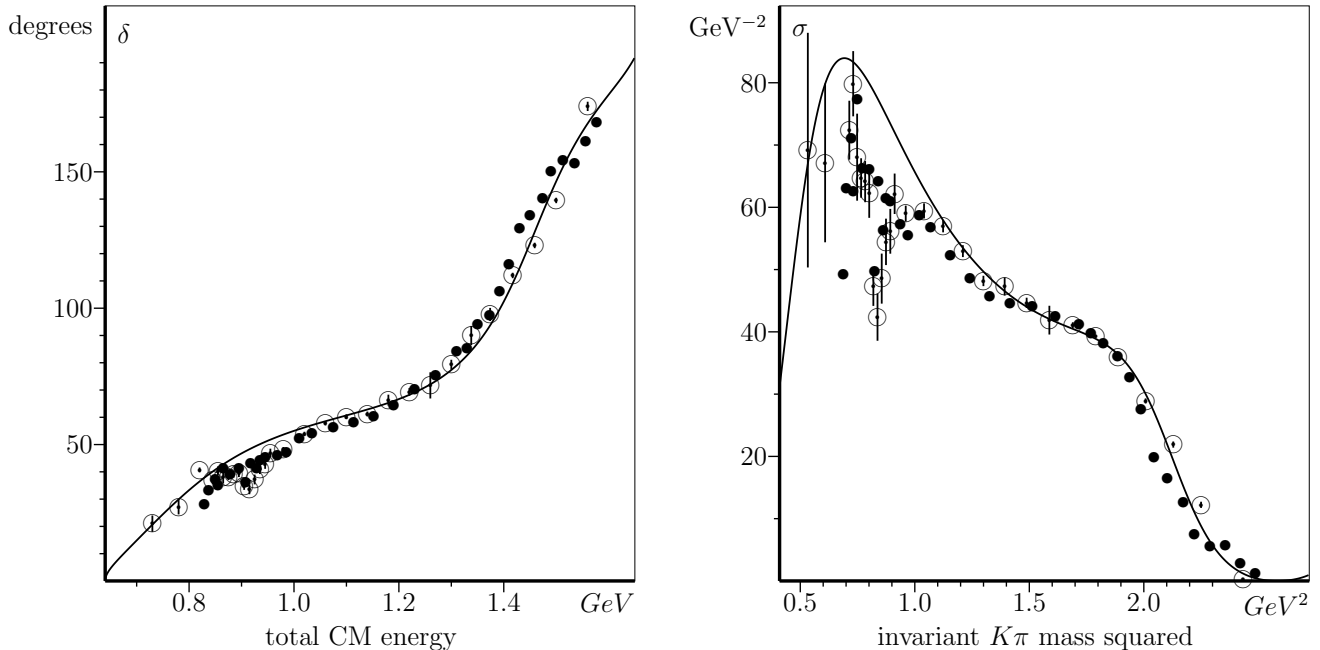


Figure 5: Fitted S -wave $K\pi$ phase shift (left) and corresponding cross section (right) from truncating the infinite sum in Eq. (43) (see text). For more details and the experimental data, see Ref. [86].

for poles, we indeed we find two of them below 1.5 GeV, namely at $(714 - i228)$ MeV for $K_0^*(700)$ and $(1458 - i118)$ MeV for $K_0^*(1430)$. These results are excellent for such a simple model, without the inelastic $K\eta'$ channel. Note that the $K\eta$ channel largely decouples [88], because of a partial cancellation between the $n\bar{n}$ and $s\bar{s}$ components of the η mesons, via $n\bar{n}$ and $s\bar{s}$ pair creation, respectively.

5.1.2 Charmed scalar mesons $D_{s0}^*(2317)$ and $D_0^*(2300)$

In April 2003, the BABAR Collaboration announced the observation of a narrow meson with a mass of about 2.32 GeV decaying to $D_s^+\pi^0$, which was published in Ref. [89]. They baptised the new state as $D_{sJ}^*(2317)^+$ (now called $D_{s0}^*(2317)^+$ [10]) and argued that the low mass of this charmed-strange meson as well as its natural parity favour a $J^P = 0^+$ assignment. If indeed confirmed as the lowest scalar $c\bar{s}$ state, its small width would be the consequence of lying below the DK threshold, with $D_s^+\pi^0$ being an isospin-violating decay mode and therefore suppressed. However, such a low mass is in conflict with the GI [2] and similar static quark models, as already mentioned above.

After learning about the discovery, we immediately realised [33] that this enigmatic new meson, if confirmed as a scalar, couples strongly to the S -wave DK channel, which may significantly alter its mass resulting from the confinement potential alone. Moreover, with its $c\bar{s}$ quark content and only one nearby OZI-allowed decay channel, it has strong similarities with the coupled $K_0^*(700)$ - $K\pi$ system. The problem is that in the $D_{sJ}^*(2317)$ case no DK phase shifts are and probably never will be available. So we decided to leave several parameters resulting from the RSE fit to the S -wave $K\pi$ phase shifts unaltered, namely λ , a , and the three constants replacing the infinite sum in Eq. (43). The only obvious changes were replacing the $K\pi$ threshold by the DK threshold at 2363 MeV, besides taking two fixed bare energy levels instead of fitting them as in the $K\pi$ case. To choose these, we resorted to the Nijmegen model for pseudoscalar and vectors mesons [9], taking the charm quark mass at 1562 MeV, the strange quark mass at 508 MeV, and the first two radial levels of the harmonic-oscillator spectrum, with frequency $\omega = 190$ MeV. This results in bare $c\bar{s}$ energy levels at 2545 MeV and 2925 MeV. Furthermore, we also included the isodoublet charmed-light scalar meson [33], with bare $c\bar{n}$ energy levels at 2443 MeV and

2823 MeV, from $m_n = 406$ MeV [9], as there was already some indication [90] of a very broad charmed scalar resonance decaying to $D\pi$ in an S -wave.

The thus found lowest charmed-strange and charmed-light scalar poles are [33]

$$c\bar{s} : (2.28 + i0) \text{ GeV} , \quad c\bar{n} : (2.03 - i0.075) \text{ GeV} . \quad (45)$$

The $c\bar{s}$ bound state pole clearly represents $D_{s0}^*(2317)$, with the pole coming out remarkably close to 2.317 GeV in view of the lack of any fit and just the use of parameters fixed in previous work [9, 86]. As for the $c\bar{n}$ pole, it seems to lie much too low to stand for the D_0^{*0} resonance first observed [90] and then confirmed [91] by the Belle Collaboration, with mass $2308 \pm 17 \pm 15 \pm 28$ MeV and width $276 \pm 21 \pm 18 \pm 60$ MeV, now listed by the PDG [10] with average mass 2300 MeV and width 274 MeV. However, one should realise that the precise position of this resonance pole is extremely sensitive to the employed parameters, in particular λ and a . As a matter of fact, using the flavour-symmetry [92] arguments underlying the Nijmegen model [8, 9], λ and a should scale as [93]

$$\lambda\sqrt{\mu_{q_1q_2}} = C_1 , \quad a\sqrt{\mu_{q_1q_2}} = C_2 , \quad (46)$$

where $\mu_{q_1q_2}$ is the reduced mass of a meson composed of quarks q_1 and q_2 , and the constants C_1, C_2 are fixed by $\lambda = 0.75 \text{ GeV}^{-3/2}$ and $a = 3.2 \text{ GeV}^{-1}$ for the scalar $n\bar{s}$ system (see above), with $m_n = 406$ MeV and $m_s = 508$ MeV [9]. When the values of λ and a resulting from Eq. (46) are used to determine the lowest scalar $c\bar{s}$ and $c\bar{n}$ poles, we find [93]

$$c\bar{s} : (2.33 + i0) \text{ GeV} , \quad c\bar{n} : (2.14 - i0.16) \text{ GeV} , \quad (47)$$

which is a further improvement as compared to Eq. (45), especially for the $D_0^*(2300)$ resonance. In a more complete model calculation [94], with all relevant pseudoscalar-pseudoscalar and vector-vector channels included, the S -wave $D\pi$ cross section representing $D_0^*(2300)$ peaks close to 2.19 GeV (also see below).

In Fig. 6 we depict the complex-energy pole trajectories in the amplitudes of S -wave $D\pi$ (left) and DK (right) scattering as a function of the coupling λ , for the simple model of Ref. [33]. In both cases we see a pole arising from deep down in the complex-energy plane for small coupling, but then settling relatively close to ($D_0^*(2300)$) or on top of ($D_{s0}^*(2317)$) the real axis for the physical value of λ . On the other hand, for either meson, there is a pole that starts at the ground-state bare energy level for zero coupling, moving into the complex plane for increasing λ . So the former poles are of a dynamical nature, whereas the latter, intrinsic ones correspond to usual resonances that can be clearly linked to states in the bare $q\bar{q}$ confinement spectrum. These dynamical poles are of the same nature as the light scalar mesons [63] and their manifestation as a broad or narrow resonance, or even a bound state like $D_{s0}^*(2317)$ ⁵, depends on details of where their most relevant thresholds lie. For the latter state, whose lowest (OZI-allowed) decay mode is DK , the pole ends up below threshold, owing to the relatively large kaon mass. Note that the pole's movement, becoming first a virtual bound state and only a true bound state after passing through the "eye" of the DK threshold, is typical for S -waves [18]. This is symbolically depicted in Fig. 6 by displacing the virtual and genuine bound-state pole trajectories slightly downwards or upwards, respectively. In contrast, the $D_0^*(2300)$ pole slows down while approaching the real axis, remaining complex. This is due to the presence of a kinematical Adler-type zero [80] in the amplitude just below the $D\pi$ threshold, due to the small pion mass. Similar Adler zeros are to a large extent responsible [25, 95] for the broad σ and κ scalar resonances.

A final comment is due concerning these dynamical poles. Namely, the only physically relevant poles are those for parameter values that reproduce the data and not the trajectories as a function of λ that

⁵As already mentioned, $D_{s0}^*(2317)$ is not really a bound state, because it can decay to $D_s\pi$ in an isospin-violating and OZI-suppressed process, which gives rise to a very small width.

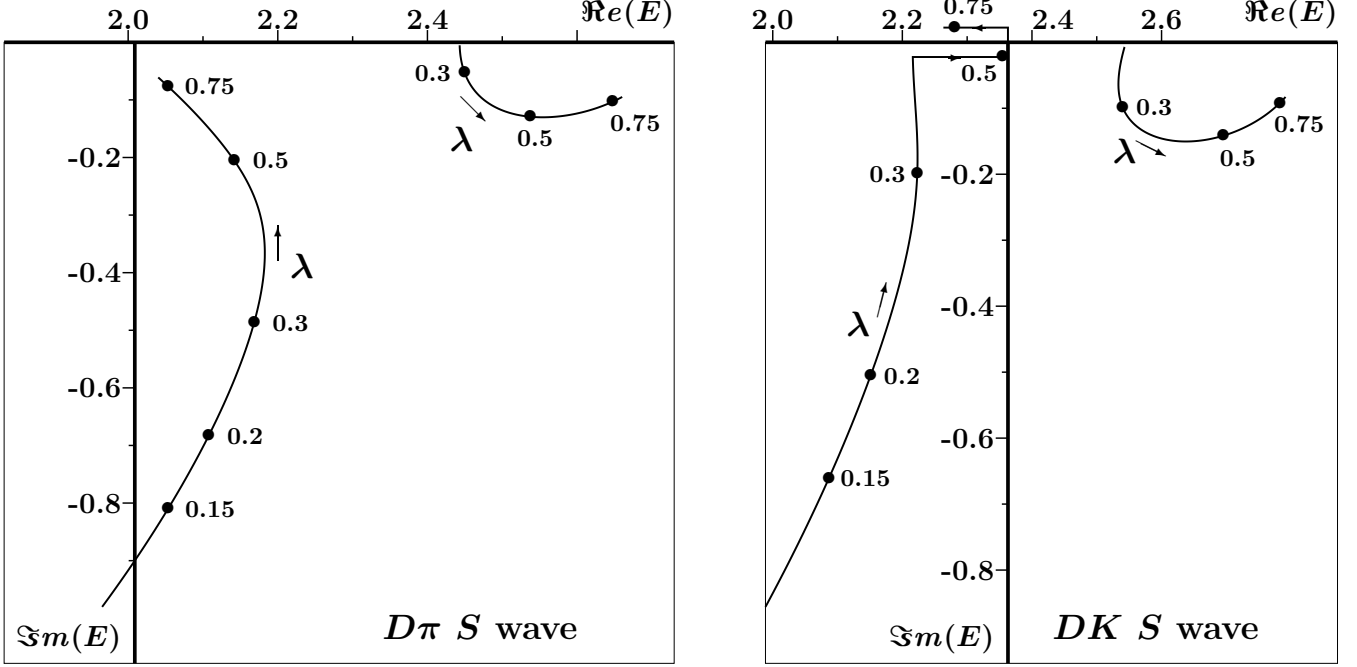


Figure 6: $D_0^*(2300)$ (left) and $D_{s0}^*(2317)$ (right) pole trajectories as a function of λ (also see text and Ref. [33]).

lead to the eventual pole positions. Now, it turns out that these trajectories are very sensitive to minor changes in other parameters and also to the included meson-meson channels. For instance, in Ref. [96] it was shown that very small variations in the delta-shell radius a can make the dynamical $D_{s0}^*(2317)$ pole become intrinsic and vice versa (see Fig. 4a in Ref. [96]). In other words, there can be a sudden crossover of the two pole trajectories for certain parameter values. However, the final pole positions hardly change with such tiny variations, so the very definition of dynamical vs. intrinsic resonance can be highly questionable for certain mesons. We shall come back to this issue when dealing with the axial-vector charmonium state $\chi_{c1}(3872)$ in Subsecs. 6.3, 6.4, and 6.5 below.

5.1.3 Charmed axial-vector mesons $D_{s1}(2460)$, $D_{s1}(2536)$, $D_1(2430)$, and $D_1(2420)$

Shortly after the discovery of $D_{s0}^*(2317)$ by BABAR [89], the Belle Collaboration not only announced [97] a confirmation of this charmed-strange scalar meson, but also evidence of a another new charmed-strange state, viz. $D_{sJ}(2457)$, decaying to D^*K and meanwhile confirmed as the axial-vector $D_{s1}(2460)$ [10]. Moreover, Belle had already indicated [90] a new and very broad charmed-light axial-vector meson, confirming its observation in Ref. [91], which is now listed [10] as $D_1(2430)^0$. Now, axial-vectors with open charm have no definite C -parity, so that each of them gives rise to two physical $J^P = 1^+$ mesons as different and orthogonal mixtures of the spectroscopic states 3P_1 and 1P_1 , just like the two strange mesons $K_1(1270)$ and $K_1(1400)$ [10]. The two new states $D_{s1}(2460)$ and $D_1(2430)^0$, together with the then already established mesons $D_{s1}(2536)$ and $D_1(2420)$, unfold a very puzzling pattern of axial-vector masses and widths. On the one hand, $D_{s1}(2460)$ and $D_{s1}(2536)$ are both very narrow, but separated in mass by 75 MeV, which is difficult to explain with standard spin-orbit splittings. On the other hand, $D_1(2430)$ and $D_1(2420)$ are almost degenerate in mass, but the former resonance is extremely broad ($\Gamma \sim 300\text{--}400$ MeV), whereas the latter is relatively narrow ($\Gamma \approx 25$ MeV) and all the more

so when considering that it can decay to $D^*\pi$ in an S -wave, with a phase space of about 280 MeV. Furthermore, the approximate mass degeneracy of $D_1(2430)$ and $D_1(2420)$ destroys any attempt to explain the mass difference between $D_{s1}(2460)$ and $D_{s1}(2536)$ with spin-orbit interactions. Clearly, unitarity must somehow come to the rescue.

In order to describe [98] these four charmed axial-vector mesons with the above simple model and its parameters fitted to $K\pi$ S -wave phase shifts, we faced the problem of needing to deal with two instead of one $q\bar{q}$ channel, viz. 3P_1 and 1P_1 . So in order to be able to apply this model again, just like in the case of $D_{s0}^*(2317)$ and $D_0^*(2300)$, we showed how a Schrödinger system of two degenerate $q\bar{q}$ channels coupled in the same way to one continuum state naturally gives rise to two orthogonal solutions that either completely decouple from the continuum or fully couple. Of course, this is an approximation in the case of the charmed axial-vector mesons, since they couple to several continuum channels and moreover in a different way. For instance, the 3P_1 and 1P_1 $c\bar{n}$ ground states couple to the S -wave $D^*\pi$ channel with strengths $g_{^3P_1}^2 = 1/36$ and $g_{^1P_1}^2 = 1/72$, respectively [64]. However, for the corresponding couplings to the D -wave $D^*\pi$ channel, the roles are reversed, yielding the values $g_{^3P_1}^2 = 5/144$ and $g_{^1P_1}^2 = 5/72$, respectively [64]. The 3P_1 and 1P_1 $c\bar{s}$ ground states have the same kind of relative couplings to the S -wave and D -wave D^*K channel. Also for the other meson-meson channels, which are all closed, there is a clear tendency for the several coupling strengths of the 3P_1 and 1P_1 components to average out. So we expect our argument based on diagonalising the above very simple Hamiltonian for two degenerate states to largely hold. The same procedure was employed in Ref. [98] to rather successfully model the tiny mass difference between K_L and K_S , besides predicting axial-vector resonances in the open-bottom sector.

When applying this approach to the pair $D_{s1}(2460)$ and $D_{s1}(2536)$, the latter state just remains as a continuum bound-state at its bare energy level of 2545 MeV resulting from the fixed model parameters of Ref. [9], whereas the pole of the former state first moves downwards into the complex-energy plane before settling as a bound state at 2446 MeV on the real axis, below the D^*K threshold (see Fig. 3 in Ref. [98]). The resulting small deviations of -14 MeV and +9 MeV from the experimental $D_{s1}(2460)$ and $D_{s1}(2536)$ masses, respectively, are insignificant in view of this parameter-free prediction. In the charmed-light case, the continuum bound state $D_1(2420)$ stays at 2443 MeV, i.e., 20 MeV higher than in experiment [10], while the resonance pole settles with a real part of about 2.3 GeV and an imaginary part of roughly 0.1 GeV, being again very sensitive to small parameter changes. Clearly, the used model is too coarse to describe very broad resonances. In particular, the inclusion of additional meson-meson channels may significantly alter the trajectories of such poles. In Subsec. 6.1 we shall come back in detail to these four charmed axial-vector mesons, in the context of the full RSE model.

5.1.4 Replacing the infinite RSE sum by channel recoupling coefficients

The way we have so far replaced the infinite sum over the confinement wave function at the string-breaking distance a in Eq. (43) was useful in the considered cases, but is not general enough to describe a large variety of meson resonances. Namely, the few constants replacing the infinite sum as determined by fitting the S -wave $K\pi$ phase shifts only make sense when dealing with similar situations, namely coupling essentially only one $q\bar{q}$ channel to one dominant S -wave meson-meson channel. On the other hand, the values of λ and a resulting from the S -wave $K\pi$ fit cannot be applied to other systems, as the P -wave $K\pi$ already showed, by leading to a quite different value of a . So a scheme is needed to replace the — in principle — infinite number of real constants in the RSE sum by other numbers that make sense physically. At this point we recall the microscopic formalism [76] developed by one of us (EvB), which amounts to deriving the recoupling constants of a meson with any quantum numbers, as well as of its radial and angular excitations, to all OZI-allowed two-meson decay channels via ground-state 3P_0 pair creation, while conserving total spin J , parity P , and (when applicable) C -parity. It is based on overlaps of wave functions for the original $q\bar{q}$ pair, the created 3P_0 pair, and the two resulting mesons,

in a harmonic-oscillator (HO) basis. These recouplings for the lowest radial quantum number have already been used in the coordinate-space model [63] for the light scalar mesons. In this calculation, the Schrödinger equation ensures that higher radially excited solutions for the $q\bar{q}$ wave functions have smaller and smaller effective couplings to the decay channels. However, in the RSE model formulated in momentum space, these wave functions only enter through the moduli of their values at the radius a , which *a priori* are not known. Nevertheless, it makes perfect sense to replace these real numbers by the recouplings constants determined with the HO overlap method of Ref. [76], which then automatically provides a suppression of higher radial excitations just like in the coordinate-space approach. Moreover, the standard normalisation of solutions of the Schrödinger equations is reflected in the normalised HO wave functions used in Ref. [76], which ensures that the sum of the squares of the recouplings to all allowed decay channels is equal to 1. Therefore, mass shifts resulting from coupling an increasing number of decay channels will never grow indefinitely and will even tend to rapidly converge in practice.

Thus, we can write down [96] the partial-wave T -matrix for the still quite simple case of one $q\bar{q}$ channel coupled to N meson-meson channels yet all with the same radial dependence of the corresponding recoupling constants as

$$[T_\ell]_{ij}(p) = \frac{\lambda^2 \left\{ \sum_{n=0}^{\infty} \frac{r_i(n)r_j(n)}{\sqrt{s - E_{nl}}} \right\} 2a \sqrt{\frac{\mu_i \mu_j}{p_i p_j}} p_i p_j j_{\ell_i}(p_i a) j_{\ell_j}(p_j a)}{1 + \lambda^2 \sum_{m=1}^N \left\{ \sum_{n=0}^{\infty} \frac{|r_m(n)|^2}{\sqrt{s - E_{nl}}} \right\} 2ia \mu_m p_m j_{\ell_m}(p_m a) h_{\ell_m}^{(1)}(p_m a)}, \quad (48)$$

where j_{ℓ_i} is the usual spherical Bessel function for channel i , $h_{\ell_i}^{(1)}$ is the corresponding spherical Hankel function of the first kind, defined by $h_{\ell_i}^{(1)} = j_{\ell_i} + in_{\ell_i}$, with n_{ℓ_i} the spherical Neumann function, and the coefficient $r_i(n)$ is the recoupling constant of the n -th bare radial $q\bar{q}$ state to the i -th decay channel, as determined with the formalism of Ref. [76]. As an example, we show in Table 2 the recouplings of generic scalar meson to its allowed meson-meson channels. Note that these constants still must be multiplied by $SU(3)_{\text{flavour}}$ relative couplings. For detailed cases, see Refs. [22, 92]. Let us here just pick two typical examples from Table 2, as illustrations. First, we see in row no. 6 a decay to two ground state vector mesons in a D -wave and with total intrinsic spin $S = 2$, though total $J = 0$ of course. This process has a relatively large recoupling constant. Another example is row no. 3, with a decay to two radially excited pseudoscalar mesons ($n = 1$) with a very small recoupling. Note that all coefficients in the fourth column still must be divided by 4^n , with n the radial quantum number of the bare scalar state.

5.1.5 Light scalar mesons in a multichannel RSE approach

The first detailed application [95] of the multichannel RSE formalism as given by Eq. (48) was a fit to S -wave $\pi\pi$ and $K\pi$ phase shifts as well as $f_0(980)$ and $a_0(980)$ line shapes, by including all pseudoscalar-pseudoscalar channels for the different scalar mesons. A further extension of the model was required, in order to deal with the coupled σ - $f_0(980)$ system by taking into account two instead of only one quark-antiquark channels, viz. $n\bar{n}$ and $s\bar{s}$. The corresponding expressions for the T -matrix became much more complicated than in Eq. (48) (see Eqs. (4,5) in Ref. [95]), but exact T -matrix unitarity is still guaranteed, as the dependence of the recouplings on the radial quantum number is the same in all cases. Since the only free fit parameters were λ and a , with the quark masses and bare energy levels fixed at the values from Ref. [9], a very accurate description of the experimental data was not to be expected. Nevertheless, all essential features of the mentioned phase shifts and line shapes were reproduced for λ and a values varying at most about 10% about the averages for the cases σ only, κ , σ coupled to $f_0(980)$, and $a_0(980)$. Also, the found scalar-meson poles came out fully compatible with contemporary and also present-day PDG [10] limits.

Meson 1	Meson 2	Relative	Recoupling Coefficients
$(nj\ell s)_1 (j^{PC})$	$(nj\ell s)_2 (j^{PC})$	LS	$\{r(n)\}^2 \times 4^n$
$(0, 0, 0, 0) (0^{-+})$	$(0, 0, 0, 0) (0^{-+})$	0, 0	$\frac{1}{24}(n+1)$
$(0, 0, 0, 0) (0^{-+})$	$(1, 0, 0, 0) (0^{-+})$	0, 0	$\frac{1}{144}(2n+3)(n-1)^2$
$(1, 0, 0, 0) (0^{-+})$	$(1, 0, 0, 0) (0^{-+})$	0, 0	$\frac{1}{3456}n(2n+1)(2n+3)(n-3)^2$
$(0, 0, 0, 0) (0^{-+})$	$(0, 1, 1, 1) (1^{++})$	1, 1	$\frac{1}{6}$
$(0, 1, 0, 1) (1^{--})$	$(0, 1, 0, 1) (1^{--})$	0, 0	$\frac{1}{72}(n+1)$
$(0, 1, 0, 1) (1^{--})$	$(0, 1, 0, 1) (1^{--})$	2, 2	$\frac{1}{18}(2n+5)$
$(0, 1, 0, 1) (1^{--})$	$(1, 1, 0, 1) (1^{--})$	0, 0	$\frac{1}{432}(2n+3)(n-1)^2$
$(0, 1, 0, 1) (1^{--})$	$(0, 1, 2, 1) (1^{--})$	0, 0	$\frac{1}{540}(2n+3)(2n-5)^2$
$(0, 1, 0, 1) (1^{--})$	$(0, 1, 1, 0) (1^{+-})$	1, 1	$\frac{1}{6}$
$(0, 0, 1, 1) (0^{++})$	$(0, 0, 1, 1) (0^{++})$	0, 0	$\frac{1}{432}(2n+3)(n-3)^2$
$(0, 1, 1, 1) (1^{++})$	$(0, 1, 1, 1) (1^{++})$	0, 0	$\frac{1}{144}(2n+3)(n-2)^2$
$(0, 1, 1, 0) (1^{+-})$	$(0, 1, 1, 0) (1^{+-})$	0, 0	$\frac{1}{144}(2n+3)(n-1)^2$

Table 2: Recoupling coefficients as a function of radial excitation n , for scalar ($J = 0$, $\ell = 1$, $s = 1$, n) decay into two mesons. Note that the squared recoupling coefficients for $n = 0$ add up to one. This means that, in the harmonic-oscillator approach, there are no additional two-meson channels that can couple to the ground state of the confinement spectrum. For the higher radial excitations, the table is still very incomplete.

In Table 3 we illustrate the dynamical nature of these scalar-meson poles by presenting a number of pole positions for small, medium, and large couplings. The physical poles lie at the complex energies for λ values close to $3.0 \text{ GeV}^{-3/2}$ in all cases. The σ and κ poles clearly originate in the scattering continuum and only turn into bound-state poles for very large values of λ , below the $\pi\pi$ and $K\pi$ thresholds, respectively. This slowing down of either pole is due to the kinematical Adler-type zero just below the corresponding lowest threshold, as we have seen above in the case of the $D_0^*(2300)$ resonance. As for the $a_0(980)$ second-sheet pole, it appears to be strongly attracted by the $K\bar{K}$ threshold, but becoming again a bound state below the $\eta\pi$ threshold for very large coupling. For small values of λ , it disengages from the $K\bar{K}$ threshold, moving further upwards as a more and more unphysical second-sheet pole. The behaviour of the $f_0(980)$ pole is similar, although now an extremely large value of λ is needed to make it turn it into a bound-state pole below the $\pi\pi$ threshold. This is probably due to repulsion by the σ pole.

5.1.6 Multichannel RSE prediction of radial excitations of $D_{s_0}^*(2317)$ and $D_0^*(2300)$

In our simple RSE description [33] of $D_{s_0}^*(2317)$ and $D_0^*(2300)$, we observed how the lowest confinement states turned into relatively broad ($\Gamma \sim 200 \text{ MeV}$) resonances as poles moving upwards in the complex-

λ	σ	κ	$f_0(980)$	$a_0(980)$
1.5	942 - i794	—	—	—
2.0	798 - i507	—	—	—
2.2	738 - i429	791 - i545	—	1081 - i8.0
2.4	682 - i368	778 - i472	—	1051 - i25
2.6	633 - i319	766 - i409	1041 - i13	1024 - i45
2.8	589 - i278	754 - i355	1028 - i26	998 - i61
3.0	549 - i243	743 - i309	1015 - i35	978 - i60
3.5	468 - i174	717 - i219	976 - i37	896 - i142
4.0	404 - i123	693 - i155	948 - i38	802 - i103
5.0	308 - i50	651 - i69	889 - i34	711 - i40
7.5	216 + i0	610 + i0	752 - i25	632 + i0
10.0	142 + i0	560 + i0	633 - i17	577 + i0

Table 3: Movement of the σ , κ , $f_0(980)$, and $a_0(980)$ poles as the coupling constant λ is varied. Bound states are indicated by “+i0”. Units are MeV for the poles and $\text{GeV}^{-3/2}$ for λ . For further details, see Ref. [95].

energy plane (see Fig. 6). However, in the corresponding energy region, several other meson-meson channels become relevant and may even allow decay to occur. Therefore, a more realistic description at higher energies requires the inclusion of several additional channels. In Ref. [94] such a calculation was carried out, employing Eq. (48) like in Subsubsec. 5.1.5 for $K_0^*(700)$ and $a_0(980)$, but now also including S -wave and D -wave vector-vector (VV) channels, besides the S -wave pseudoscalar-pseudoscalar (PP) channels. In order to allow reliable predictions at higher energies, the parameter λ is calibrated so as to reproduce the $D_{s_0}^*(2317)$ mass, with the parameter a in the $c\bar{s}$ and $c\bar{n}$ cases separately related to the value 3.2 GeV^{-1} found for $K_0^*(700)$ via flavour symmetry of the equations. Moreover, a subthreshold suppression of closed meson-meson channels is included via the same form factor as used in Ref. [95]. For further details, see Ref. [94]. Thus, apart from the $D_{s_0}^*(2317)$ bound-state, the following resonance poles are found (all in MeV):

$$c\bar{s} : (2779 - i233), (2842 - i23.6) ; \quad c\bar{n} : (2174 - i96.4), (2703 - i228), (2737 - i24.0) . \quad (49)$$

Starting with the charmed-strange scalars, the calibrated $D_{s_0}^*(2317)$ pole now originates in the lowest $c\bar{s}$ state at 2545 MeV, as was checked by slowly increasing λ from 0 to its final value. This is to be contrasted with the simple RSE model calculation [33] in which $D_{s_0}^*(2317)$ showed up as a dynamical pole. Conversely, the broad $c\bar{s}$ resonance found here at $(2779 - i233)$ MeV now turns out to be a dynamical state, whereas the nearby resonance at a mass of about 2.79 GeV seen in Ref. [33] corresponded to the ground state of the confinement spectrum but pushed to higher energies (see Fig. 2 in Ref. [33]). As for the $c\bar{s}$ pole at $(2842 - i23.6)$ MeV, it is simply linked to the first radial excitation in the bare spectrum.

Coming now to the $c\bar{n}$ resonances, we see that the $D_0^*(2300)$ pole, with peak mass near 2.19 GeV [94], improves as compared to the values found in Refs. [33, 93], albeit still lying roughly 100 MeV too low as for its real part. This is not very worrying in view of the sensitivity of this pole to details of the model’s parameters, besides the problem of reliably extracting mass and width of a very broad resonance from the data employing Breit-Wigner parametrisations (see our above discussion on this issue). Here, it is worthwhile to note that this resonance is now called $D_0^*(2300)$ by the PDG [10], whereas in prior PDG editions it was designated as $D_0^*(2400)$. The next $c\bar{n}$ resonance, with pole at $(2703 - i228)$ MeV, is the bare confinement ground state yet displaced by the dynamics to much higher energies and acquiring a large imaginary part. This pole can be compared to the one found in Ref. [33] at about 2.64 GeV,

which was also of an intrinsic nature. Finally, the pole at $(2737 - i24.0)$ MeV comes again from the first radial excitation in the bare scalar $c\bar{n}$ spectrum.

Focusing now on the $c\bar{s}$ pole at $(2842 - i23.6)$ MeV, when we presented [99] our above findings, in particular on this D_{s0}^* resonance with a peak mass of 2847 and a width of 47 MeV, we were informed about a new charmed-strange state decaying to DK , called $D_{sJ}(2860)^+$, with mass 2857 MeV and width 47 MeV, observed by the BABAR Collaboration and later published in Ref. [100]. Naturally, we associated our prediction with the BABAR observation. However, a few years later the BABAR Collaboration published [101] new results on $D_{sJ}(2860)$, most notably the observation of D^*K decays, which would exclude a scalar assignment. In a Comment [102] on this paper, we argued on the basis of e.g. branching ratios of 2^3P_2 and 1^3F_2 $c\bar{s}$ states decaying to DK and D^*K , as well as an inevitable mixing of 2^3P_2 with 1^3F_2 , that the observed $D_{sJ}(2860)$ structure may correspond to overlapping $J^P = 0^+$ and $J^P = 2^+$ resonances. Then, in 2012, the LHCb Collaboration again confirmed [103] $D_{sJ}(2860)$, with unknown J^P , as decaying to DK and D^*K , but now with a slightly increased mass of 2866 MeV and a very significantly larger width of 70 MeV. Two years later, the same LHCb Collaboration claimed [104], from a Dalitz-plot analysis, that the $D_{sJ}(2860)$ structure is after all composed of two overlapping resonances, namely a D_{s1}^* $J^P = 1^-$ state with mass 2859 MeV and width 159 MeV and a D_{s3}^* $J^P = 3^-$ state with mass 2860.5 MeV and width 53 MeV. These are the states listed as such in the PDG tables [10]. In Ref. [105] we argued, on the basis of structures resulting from threshold enhancements due to the opening of the DK^* and D^*K^* channels, that the $D_{sJ}(2860)$ bump may hide several much narrower states than the extracted [104] surprisingly broad ($\Gamma = 159$ MeV) D_{s1}^* resonance and possibly with completely different J^P assignments. We shall come back to threshold enhancements in Sec. 8.

5.2 Fully unitary multichannel RSE model in momentum space

The most straightforward way to derive the general RSE expression for the T -matrix describing a system of several quark-antiquark channels coupled to an arbitrary number of meson-meson (MM) channels is by realising that the thus constructed effective meson-meson potential is separable. Namely, we do not consider t -channel exchanges between the two scattered mesons, only s -channel exchanges amounting to towers of bare $q\bar{q}$ states, which resemble [106] Regge propagators. Because of the separability of the MM potential, the Lippmann-Schwinger equation for the T -matrix can be solved in closed form, even for energy-dependent potentials, which is the case here. Graphically we can depict the Born series for the T -matrix as [106]

Here, the first diagram on the right-hand side stands for the effective MM potential V generated by the $MMq\bar{q}$ vertices and the RSE $q\bar{q}$ propagator in the intermediate state. The wiggly lines indicate that this is not just one $q\bar{q}$ state but a whole tower, consisting in principle of an infinite number of $q\bar{q}$ states with the same quantum numbers. The second diagram is the once-iterated V , with an MM loop in between, and so the second term in the Born series. The whole series can be summed up easily, giving rise to a closed-form expression for the T -matrix. The explicit momentum-space formulae for V read [107]

$$V_{ij}^{L_i, L_j}(p_i, p'_j; E) = \lambda^2 j_{L_i}^i(p_i a) \mathcal{R}_{ij}(E) j_{L_j}^j(p'_j a), \quad (50)$$

$$\mathcal{R}_{ij}(E) = \sum_{i_{q\bar{q}}=1}^{N_{q\bar{q}}} \sum_{n=0}^{\infty} \frac{g_{(i_{q\bar{q}}, n)}^i g_{(i_{q\bar{q}}, n)}^j}{E - E_n^{(i_{q\bar{q}})}}, \quad (51)$$

where the RSE propagator \mathcal{R} contains an infinite tower of s -channel bare $q\bar{q}$ states, corresponding to the discrete spectrum of an arbitrary confining potential. Here, $E_n^{(i_{q\bar{q}})}$ is the energy level of the n -th recurrence in the $i_{q\bar{q}}$ -th $q\bar{q}$ channel, with $N_{q\bar{q}}$ the number of $q\bar{q}$ channels having the same quantum numbers, and $g_{(i_{q\bar{q}},n)}^i$ is the corresponding coupling to the i -th MM channel. Furthermore, in Eq. (50), λ is the overall coupling constant for 3P_0 decay (now with dimensions $\text{GeV}^{1/2}$), and $j_{L_i}^i(p_i)$ and p_i are the L_i -th order spherical Bessel function and the (relativistically defined) off-shell relative momentum in MM channel i , respectively. The spherical Bessel function originates in our string-breaking picture of OZI-allowed decay, being just the Fourier transform of a spherical delta-shell of radius a . The channel couplings $g_{(i_{q\bar{q}},n)}^i$ in Eq. (51) are computed following the formalism developed in Ref. [76], namely from overlaps of HO wave functions for the original $q\bar{q}$ pair, the created 3P_0 pair, and the quark-antiquark states corresponding to the outgoing two mesons. In most cases, this method produces the same couplings for ground-state mesons as the usual point-particle approaches, but also provides a clear prescription for excited mesons, with the additional advantage of always resulting in a finite number of non-vanishing couplings. Because of their fast decrease for increasing radial quantum number n , practical convergence of the infinite sum in Eq. (51) is achieved by truncating it after at most 20 terms.

With this effective energy-dependent MM potential, the T -matrix reads explicitly [107]

$$T_{ij}^{(L_i, L_j)}(p_i, p'_j; E) = -2a\lambda^2 \sqrt{\mu_i p_i} j_{L_i}^i(p_i a) \times \sum_{m=1}^N \mathcal{R}_{im} \left\{ [\mathbb{1} - \Omega \mathcal{R}]^{-1} \right\}_{mj} j_{L_j}^j(p'_j a) \sqrt{\mu_j p'_j}, \quad (52)$$

with the loop function

$$\Omega_{ij}(k_j) = -2ia\lambda^2 \mu_j k_j j_{L_j}^j(k_j a) h_{L_j}^{(1)j}(k_j a) \delta_{ij}, \quad (53)$$

where $h_{L_j}^{(1)j}(k_j a)$ is the spherical Hankel function of the first kind, k_j and μ_j are the on-shell relative momentum and reduced mass in MM channel j , respectively, and the matrix $\mathcal{R}(E)$ is given by Eq. (51). Note that no regularisation is needed in this all-orders model, since the Bessel functions at the vertices make the meson loops finite. The fully on-shell and unitary S -matrix is then given by

$$S_{ij}^{(L_i, L_j)}(k_i, k_j; E) = \delta_{ij} + 2iT_{ij}^{(L_i, L_j)}(k_i, k_j; E). \quad (54)$$

This RSE S -matrix can be used to describe a large variety of non-exotic mesons coupling to several open and closed two-meson decay channels, even when some of these involve resonances themselves, by applying a mathematical procedure (see Appendix B of Ref. [36]) to re-unitarise the resulting non-unitary S -matrix.

6 Understanding the charmed axial-vector mesons and χ_{c1} (3872)

6.1 Revisiting D_{s1} (2460), D_{s1} (2536), D_1 (2430), and D_1 (2420)

When describing the charmed axial-vector mesons with the basic RSE model of Subsubsec. 5.1.3, we were limited to only one quark-antiquark channel. We then argued that diagonalising a simple Hamiltonian for two degenerate $q\bar{q}$ states coupled in the same way to one continuum channel would give rise to one eigensolution that decouples and an orthogonal one that fully couples. This allowed to study [98] D_{s1} (2460) and D_1 (2430) by using Eq. (43). Here we review results [64] obtained by employing the full RSE formalism as given in Eqs. (51–53). So in both the $c\bar{s}$ and $c\bar{n}$ cases, we take two $q\bar{q}$ channels with $\ell = 1$, viz. for the 3P_1 and 1P_1 spectroscopic states, which are degenerate in energy without explicit spin-orbit interactions.

Taking for the bare $q\bar{q}$ state the usual values of quark masses and HO radial levels from Ref. [9], we optimise λ and a for the broad $D_{s1}(2430)$ resonance, whose pole is extremely sensitive to especially the decay radius (see below). In the $c\bar{s}$ case, these λ and a values are then scaled with the reduced quark masses, as successfully done before in Refs. [93, 94] for the charmed scalar mesons. So we have only two relatively free parameters, albeit within the ranges expected [64] from previous work, to fit the four masses as well as the four widths of the ground-state charmed axial-vectors. The corresponding pole positions [64] are given in Table 4, together with the predictions for the first radial excitations. We

Quark Content	Radial Excitation	Pole in MeV
$c\bar{q}$	0	$2439 - i \times 3.5$
$c\bar{q}$	0	$2430 - i \times 191$
$c\bar{s}$	0	$2540 - i \times 0.7$
$c\bar{s}$	0	$2452 + i \times 0.0$
$c\bar{q}$	1	$2814 - i \times 7.8$
$c\bar{q}$	1	$2754 - i \times 47.2$
$c\bar{s}$	1	$2915 - i \times 6.7$
$c\bar{s}$	1	$2862 - i \times 25.7$

Table 4: Poles of ground-state ($n=0$) and first radially excited ($n=1$) charmed axial-vector mesons. Parameters: $\lambda = 1.30$ (1.19) $\text{GeV}^{1/2}$ and $r_0 = 3.40$ (3.12) GeV^{-1} for $c\bar{q}$ ($c\bar{s}$) states. For further details, see Ref. [64].

immediately see that the dynamics of the RSE coupled-channel equations generates the right mixture of the included 3P_1 and 1P_1 $q\bar{q}$ components, which is simply imposed in other approaches (see discussion in Ref. [64]). Thus, on the one hand we end up with two resonances, i.e., $D_{s1}(2536)$ and $D_1(2420)$, that are much narrower than what could be expected from their S -wave decays and available phase space, becoming quasi-bound states in the continuum. On the other hand, we find a strongly coupling state, i.e., $D_{s1}(2460)$, shifting so much downwards that it settles as a bound-state pole on the real axis, below the D^*K threshold, in much the same way as $D_{s0}^*(2317)$ with respect to the DK threshold. Finally, the other strongly coupling state, i.e., $D_1(2430)$, becomes a very broad resonance and in a highly non-linear fashion, with its real part first decreasing and then increasing again, at least for the optimum parameter values. The corresponding pole trajectory as a function of λ is depicted in Fig. 7, together with those of $D_{s1}(2460)$ and $D_{s1}(2536)$. The behaviour of the $D_1(2430)$ pole is again related to the Adler-type zero just below the $D^*\pi$ threshold, which prevents the latter channel from attracting the pole so as to become a bound state. To conclude this topic, it is most remarkable that with only two quite restricted parameters the very unusual pattern of masses and widths of the charmed axial-vector mesons can be reproduced, with rather insignificant deviations from the experimentally observed [10] values. This lends further support to the predictive power of the RSE model.

6.2 Describing $\chi_{c1}(3872)$ in momentum and coordinate space

Hundreds of papers have been published on the axial-vector charmonium-like state $\chi_{c1}(3872)$, after its first observation [35] in 2003 by the Belle Collaboration, having been called $X(3872)$ for many years. The main reason for this excitement is the extreme closeness of its mass to the $\bar{D}^{*0}D^0$ threshold, now within 0.01 MeV according to the PDG average [10]. Moreover, if confirmed as a $J^{PC} = 1^{++} c\bar{c}$ state, its mass would be about 80 MeV lower than in the GI [2] and similar static quark models, which is much more than any other discrepancy found for established charmonium states in most of such models. Another coincidence is that the $\chi_{c1}(3872)$ mass lies less than 1 MeV below the central $\rho^0 J/\psi$ threshold, which is one of the main observed hadronic decay modes, besides e.g. $\omega J/\psi$ and $\bar{D}^{*0}D^0$. Since the $\rho^0 J/\psi$ decay

of $\chi_{c1}(3872)$ is both isospin violating and OZI-forbidden, its contribution to the width is small despite the available phase space owing to the large ρ width. For a summary of different model approaches to $\chi_{c1}(3872)$, see the more general review on hidden-charm pentaquark and tetraquark states [12].

Next we shall briefly review three different model calculation of $\chi_{c1}(3872)$, with each one focusing on specific aspects.

6.3 RSE modelling of $\chi_{c1}(3872)$

In Ref. [36] the $\chi_{c1}(3872)$ state was studied by employing the full RSE formalism, with an emphasis on the behaviour of the $2^3P_1 c\bar{c}$ pole and $\bar{D}^{*0}D^0$ amplitude in the vicinity of the latter threshold, and also on the effect of the OZI-forbidden decays $\rho^0 J/\psi$ and $\omega J/\psi$. So the goal was not to predict the precise mass of $\chi_{c1}(3872)$, which would anyhow be impossible due to the needed fine-tuning of parameters, but rather to demonstrate that this meson can be understood as a strongly unitarised 2^3P_1 charmonium state. Thus, the bare RSE $J^{PC} = 1^{++}$ spectrum is coupled to the OZI-allowed vector-pseudoscalar channels $\bar{D}^{*0}D^0$, $D^{*\mp}D^\pm$, and $D_s^{*\mp}D_s^\pm$, allowed in both S - and D -waves, as well as the charge-averaged vector-vector channel \bar{D}^*D^* in D -waves only. Furthermore, the already mentioned OZI-forbidden channels $\rho^0 J/\psi$ (also isospin violating) and $\omega J/\psi$ are coupled as well. Upon increasing the overall coupling λ , the bare $2^3P_1 c\bar{c}$ pole at 3979 MeV (for $m_c = 1562$ MeV and HO frequency $\omega = 190$ MeV [9]) moves about 100 MeV downwards in the complex-energy plane, crossing the $\rho^0 J/\psi$ and $\bar{D}^{*0}D^0$ thresholds as depicted on the left-hand plot of Fig. 8 for different sets of parameters. Note that in this calculation the $\chi_{c1}(3872)$ pole will not end up as a bound state on the real axis below the $\bar{D}^{*0}D^0$ threshold, because the $\rho^0 J/\psi$ channel is included with a complex ρ^0 mass in order to mimic the broadness of this resonance. Nevertheless, the resulting S -matrix has been made unitary again with an empirical yet mathematical transformation [36] using the fact that S is always a symmetric matrix. For further details, see Ref. [36].

The pole trajectories as well as the amplitudes shown in Fig. 8 support the interpretation of $\chi_{c1}(3872)$

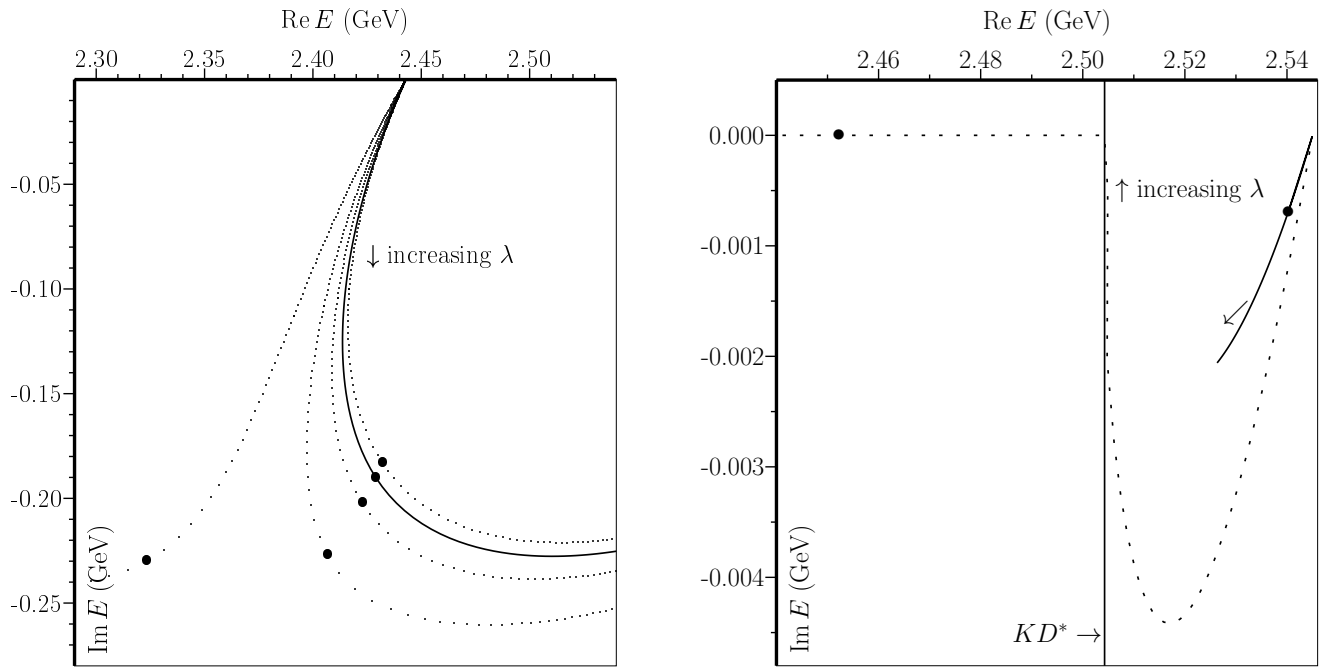


Figure 7: Left-hand plot: $D_1(2430)$ pole trajectories as a function of λ , for $r = 3.2, 3.3, 3.4,$ and 3.5 GeV^{-1} (left to right); solid curve and bullets correspond to $r = 3.4$ GeV^{-1} and $\lambda = 1.30$, respectively. Right-hand plot: $D_{s1}(2460)$ (left) and $D_{s1}(2536)$ (right) pole trajectories as a function of λ for $r = 3.4$ GeV^{-1} ; bullets correspond to $\lambda = 1.19$ (also see text and Ref. [64]).

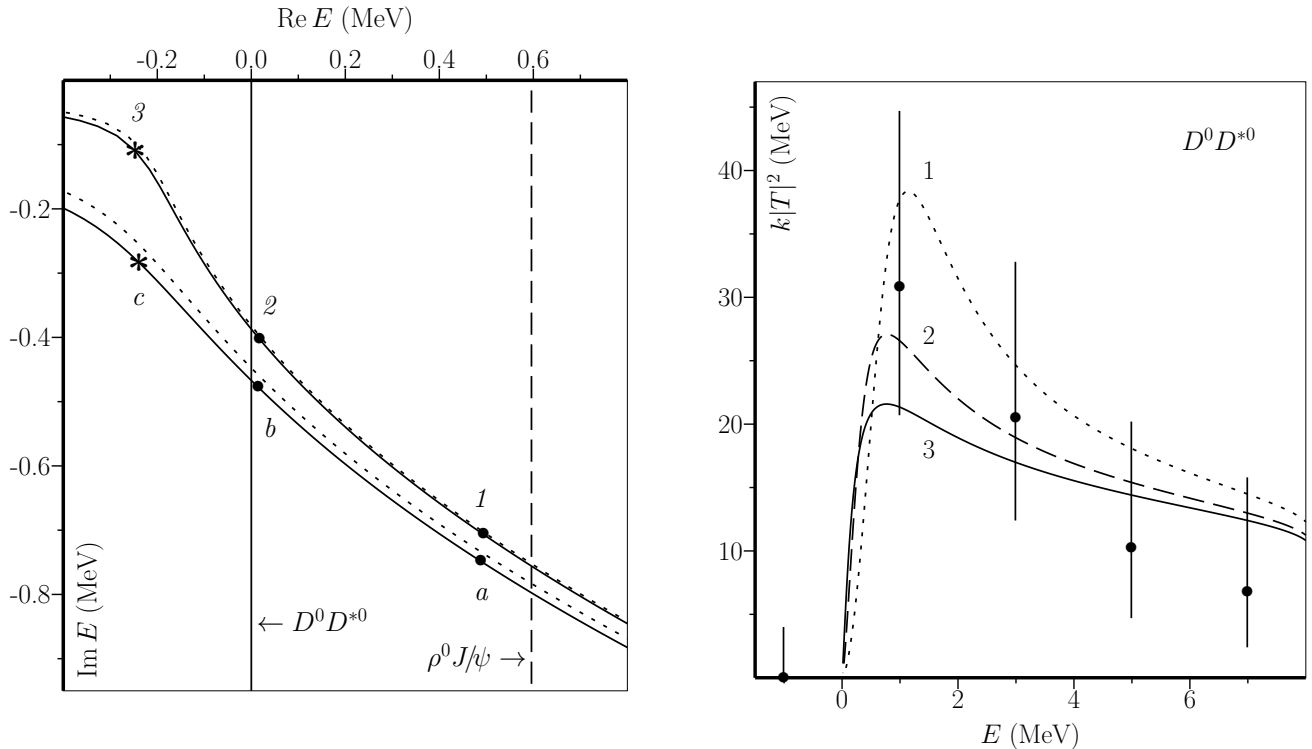


Figure 8: Left: Pole trajectories of $\chi_{c1}(3872)$ as a function of overall coupling λ ; pole positions 1, 2, 3 and a, b, c for two different values of OZI-forbidden coupling (see text); dotted curves - different decay radius. Right: corresponding (1, 2, 3) elastic $\bar{D}^{*0} D^0$ amplitudes with arbitrarily normalised data. See Ref. [36] for more details.

as a regular 2^3P_1 $c\bar{c}$ state, but strongly influenced by the S -wave $\bar{D}^{*0} D^0$ decay channel and — to a lesser extent — by the OZI- and isospin-violating $\rho^0 J/\psi$ channel.

6.4 Coordinate-space modelling of $\chi_{c1}(3872)$ wave function and pole

In Ref. [37] the simple coordinate-space model of Ref. [108] was employed to find out whether it is reasonable to call $\chi_{c1}(3872)$ a $\bar{D}^{*0} D^0$ molecule. Thus, a harmonically confined 3P_1 $c\bar{c}$ state is coupled to the $\bar{D}^{*0} D^0$ channel through a delta-shell interaction at a radius a and with coupling constant g , similarly to the RSE modelling. The advantage of the r -space formulation is that one can easily obtain the bound-state wave function for a pole on the real axis below threshold. One can then study how variations in the binding energy with respect to this threshold affects the $c\bar{c}$ and $\bar{D}^{*0} D^0$ wave-function components, in particular their relative probabilities, besides computing the r.m.s. radius of the system in the different situations.

As one of the main results, we find that for the then experimentally reported average binding energy of 0.16 MeV, the $c\bar{c}$ probability varies as 7.48%–11.18% for $a = 2.0$ – 3.0 GeV $^{-1}$, and the corresponding $\bar{D}^{*0} D^0$ probability as 92.52%–88.82%. Nevertheless, the $c\bar{c}$ and $\bar{D}^{*0} D^0$ wave functions are of comparable size in the inner region, with the $\bar{D}^{*0} D^0$ probability only being so large because of its very long tail, owing to the small binding energy. As for the r.m.s. radius, it is quite stable at almost 8 fm for either value of a and again a binding of 0.16 MeV. For the present PDG value of the binding energy, the $\bar{D}^{*0} D^0$ probability would be larger than 99% and the r.m.s. radius of the order of 100 fm, but the two wave-function components would still be of similar size in the interior. For further variations, see Ref. [37]. A more complete study of the $\chi_{c1}(3872)$ wave function will be presented in Subsec. 6.5.

The coordinate-space formalism also allows to search for S -matrix poles and Fig. 9 shows how a

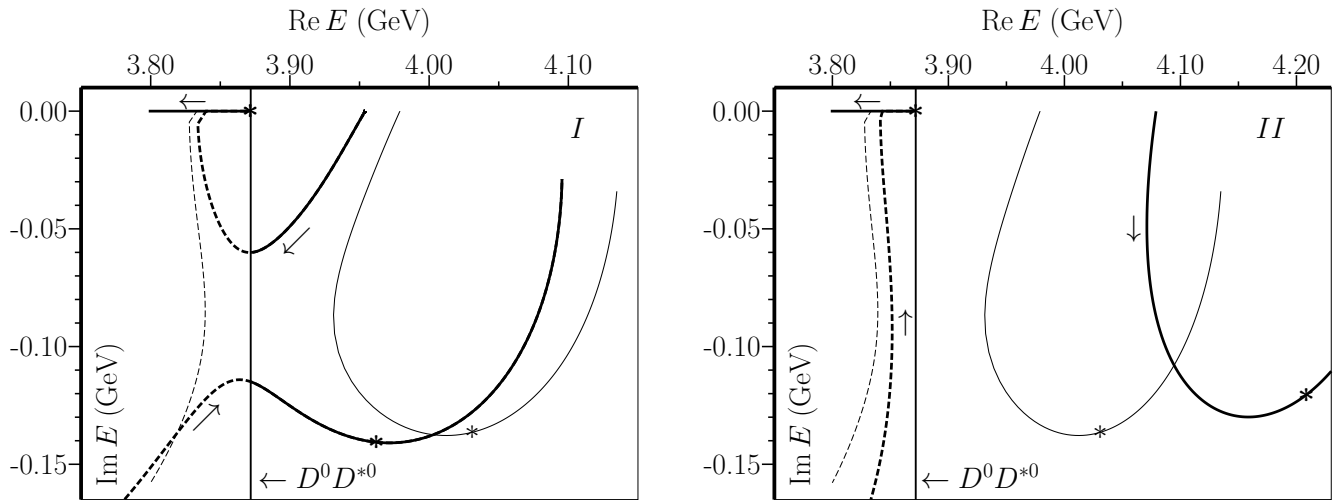


Figure 9: Left: $\chi_{c1}(3872)$ pole trajectories for 2^3P_1 bare $c\bar{c}$ mass at 3954 MeV (boldface) and 3979 MeV (non-boldface). Right: same but now for bare mass at 4079 MeV (boldface) and again 3979 MeV (non-boldface). Also see text and Ref. [37].

small change in the energy of the bare state can affect the pole trajectories. If we take the bare state at 3979 MeV just like in Ref. [36], the $\chi_{c1}(3872)$ pole now turns out to be dynamical instead of intrinsic (cf. non-boldface dashed trajectories on both plots). At first sight, this qualitative difference might be due to our much simpler modelling here, with only one meson-meson channel. However, if we lower the 2^3P_1 bare $c\bar{c}$ mass by only 25 MeV to 3954 MeV, which is almost exactly the value predicted in the GI model [2], the $\chi_{c1}(3872)$ pole trajectory suddenly connects to this bare energy level and so becomes of an intrinsic nature (upper boldface trajectory on left-hand plot). The corresponding dynamical pole then moves close to the intrinsic pole in the standard situation (lower boldface trajectory and non-boldface solid trajectory, respectively, on the same plot). So we witness a crossover of poles for small parameter variations, just as in the case of $D_{s0}^*(2317)$ [96] and discussed above. We must conclude that also for $\chi_{c1}(3872)$ its assignment as either a dynamical or intrinsic state is very problematic. The right-hand plot in Fig. 9 displays the situation when the 2^3P_1 bare $c\bar{c}$ mass is increased by 100 MeV. Although this does not represent a very likely scenario compared to other models, it does show how insensitive the $\chi_{c1}(3872)$ pole is to very significant changes in the confinement spectrum (cf. the non-bold and bold dashed trajectories on the right-hand plot). So our findings appear to be quite model independent.

From the studied $\chi_{c1}(3872)$ wave function and pole trajectories we conclude [37] that this enigmatic meson is not a $\bar{D}^{*0}D^0$ molecule.

6.5 Multichannel coordinate-space modelling of $\chi_{c1}(3872)$

In Ref. [38] electromagnetic transition rates of $\chi_{c1}(3872)$ to J/ψ and $\psi(2S)$ were calculated in a multichannel coordinate-space model like the one employed in Refs. [8, 109], which is a generalisation of the model used in Subsec. 6.4. In order to ensure the derivation of realistic wave functions for the involved three charmonium states, several open-charm decay channels that should acquire appreciable probabilities in the total wave function are coupled to the $c\bar{c}$ channel(s) in each case. Using an abbreviated notation in which D represents D^0 , D^+ , or D_s^+ , we get for the vectors J/ψ and $\psi(2S)$ the channels $\bar{D}D$, \bar{D}^*D , and \bar{D}^*D^* coupling in P -waves to the 3S_1 $c\bar{c}$ wave-function component, and \bar{D}^*D^* coupling only in an F -wave to the 3D_1 $c\bar{c}$ component. In the $\chi_{c1}(3872)$ case, we must couple the $\bar{D}^{*0}D^0$ and $D^{*\mp}D^\pm$ channels separately, with the correct mass splitting and relative couplings, in view of the closeness of the pole to the former threshold. Moreover, there is now only one $c\bar{c}$ component, viz. 3P_1 , to which we couple the mentioned $\bar{D}^{*0}D^0$ and $D^{*\mp}D^\pm$ channels, as well as $D_s^{*\mp}D_s^\pm$, in both S - and D -waves, and

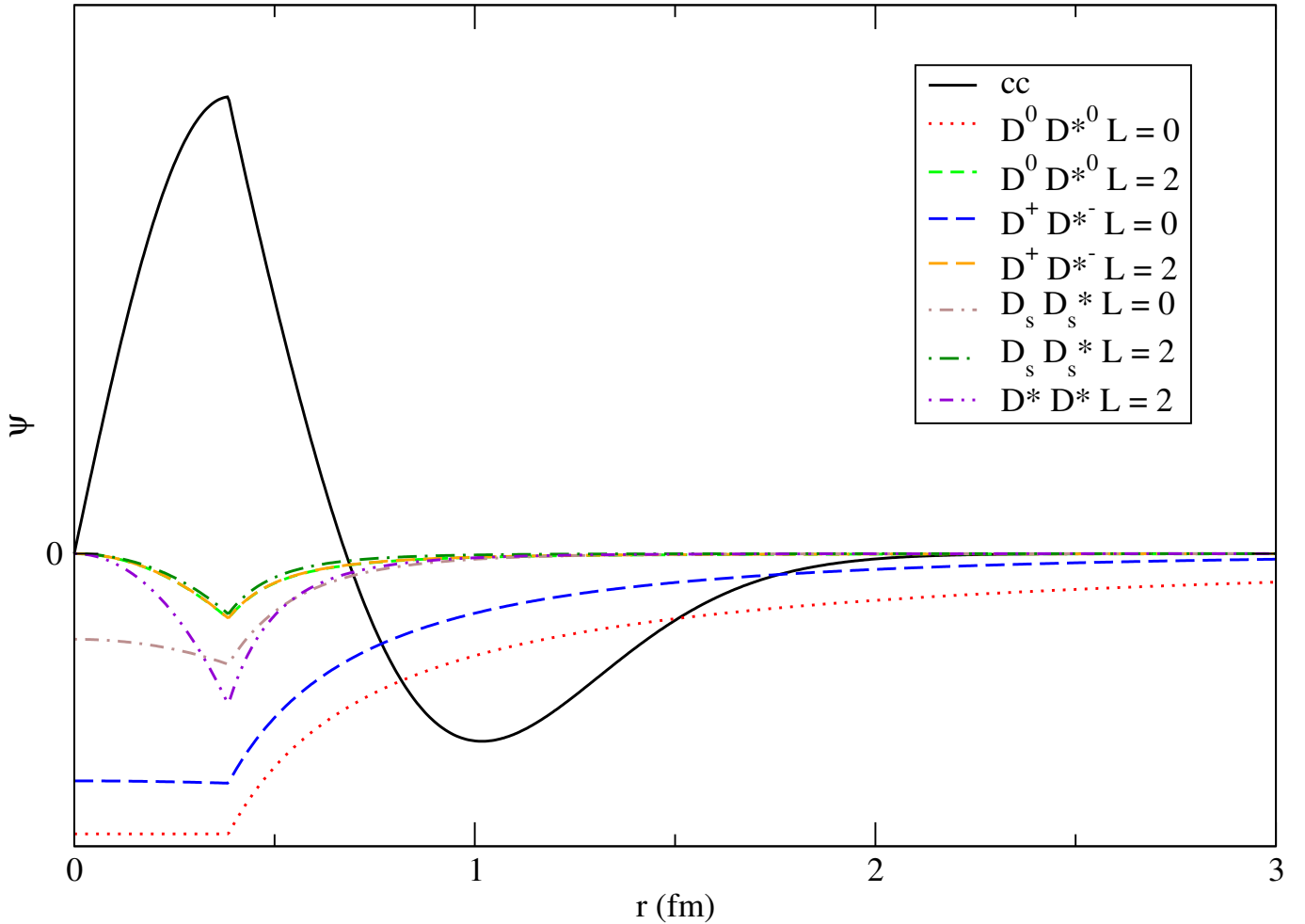


Figure 10: Radial wave function of $\chi_{c1}(3872)$; see text and Ref. [38].

finally $\bar{D}^* D^*$ (with $D = D^0, D^\pm, D_s$) only in D -waves.

The parameters λ and a are fixed such that the masses of the three charmonia are exactly reproduced. This can be done with the same a , but two λ values are needed, differing by about 15% between the two vectors and the axial-vector. This is perfectly reasonable, as the included meson-meson channels have different orbital angular momenta (also see the discussion in Ref. [38]). The resulting multicomponent radial wave function of $\chi_{c1}(3872)$ is depicted in Fig. 10. For clarity, the meson-meson components are plotted with a negative sign. We see that now the $c\bar{c}$ channel is clearly dominant in the interior region, followed by the S -wave channels $\bar{D}^{*0} D^0$ and $D^{*\mp} D^\pm$. This is logical, since their thresholds lie much closer to the $\chi_{c1}(3872)$ mass and so are less suppressed kinematically.

With the $\chi_{c1}(3872)$ wave function at hand, we can again compute the r.m.s. radius of the system as well as the $c\bar{c}$ and $\bar{D}^{*0} D^0$ probabilities, which come out at 6.57 fm, 26.76%, and 65.03%, respectively. The at first sight surprisingly large $c\bar{c}$ percentage as compared to the value found in the simple model of Subsec. 6.4 can be understood by realising that all channels contribute to the negative mass shift of the bare 2^3P_1 $c\bar{c}$ state at 3979 MeV, and in particular the now also quite nearby $D^{*\mp} D^\pm$ threshold. This reduces the relative importance of the $\bar{D}^{*0} D^0$ component in the wave function, which is precisely the one with by far the longest tail, and so its probability is significantly reduced. This benefits primarily the $c\bar{c}$ component, which is most prominent in the interior region. For further details, see Ref. [38].

After also solving for the radial wave functions of J/ψ and $\psi(2S)$, the formalism developed in

Ref. [110] allows to compute [38] the electromagnetic branching ratio

$$\mathcal{R}_{\gamma\psi} = \frac{\Gamma(X(3872) \rightarrow \gamma\psi(2S))}{\Gamma(X(3872) \rightarrow \gamma J/\psi)} = 1.17. \quad (55)$$

This value is too low as compared to the PDG [10] average of 2.6 ± 0.6 , but a huge improvement due to unitarisation as compared to a static calculation with the same confinement mechanism. For further discussion on possible theoretical and experimental improvements, see Ref. [38].

This concludes our extensive discussion of this fascinating meson. We are very well aware that there are many other descriptions of $\chi_{c1}(3872)$, as e.g. a dynamical pole in a coupled-channel model [111], a purely molecular state from t -channel meson exchanges [112], or using effective field theory [113] (see, however, Ref. [114]). For many more references, see Ref. [12]. Nevertheless, we believe a unitarised quark-model formulation is the most promising one in the context of general meson spectroscopy. The lattice appears to confirm this (see Sec. 7).

7 Recent Lattice Results on Meson Resonances

Lattice QCD is a non-perturbative approach to the non-Abelian gauge theory of quarks and gluons, which uses Monte-Carlo techniques to numerically simulate gauge configurations in discretised Euclidean space-time. Originally, quarks were taken as static sources of the colour fields, in view of the enormous numerical effort needed in treating also the quarks dynamically, i.e., via a fermion determinant. This approximative handling of the theory is generally called quenched lattice QCD. However, present-day computer power allows to go beyond the quenched approximation, doing realistic calculations of mesons in 3+1 dimensions. Now, in unquenched lattice QCD, effects of $q\bar{q}$ loops are fully taken into account, by including dynamical quark degrees of freedom. Nevertheless, allowing for virtual $q\bar{q}$ pairs does not paint a complete picture, as the created quark and antiquark may recombine with the original (anti)quarks so as to form two new colourless mesons. Even if the mass of the initial meson is smaller than the sum of the new mesons' masses, so that no real decay can take place, the corresponding virtual processes via meson-meson loops will contribute to the total mass. This is expected to be all the more significant according as the decay-threshold energy lies closer to the original meson's mass. On the other hand, if the latter mass is above threshold, the meson actually becomes a resonance, whose properties are determined by S -matrix analyticity and unitarity.

In recent years, different lattice groups employing Lüscher's method [115] or extensions thereof (see Refs. [116, 117] for a list of references) have managed to extract unitary scattering phase shifts and/or resonance properties from unquenched finite-volume simulations that include meson-meson or meson-baryon interpolating fields, besides the usual $q\bar{q}$ or qqq ones, respectively (see Ref. [116] for a recent review). Some of these works on mesonic resonances [10] show that sizeable mass shifts may result from unitarisation, even when analytically continued to underneath the lowest strong-decay threshold. On the other hand, dynamical resonances, not present in the quenched meson spectrum, may show up as well. Finally, there is even an indication that radial level spacings can be affected considerably. In the following we shall briefly review a typical selection of such recent lattice applications.

7.1 $\chi_{c1}(3872)$ as a $\bar{c}c + \bar{D}^*D$ state

In Ref. [118] a lattice study of charmonium-like mesons with $J^{PC} = 1^{++}$ was performed, considering three types of quark contents, viz. $\bar{c}c\bar{d}u$, $\bar{c}c(\bar{u}u + \bar{d}d)$, and $\bar{c}c\bar{s}s$, where the latter two can mix with $\bar{c}c$. The corresponding simulation with $N_f = 2$ and $m_\pi = 266$ MeV aimed at finding possible signatures of exotic tetraquark states. A large basis of $\bar{c}c$, two-meson, and diquark-antidiquark interpolating fields was employed, with diquarks in both antitriplet and sextet colour representations. Thus, a lattice

candidate for $X(3872)$ (alias $\chi_{c1}(3872)$) with $I = 0$ is observed very close to the experimental state, but only if both $\bar{c}c$ and \bar{D}^*D interpolators are included. The candidate is not found if diquark-antidiquark and \bar{D}^*D are used without a $\bar{c}c$ interpolating field. Furthermore, no candidate for a neutral or charged $X(3872)$ or any other exotic candidates are found in the $I = 1$ channel. Also no signatures of exotic $\bar{c}c\bar{s}s$ candidates are found below 4.2 GeV, such as $Y(4140)$ (alias $X(4140)$) or $\chi_{c1}(4140)$ [10].

Besides these very significant results concerning $\chi_{c1}(3872)$ in particular, it is worthwhile to pay attention to the following quote from Ref. [118]:

“In the physical world with $N_c = 3$, it is argued that tetraquarks could exist at subleading orders [119] of large N_c QCD. However, in the presence of the leading order two-meson terms, one should take caution in interpreting the nature of the levels purely based on their overlap factors onto various four-quark interpolators.”

The latter warning about not jumping to conclusions concerning evidence of tetraquarks also applies to other approaches involving four-quark components in the employed formalism. For a discussion focusing on the light scalar mesons, see Ref. [62].

7.2 $D_{s0}^*(2317)$ as a $c\bar{s} + DK$ state

In the lattice calculation of Ref. [26], the charmed-strange scalar meson $D_{s0}^*(2317)$ is found 37 ± 17 MeV below the DK threshold, in a simulation of the $J^P = 0^+$ channel using, for the first time, both DK and $\bar{s}c$ interpolating fields. The simulation is done on $N_f = 2 + 1$ gauge configurations with $m_\pi \simeq 156$ MeV, and the resulting $M_{D_{s0}^*} - \frac{1}{4}(M_{D_s} + 3M_{D_s^*}) = (266 \pm 16)$ MeV is close to the experimental value (241.5 ± 0.8) MeV. The energy level related to the scalar meson is accompanied by additional discrete levels due to DK scattering states. The levels near threshold lead to the negative DK scattering length $a_0 = -(1.33 \pm 0.20)$ fm that indicates the presence of a state below threshold.

These results were published with more details in Ref. [120], with additionally a lattice confirmation of the $J^P = 1^+$ charmed-strange meson $D_{s1}(2460)$ as a unitarised $\bar{s}c$ state below the D^*K threshold, similarly to $D_{s0}^*(2317)$ below the DK threshold. (Also see Ref. [121] for charmed-light mesons with $J^P = 0^+$ or $J^P = 1^+$.) Very recently, another lattice collaboration [27], by including quark-antiquark, tetraquark, and two-meson interpolators in their computation, obtained essentially the same results for $D_{s0}^*(2317)$, while even concluding:

“The coupling to the tetraquark interpolating fields is essentially zero, rendering a tetraquark interpretation of the $D_{s0}^(2317)$ meson rather unlikely.”*

7.3 Light scalar mesons as $q\bar{q}$ states with meson-meson components

The light scalar mesons $f_0(500)$, $f_0(980)$, $K_0^*(700)$, and $a_0(980)$ were studied by the same lattice collaboration in Refs. [117, 122–124], respectively. In the $f_0(500)$ (σ) case, two types of interpolating fields were included in the simulation [122], namely single-meson-like operators resembling $q\bar{q}$ constructions of both $(u\bar{u} + d\bar{d})$ and $s\bar{s}$ flavours, as well as operators resembling a pair of pions $\pi\pi$ with definite relative and total momentum, projected onto isospin $I = 0$. The calculations were done for two u, d quark masses, corresponding to pion masses of 261 and 391 MeV, respectively. The resulting amplitudes are described in terms of a σ meson which evolves from a bound state below the $\pi\pi$ threshold at the heavier quark mass to a broad resonance at the lighter quark mass. A precise determination of the σ 's pole position is not possible yet, because the employed parametrisations, while maintaining elastic unitarity, do not necessarily respect the analytical constraints placed on them by causality and crossing symmetry, apart from the need to extrapolate to the physical pion mass. So for future simulations, adaptation dispersive approaches and the use of smaller u, d quark masses are planned [122].

In Ref. [117] the first lattice-QCD study of S -wave and D -wave scattering in the coupled isoscalar $\pi\pi$, $K\bar{K}$, and $\eta\eta$ channels was carried out from discrete finite-volume spectra computed on lattices for a light-quark mass corresponding to $m_\pi \sim 391$ MeV. In the $J^P = 0^+$ sector analogues of the experimental σ and $f_0(980)$ states are found, where the σ appears as a stable bound-state below the $\pi\pi$ threshold and $f_0(980)$ manifests itself as a dip in the $\pi\pi$ cross section in the vicinity of the $K\bar{K}$ threshold, as also seen in experiment. For $J^P = 2^+$ two states resembling $f_2(1270)$ and $f_2'(1525)$, observed as narrow peaks, with the lighter state dominantly decaying to $\pi\pi$ and the heavier state to $K\bar{K}$, in agreement with experiment [10]. The presence of all these states is determined rigorously by finding the pole singularity content of scattering amplitudes, and their couplings to decay channels are established using the residues of the poles. As an extension of Lüscher's method [115], an approach which has proven successful proceeds by parametrising the energy dependence of coupled-channel amplitudes and fitting a large set of energy levels, from one or more lattice volumes, within a kinematic window. A dense spectrum of energy levels will tightly constrain the possible energy dependence of the scattering t -matrix, and to acquire as many energy levels as possible, systems with various total momenta may be considered. For further details and references, see Ref. [117].

Coupled-channel πK and ηK scattering amplitudes for $J^P = 0^+$, 1^- , and 2^+ were determined in Ref. [123] by studying the finite-volume energy spectra obtained from dynamical lattice-QCD calculations. Using a large basis of interpolating operators, including both those resembling a $q\bar{q}$ construction and those resembling a pair of mesons with definite relative momentum, a reliable excited-state spectrum can be obtained. Working at $m_\pi = 391$ MeV, a gradual increase in the $J^P = 0^+$ πK phase shift is found, which may be identified with a broad scalar resonance that couples strongly to πK and weakly to ηK . The low-energy behaviour of this amplitude suggests a virtual bound state that may be related to the κ ($K_0^*(700)$) resonance. At higher energies, a broad resonance is found that couples dominantly to πK and not ηK , with a pole mass of $m = (1370 \pm 45)$ MeV and width of $\Gamma = (530 \pm 45)$ MeV. This should represent the $K_0^*(1430)$ [10] resonance, although the here found width is clearly too large. The (approximate) decoupling of the ηK channel is in agreement with what was observed in Ref. [88]. For a more definite determination of the $K_0^*(700)$ resonance, the use of considerably smaller pion masses will be necessary.

In Ref. [124] the first lattice-QCD calculation of coupled-channel meson-meson scattering in the $I^G = 1^-$ sector was carried out, with the channels $\pi\eta$, $K\bar{K}$, and $\pi\eta'$, for a pion mass of 391 MeV and a strange-quark mass approximately tuned to its physical value. The energy dependence of the S -matrix is determined and a prominent cusp-like structure in the S -wave $\pi\eta \rightarrow \pi\eta$ amplitude close to the $K\bar{K}$ threshold is observed, coupled with a rapid turn-on of amplitudes leading to the $K\bar{K}$ final state. This behaviour is traced to an $a_0(980)$ -like resonance, strongly coupled to both $\pi\eta$ and $K\bar{K}$, which is identified with a pole in the complex energy plane, appearing on only a single unphysical Riemann sheet. Explicit lattice calculations at a smaller quark mass will be needed in order to confirm an $a_0(980)$ resonance in agreement with experiment.

7.4 $K^*(1410)$ and the issue of radial splittings

As already shown above in our discussion of the GI model [2], the $K^*(1410)$ first radial excitation of lowest strange vector meson $K^*(892)$ is one of the many examples of a considerably smaller radial mass splitting than predicted in the GI and similar static quark models. This makes any possible lattice prediction of the $K^*(1410)$ all the more interesting. Now, in Ref. [31] excited states in unquenched lattice QCD were computed, though without meson-meson interpolators, with the resulting bound-state spectra for strange and isovector mesons shown in Fig. 11. In both cases, the radial splitting between the ground-state vector meson and its first radial excitation is much too large, even with the proviso that the used pion mass is around 390 MeV and that the states have been extracted in a finite volume. Therefore, it is most opportune to check similar predictions by a different lattice group.

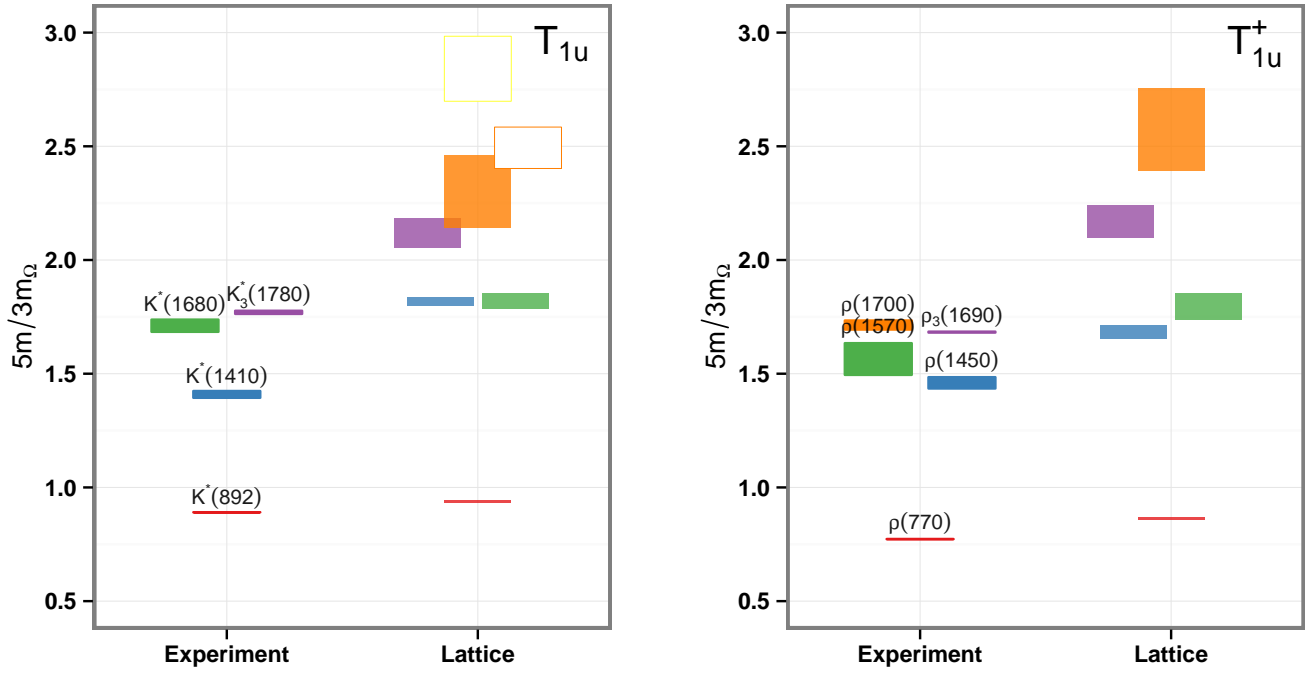


Figure 11: Left: excited strange-meson masses, as ratios with respect to $3/5$ of the Ω baryon mass m_Ω , for stationary states expected to evolve into the single-meson resonances in infinite volume. The height of each box indicates its statistical uncertainty. The hollow boxes at the top show higher-lying states extracted with less certainty due to the expected presence of lower-lying two-meson states that have not been taken into account. Right: the analogous plot for the isovector channel, the superscript in T_{1u}^+ indicating G -parity. See Ref. [31] for further details.

In the unquenched lattice calculation of Refs. [126, 127], yet again without including two-meson interpolators, results were presented for radial excitation spectra of light and strange mesons as well as positive- and negative-parity baryons. On the left-hand plot of Fig. 12 we display the corresponding radial excitations of, among other strange mesons, $K^*(892)$ and also two isoscalar mesons. We again see a too large first radial splitting in the isodoublet vector case, i.e., roughly 200 MeV more than in experiment, though not as huge as in Ref. [31]. The big surprise, though, we see on the right-hand plot

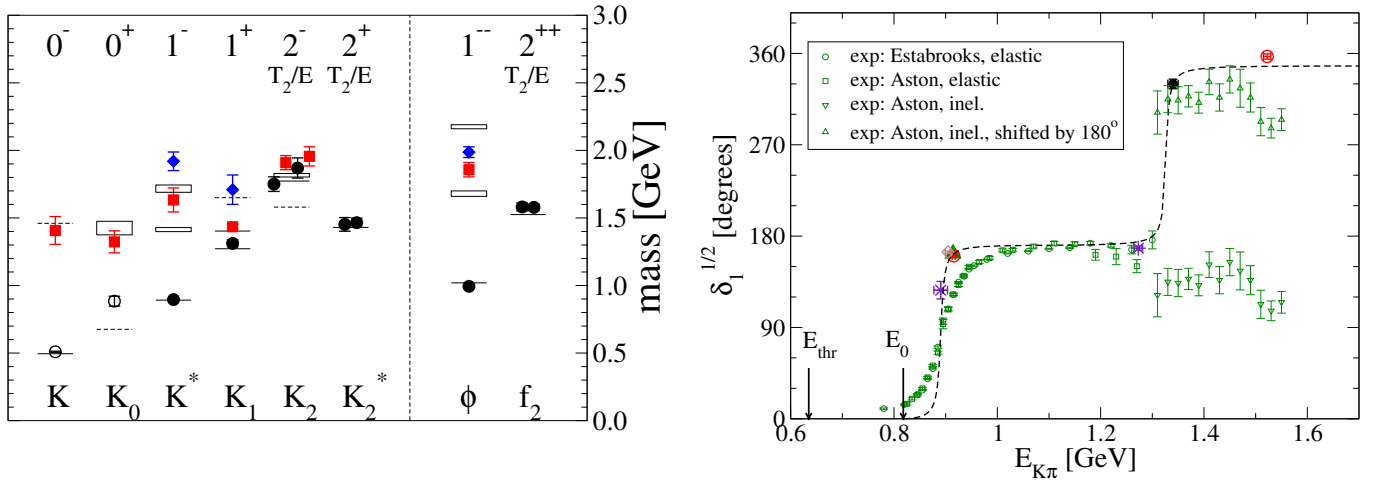


Figure 12: Left: radial excitation spectrum of several mesons including $K^*(892)$ from the lattice calculation in Refs. [126, 127]. Right: P -wave $K\pi$ phase shifts from the lattice calculation in Refs. [128, 129]. Figures reprinted from Refs. [127] (left) and [129] (right) by kind permission of the authors.

of Fig. 12, taken from Refs. [128, 129], in which P -wave $K\pi$ phase shifts were calculated by members of the same lattice group as in Refs. [126, 127]. This more realistic simulation includes $K\pi$ two-meson interpolators, which allows to extract phase shifts using Lüscher’s method [115]. As expected, the phase passes through 90° more or less at the mass of the $K^*(892)$ resonance. However, there is a second phase-shift jump of 180° right above 1.3 GeV, corresponding to the first radially excited K^* resonance, with an extracted mass of (1.33 ± 0.20) GeV, which is about 300 MeV lower than in the lattice calculation — without considering decay — of Refs. [126, 127]. Admittedly, the simulation in Refs. [128, 129] is an approximation in the $K^{*’}$ case, because it ignores the important [10] $K^*(892)\pi$ decay mode and also $K\rho$. However, it is hardly conceivable that the inclusion of these channels will drastically change the $K^{*’}$ mass, and certainly not shift it to much higher energies. So the discrepancy of roughly 300 MeV between the mass of an excited meson calculated with or without two-meson interpolators in a lattice simulation poses an enormous challenge to lattice practitioners as well as quark-model builders.

7.5 Conclusions on lattice results for some puzzling mesons

Summarising, the above lattice results in Refs. [117, 122–125] largely confirm our earlier interpretation and modelling of the light scalar mesons as dynamical $q\bar{q}$ resonances in Refs. [63, 86, 95]. Moreover, the lattice descriptions of $D_{s0}^*(2317)$ in Refs. [26, 27, 120] support our former unitarised model for this state tuned to an S -wave $K\pi$ phase-shift fit. Similarly, the lattice results for the charmed axial-vector mesons in Refs. [120, 121] are in agreement with our prior modelling of these resonances in Refs. [64, 98]. Furthermore, the lattice approach to $\chi_{c1}(3872)$ with quark-antiquark, tetraquark, and meson-meson interpolators in Ref. [118] corroborates our preceding description of this meson as a non-exotic yet strongly unitarised $2^3P_1 c\bar{c}$ state in Refs. [36–38]. Finally, the lattice calculation of P -wave $K\pi$ phase shifts in Ref. [128] lends indirect support to the $\rho(1250)$ resonance resulting from the analysis in Ref. [20], as a consequence of the low-lying $K^{*’}$ found on the lattice.

To conclude this discussion, there has been spectacular progress over the past decade in describing physical meson resonances through QCD simulations on the lattice, which promise to become very helpful in the future to further reduce model bias in determining resonance pole positions from experiment. Even certain data analyses might need to be reassessed in view of clear conflicts with solid lattice predictions.

8 Mesonic Enhancements and Production Processes

So far we have only considered a unitary S -matrix for meson-meson scattering in order to search for poles describing non-exotic meson resonances. However, because direct meson-meson scattering is not feasible experimentally, such data long ago used to be extracted from meson scattering off nucleons. For example, the still often cited and even used LASS [130] phase shifts for $K^-\pi^+$ scattering were obtained from the reaction $K^-p \rightarrow K^-\pi^+n$. However, nowadays mesonic resonances are mostly observed in e^+e^- collisions and decays of the resulting vector states, or in multiparticle decays of open-bottom and open-charm mesons. One may argue that, from a theoretical point of view, there is no fundamental difference between the various mechanisms to produce meson resonances, as their pole positions are generally accepted to be universal and so independent of the process. However, resonance line shapes may very well depend on the production mechanism, which makes it crucial to have an adequate formalism at hand for a reliable analysis of the experimental data. But still more importantly, the common feature of production processes is an initial state with only one quark-antiquark pair and not a two-meson system, as shown in Fig. 13 [131]. Here, the first diagram shows an initial $q\bar{q}$ pair (resulting from e^+e^- annihilation or heavy-meson decay) producing two mesons e.g. via 3P_0 pair creation at the vertex v followed by an OZI-allowed decay. These two mesons can and will then rescatter through

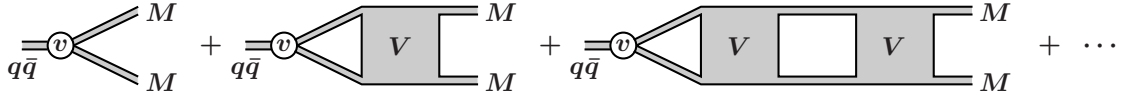


Figure 13: Schematic production process followed by rescattering; see text and Ref. [131].

iterations of the effective potential V , and so the two-body T -matrix. Now there are two essential remarks to be made. In the first place, the amplitude for the production process depicted in Fig. 13 will have the same resonance poles as T , provided the first diagram is not singular. Secondly, if one assumes that the effective potential V involves $q\bar{q}$ pair annihilation followed by a new creation, then the first term is of leading order in the strength of the creation/annihilation process, as it only amounts to one $q\bar{q}$ creation.

In Ref. [131] we derived the formalism of production processes in the context of the RSE model. The resulting relation between the production amplitude for an initial quark-antiquark state labelled α to a final meson-meson state labelled i reads

$$P_i^{(\alpha)} \propto \lambda \sum_{L,M} (-i)^L Y_M^{(L)}(p_i) Q_{\ell_{q\bar{q}}}^{(\alpha)}(E) \left\{ g_{\alpha i} j_L(p_i a) - i \sum_{\nu} \mu_{\nu} p_{\nu} h_L^{(1)}(p_{\nu} a) g_{\alpha \nu} T_{i\nu}^{(L)} \right\}, \quad (56)$$

where $T_{i\nu}^{(\ell)}$ is a partial-wave T -matrix element for transitions between the two-meson channels i and ν . Furthermore, $j_L(p_i a)$ and $h_L^{(1)}(p_i a)$ are the usual spherical Bessel and Hankel-1 functions, and the $g_{\alpha i}$ are the coupling constants for transitions between the initial $q\bar{q}$ pair, with all its quantum numbers symbolically abbreviated as α , and the i -th meson-meson channel, following again the recoupling scheme of Ref. [76]. The largely unknown function $Q_{\ell_{q\bar{q}}}^{(\alpha)}(E)$ describes the initial quark-antiquark state α with energy E , which must be determined by the precise production mechanism. Note that indeed P and T share the same resonance poles, as the spherical Bessel function in the lead term of Eq. (56) is smooth. Furthermore, the production amplitude P manifestly satisfies [131,132] the so-called extended-unitarity relation

$$\Im m(P) = T^* P, \quad (57)$$

despite the fact that the coefficients in front of the T -matrix elements in Eq. (56) are complex [132,133] due to the spherical Hankel function $h_L^{(1)}$. In Ref. [134] it was argued that these coefficients should be real, but we showed [133] this to imply that the coefficients themselves must contain T -matrix elements, whereas our definition in Eq. (56) involves purely kinematical coefficients, proportional to $h_L^{(1)}$. Besides this clear advantage, Eq. (56) explicitly displays the mentioned lead term in the production amplitude, which is linearly dependent on the coupling $g_{\alpha \nu}$ between the initial $q\bar{q}$ state and meson-meson channel ν , and has the shape of a spherical Bessel function. This term will generally result in an enhancement in the cross section right above a threshold opening, which may be mistaken for a genuine resonance or distort the signal when indeed a true resonance pole is nearby. In Ref. [131] we also showed the connection between our production formalism and the Breit-Wigner approximation as well as the K -matrix approach.

Notwithstanding these nice properties of the formalism, one should realise that actually reproducing experimental production data is much more difficult than finding resonance poles or fitting scattering phase shifts with the RSE T -matrix. Namely, in order to fit production cross sections, one would need accurate knowledge of the largely unknown function $Q_{\ell_{q\bar{q}}}^{(\alpha)}(E)$ in the lead term of Eq. 56, as well as of the generally multichannel meson-meson T -matrix. Therefore, we have limited ourselves to more empirical applications in a number of concrete cases involving puzzling resonances. Three typical examples will be dealt with next, viz. the enigmatic vector charmonium states $\psi(4260)$ and $\psi(4660)$, as well as the

usually uncontroversial [10] bottomonium resonance $\Upsilon(10580)$. For a more general discussion of the former two candidates for exotic charmonia, see the review in Ref. [12]. We also mention here Ref. [135] for our production description of several threshold and resonance structures in e^+e^- annihilation at the mass scales of strangeonium, charmonium, and bottomonium.

8.1 Non-resonant vector charmonium state $\psi(4260)$

The $\psi(4260)$ vector charmonium state, previously called $X(4260)$, has 51 listed [10] decay modes, of which 39 are “*not seen*”, one is “*possibly seen*”, and five are just mentioned. None of the “(possibly) seen” modes correspond to decays to open-charm mesons. It lies outside the scope of the present paper to mention all the published explanations of this most peculiar feature of $\psi(4260)$, usually in terms of (crypto-)exotic non- $c\bar{c}$ configurations, so we just refer to the dedicated review of exotic candidates in Ref. [12]. Instead, we briefly summarise here our non-resonant interpretation of $\psi(4260)$, as published in Ref. [39]. Assuming a very broad threshold structure in the $J/\psi\pi^+\pi^-$ channel dominated by $J/\psi f_0(500)$, we interpret the various dips in the $J/\psi\pi^+\pi^-$ event distribution as strong inelasticity effects from the opening of OZI-allowed channels with pairs of charmed mesons as well as established vector charmonia in these channels. This also helps to explain the very pronounced and puzzling dip precisely at the mass of $\psi(4415)$. Thereabove, the opening of the $\Lambda_c\bar{\Lambda}_c$ threshold and a tentative, so far unlisted $\psi(3D)$ resonance are fundamental to understand the data. These large inelasticity effects we called [39] *depletion*, which we believe to give rise to a non-resonant, apparent $\psi(4260)$ enhancement.

In Fig. 14 we show how the data can be explained stepwise with the mentioned broad structure, thresholds of open-charm meson pairs, known charmonium resonances, the $\Lambda_c\bar{\Lambda}_c$ baryon-antibaryon threshold, and finally a proposed, so far unlisted, $\psi(3D)$ resonance. Note that already in Ref. [138] we had found indirect indications of a $\psi(3D)$ resonance not far underneath the $\Lambda_c\bar{\Lambda}_c$ threshold. The here extracted $\psi(3D)$ mass and width are 4.53 GeV and 80 MeV, respectively. In the GI model, this vector charmonium state was predicted [2] at 4.52 GeV.

To conclude our discussion on $\psi(4260)$, let us just mention a very recent calculation [137] from a unitarised effective Lagrangian, which also supports the interpretation of this state as a non-resonant enhancement, due to the proximity of the $D_s^*\bar{D}_s^*$ threshold and the $\psi(4160)$ pole.

8.2 Vector charmonium $\psi(4660)$ as a $\Lambda_c\bar{\Lambda}_c$ threshold enhancement

The vector charmonium $\psi(4660)$, previously called $X(4660)$ and also known as $Y(4660)$, is listed [10] with an average mass and width of (4633 ± 7) MeV and (64 ± 9) MeV, respectively. These small errors as given by the PDG are surprising in view of the published ranges of mass and width values of 4626–4669 MeV and 42–104 MeV, respectively. Also puzzling is that the only “*seen*” open-charm decay mode of $\psi(4660)$ is $D_s^+D_{s1}^-(2536)^-$.

In Ref. [138] we analysed data on the $e^+e^- \rightarrow \Lambda_c\bar{\Lambda}_c$ cross section published [139] by the Belle Collaboration, employing a phenomenological ansatz based on our production formula in Eq. (56). From our fit we concluded that the reported structure “ $X(4630)$ ” at 4634 MeV is a non-resonant threshold enhancement due to the opening of the $\Lambda_c\bar{\Lambda}_c$ channel (also see Ref. [39]). Moreover, we found indications of the higher vector charmonia $\psi(5S)$, $\psi(4D)$, $\psi(6S)$, and $\psi(5D)$, as well as an indirect indication of $\psi(3D)$, later supported by the analysis in Ref. [39]. In Fig. 15 we show the experimental data [139] in the energy region 4.57–5.40 GeV (left-hand plot), and the data with the suggested $\psi(5S)$ and $\psi(4D)$ resonances⁶ in the interval 4.57–5.10 GeV (right-hand plot). The solid curves on both plots represent our fit based on the opening of the $\Lambda_c\bar{\Lambda}_c$ and three charmed- Σ -baryon thresholds. For details, see Ref. [138].

⁶This way of displaying the data and the proposed two new ψ states only appears in the arXiv version 0809.1151v3 [hep-ph] of Ref. [138].

8.3 $\Upsilon(10580)$ as a non-resonant enhancement between the $B\bar{B}$ and $B^*\bar{B}$ thresholds

Finally, we discuss a bottomonium state that is generally believed to be very well established, namely $\Upsilon(10580)$, which has been included in the PDG tables for many years and is listed [10] as $\Upsilon(4S)$. However, we interpreted [40, 140, 141] it rather as a non-resonant bump right between the $B\bar{B}$ and $B^*\bar{B}$ thresholds. The crucial point is that the data [142] show a small yet clear enhancement on top of the $B_s\bar{B}_s$ threshold, whereas there are unmistakable dips at the openings of the $B\bar{B}^*$ and $B^*\bar{B}^*$ thresholds (see Fig. 16). This pattern can be understood by assuming an $\Upsilon(4S)$ resonance somewhat above the $B_s\bar{B}_s$ threshold, which also allows to identify $\Upsilon(10860)$ as $\Upsilon(3D)$ and $\Upsilon(11020)$ as $\Upsilon(5S)$. From our phenomenological fit to the data, based on threshold enhancements as following from our production formalism described above, we extracted [140, 141] an Υ resonance with a mass of 10.735 GeV and a

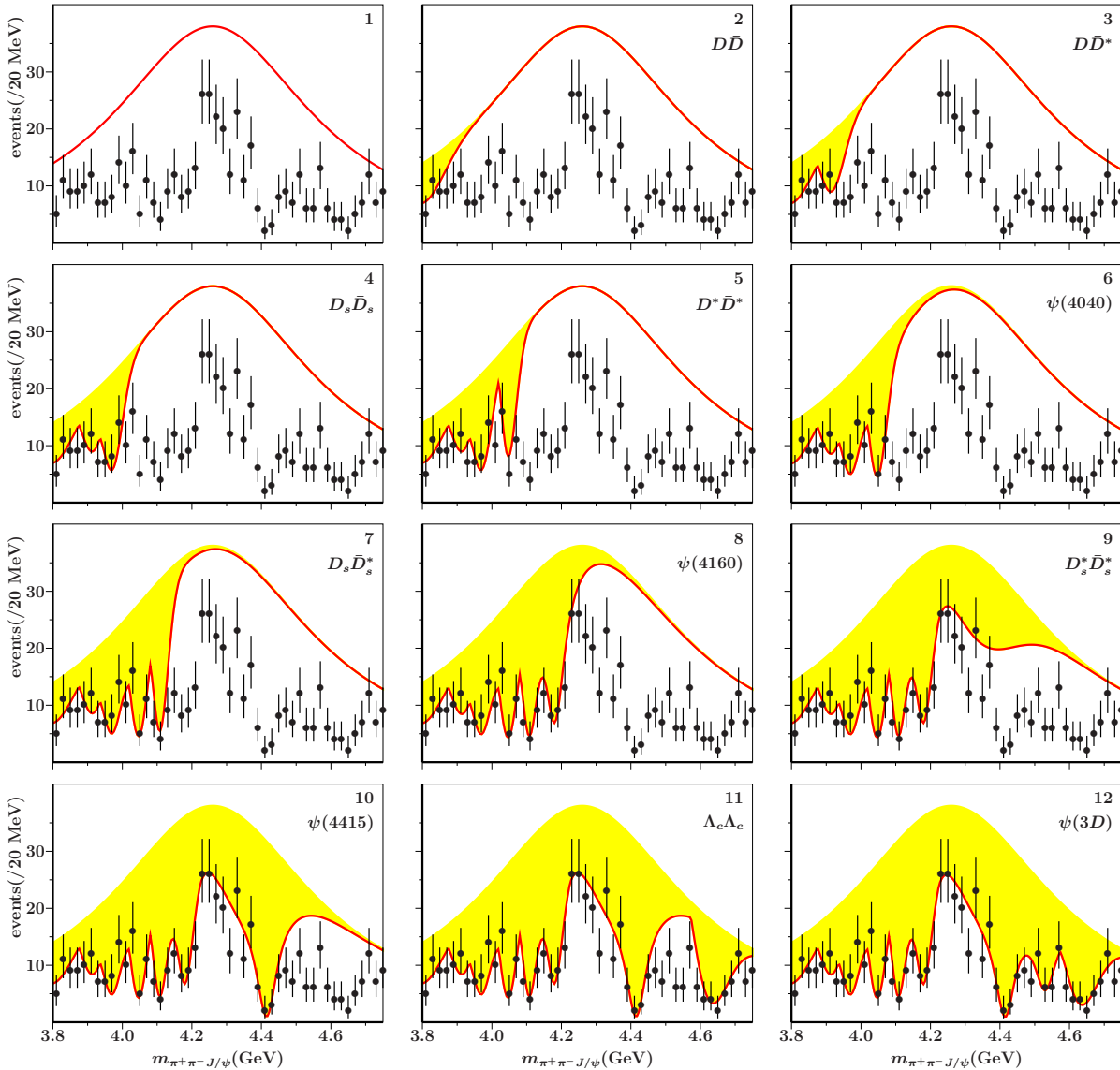


Figure 14: Reconstruction of $\psi(4260)$ data in $e^+e^- \rightarrow \pi^+\pi^- J/\psi$ [136] via a stepwise depletion of a presumed broad threshold structure by OZI-allowed inelastic processes (also see text). From upper left to lower right: broad structure (1), depletion by respectively $D\bar{D}$ (2), $D\bar{D}^*$ (3), $D_s\bar{D}_s$ (4), $D^*\bar{D}^*$ (5), $\psi(4040)$ (6), $D_s\bar{D}_s^*$ (7), $\psi(4160)$ (8), $D_s^*\bar{D}_s^*$ (9), $\psi(4415)$ (10), $\Lambda_c\bar{\Lambda}_c$ (11), and $\psi(3D)$ (12) (also see text and Ref. [39]).

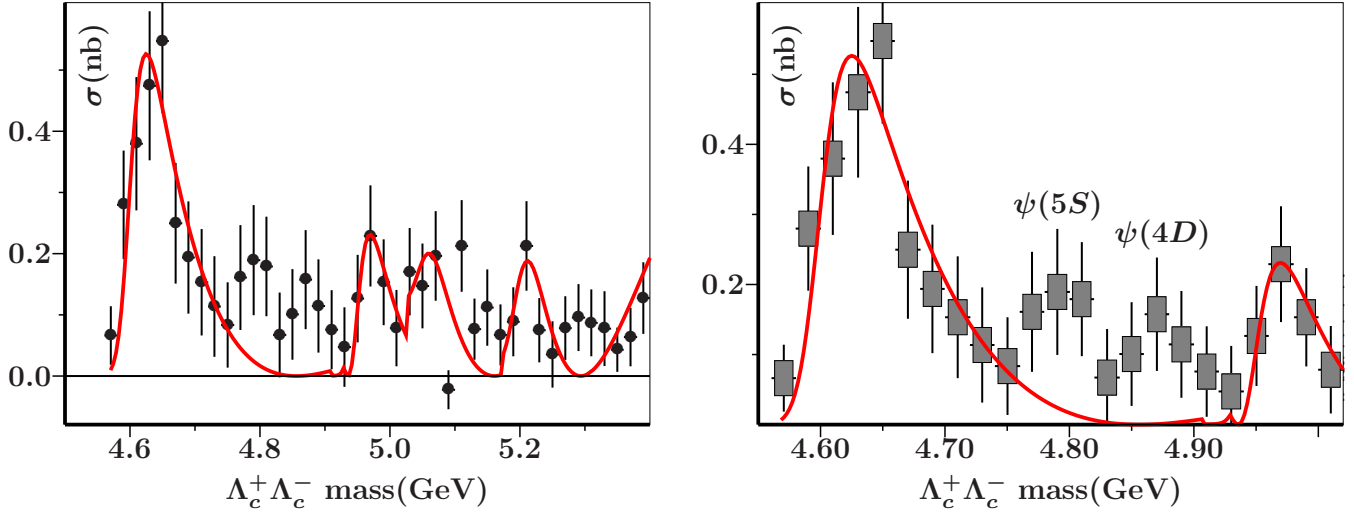


Figure 15: Left: experimental data [139] in the energy region 4.57–5.40 GeV. Right: same data with the proposed $\psi(5S)$ and $\psi(4D)$ resonances. Solid curves on both plots are from the fit in Ref. [138].

width of 38 MeV, which we interpret as the true $\Upsilon(4S)$ state. Most interestingly, the Belle Collaboration very recently observed [10,143] a new vector bottomonium state, with a mass of 10.753 GeV and a width of 35.5 MeV.

As for our non-resonant interpretation of $\Upsilon(10580)$, also very recently Υ resonances above the open-bottom threshold were studied [144] in a simple effective model based on the 3P_0 mechanism. In this paper, the vector bottomonium resonances listed in the PDG tables are described via a propagator dressed with loops of B , B^* , B_s , and B_s^* mesons. From this dressed propagator, a wave-function-renormalisation constant Z is obtained, which should be close to one for a state that is mostly $b\bar{b}$. This condition is strongly fulfilled by all Υ resonances except for $\Upsilon(10580)$, which shows a large deviation. Moreover, the high peak and relatively large width of $\Upsilon(10580)$ is argued [144] to be incompatible with a vector $b\bar{b}$ resonance decaying only to $B\bar{B}$ and with little phase space. We believe that these results lend support to considering $\Upsilon(10580)$ a non-resonant $B\bar{B}$ threshold enhancement, amplified [140] by the pole of a so far unlisted (yet also see Ref. [145]) $\Upsilon(2D)$ state not far below the $B\bar{B}$ threshold.

9 Summary and Conclusions

In this review we aimed at making the case for a systematic treatment of meson spectroscopy based on the quark model for $q\bar{q}$ states only, yet imposing the requirements of S -matrix unitarity. Thus, in Sec. 1 we started with a brief introduction to mainstream quark models of mesons using a Coulomb-plus-linear confining potential, and mentioned the inevitable problem with radial spacings in the spectra of especially mesons made of light and strange quarks. In Sec. 2 we employed a simple unitary single-channel model for the S -matrix in order to show discrepancies that may arise when using standard Breit-Wigner parametrisations, in particular when applied to very broad resonances not far above the lowest threshold, like in the case of the light scalar mesons $f_0(500)$ and $K_0^*(700)$. Section 3 was devoted to a detailed discussion of static quark models, in which the dynamical effects of strong decay or virtual meson loops on the spectra are ignored. The shortcomings of the relativised meson model of Godfrey and Isgur [2] were illustrated with many examples from particularly light-meson spectra. Furthermore, two fully relativistic static quark models were reviewed as well and shown to have similar or even worse problems. In Sec. 4 we briefly reviewed the very disparate predictions for meson mass shifts, some of them really huge, due to unitarisation or coupled channels in a series of old and more

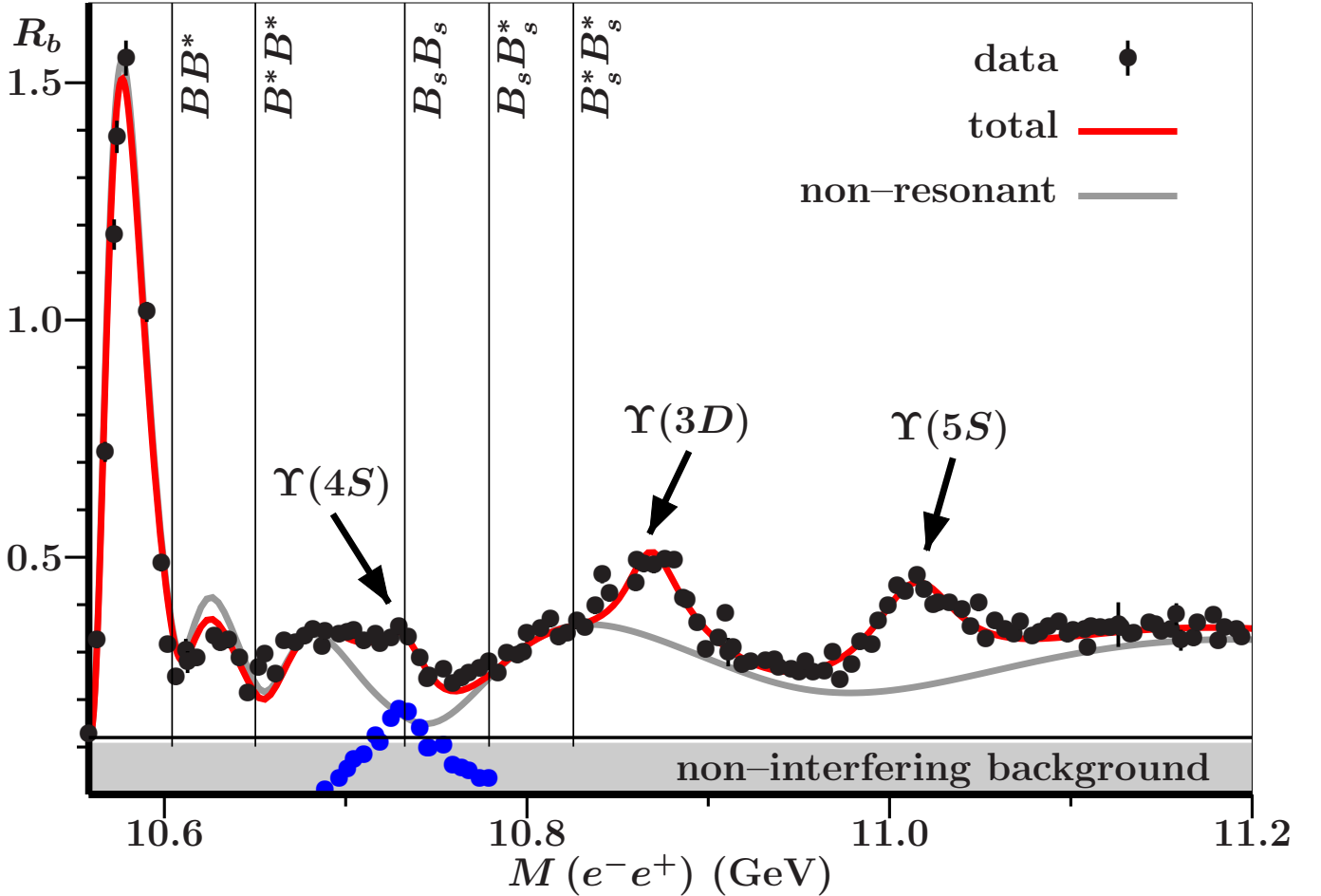


Figure 16: Fit [141] to bottomonium vector states, with open-bottom thresholds marked and locations of $\Upsilon(4S)$, $\Upsilon(3D)$, and $\Upsilon(5S)$ in the data [142]. The blue dots indicate the difference between the data and the non-resonant contribution disregarding interference. For further details, see text and Refs. [140, 141].

recent models, discussing their differences. Section 5 treated a simple unitarised model in momentum space, called Resonance Spectrum Expansion (RSE) and inspired by the unitarised quark-meson model in coordinate space developed by the Nijmegen group. Its predictive power was demonstrated by successfully describing e.g. the $K_0^*(700)$ resonance, the charmed scalar meson $D_{s0}^*(2317)$, the charmed $J^P = 1^+$ mesons, and — in a multichannel extension of the model — even the whole light scalar-meson nonet. Furthermore, the most general RSE model, applicable to systems with various quark-antiquark channels coupled to an arbitrary number of meson-meson channels, was shown to be exactly solvable, both algebraically and analytically, owing to the separability of the effective meson-meson interaction and the employed string-breaking mechanism. In Sec. 6 the latter general RSE model was used to analyse again the charmed $J^P = 1^+$ mesons, thus allowing to dynamically produce the physical states as orthogonal mixtures of the 3P_1 and 1P_1 quark-antiquark components. This gives rise to two quasi-bound states in the continuum and two strongly shifted states, thus reproducing the observed disparate pattern of masses and widths with remarkable accuracy. Moreover, the same full RSE model as well as its multichannel coordinate space version were employed to describe the axial-vector charmonium state $\chi_{c1}(3872)$, modelling it as a unitarised 2^3P_1 charmonium state. The resulting pole trajectories, wave function, and electromagnetic transitions support our interpretation of this very enigmatic meson. Section 7 was devoted to several recent lattice calculations of controversial meson

resonances that include meson-meson interpolating fields in the simulations, in order to allow for the computation of phase shifts and extract the corresponding resonance or bound-state pole positions. The results for $\chi_{c1}(3872)$, $D_{s0}^*(2317)$, the charmed $J^P = 1^+$ mesons, and the light scalars largely confirm our description of these mesons. In Sec. 8 we presented a formalism for production processes that is strongly related to our RSE model and satisfies the extended-unitary condition $\Im m(P) = T^* P$, with T the RSE T -matrix. The general expression features a purely kinematical, non-resonant real lead term, plus a combination of two-body T -matrix elements with also kinematical yet complex coefficients. Fully empirical applications of the formalism to the controversial vector charmonium states $\psi(4260)$ and $\psi(4660)$ as well as the established $\Upsilon(10580)$ bottomonium state allowed to fit all three resonance-like structures as non-resonant threshold enhancements.

Let us repeat that we did not aspire to carry out a comprehensive review of general meson spectroscopy. Therefore, several alternative descriptions of mesons with very interesting results, like e.g. unitarised chiral models [146, 147], the generalised Nambu–Jona-Lasinio model [148], or the quark-level linear σ model [149], have not been dealt with here at all. Nevertheless, we believe that these approaches have a more restricted applicability to meson spectroscopy, being usually limited to specific resonances or ground states only. In order to be able to infer information on the confining potential, it is necessary to be able to calculate radially excited states without introducing new parameters. We have also not paid attention to truly exotic meson candidates, as e.g. the charmed charmonium-like and bottomonium-like states $Z_c^\pm(3900)$, $Z_c^\pm(4430)$, $Z_b(10610)$, and $Z_b(10650)$ [10]. For a discussion of such exotics, we refer again to Ref. [12]. Nevertheless, in this context it is worthwhile to mention a very recent paper by the COMPASS Collaboration [150], in which for the first time a triangle-singularity model is fitted directly to partial-wave data, viz. for the controversial $a_1(1420)$ state reported [151] by COMPASS itself five years ago. The conclusion of this fit is that including the triangle singularity allows for a better fit to the data with fewer parameters, so that after all there is no need to introduce the new $a_1(1420)$ resonance [150]. This result may have far-reaching consequences for exotic spectroscopy, in view of the increasing number of observed enhancements in the data that cannot be accommodated as $q\bar{q}$ mesons. Clearly, all such controversial states will have to be refitted in a similar fashion. For a detailed discussion of triangle singularities, see Ref. [12].

To conclude, we recall the mentioned email exchange with a co-spokesperson [83] of the E791 Collaboration about the need for easy formulae to fit the data and a related discussion at the LHCb workshop ‘*Multibody decays of D and B mesons*’, in Rio de Janeiro, 2015 [152]. The latter meeting focused on alternatives to the usual Breit-Wigner (BW) and Flatté parametrisations that guarantee multichannel unitarity, even in the case of overlapping broad resonances. In that spirit, we proposed (see Ref. [152], pages 36–39) our general RSE formalism (cf. Eqs. (51–54)), yet with the bare HO energies replaced by a few to-be-fitted real energies and possibly also the Bessel and Hankel-1 functions by more flexible expressions, thus allowing much more accurate fits to the data. Apart from thus guaranteeing manifest multichannel unitarity, the usual two BW parameters for each resonance could then be replaced by only one real energy. Finally, a similar generalisation of our production formalism should also be possible.

10 Acknowledgement

We thank R. Kamiński for demonstrating the importance of a fully unitary S -matrix description instead of the usual Breit-Wigner parametrisation even in the simplest case of elastic resonances, which was one of our motivations to write the present review.

References

- [1] G. S. Bali, K. Schilling, and C. Schlichter, *Phys. Rev. D* 51 (1995) 5165

- [2] S. Godfrey and N. Isgur, *Phys. Rev. D* 32 (1985) 189
- [3] G. Rupp, S. Coito, and E. van Beveren, *Acta Phys. Pol. B Proc. Suppl.* 5 (2012) 1007
- [4] E. Eichten, K. Gottfried, T. Kinoshita, K. D. Lane, and T. M. Yan, *Phys. Rev. D* 17 (1978) 3090
[*Erratum-ibid* 21 (1980) 313]
- [5] E. Eichten, K. Gottfried, T. Kinoshita, K. D. Lane, and T. M. Yan, *Phys. Rev. D* 21 (1980) 203
- [6] E. Eichten, *Phys. Rev. D* 22 (1980) 1819
- [7] J. L. Richardson, *Phys. Lett. B* 82 (1979) 272
- [8] E. van Beveren, C. Dullemond, and G. Rupp, *Phys. Rev. D* 21 (1980) 772 [*Erratum-ibid* 22 (1980) 787]
- [9] E. van Beveren, G. Rupp, T. A. Rijken, and C. Dullemond, *Phys. Rev. D* 27 (1983) 1527
- [10] P. A. Zyla *et al.* [Particle Data Group], *Prog. Theor. Exp. Phys.* 2020 (2020) 083C01
- [11] D. V. Bugg, *Phys. Rep.* 397 (2004) 257
- [12] H. X. Chen, W. Chen, X. Liu, and S. L. Zhu, *Phys. Rep.* 639 (2016) 1
- [13] V. Crede and C. A. Meyer, *Prog. Part. Nucl. Phys.* 63 (2009) 74
- [14] S. R. Cotanch, *Prog. Part. Nucl. Phys.* 50 (2003) 353
- [15] G. Eichmann, H. Sanchis-Alepuz, R. Williams, R. Alkofer, and C. S. Fischer, *Prog. Part. Nucl. Phys.* 91 (2016) 1
- [16] R. Kamiński and P. Bochnacki, *Acta Phys. Pol. B* 50 (2019) 1911
- [17] G. Rupp and E. van Beveren, *Acta Phys. Pol. B Proc. Suppl.* 13 (2020) 51
- [18] J. R. Taylor, “*Scattering Theory: The Quantum Theory of Nonrelativistic Collisions*”, John Wiley & Sons, Inc., New York, London, Sydney, Toronto (1972), ISBN 0-471-84900-6; see page 220
- [19] E. Bartoš, S. Dubnička, A. Liptaj, A. Z. Dubničková, and R. Kamiński, *Phys. Rev. D* 96 (2017) 113004, see Table II
- [20] N. Hammoud, R. Kamiński, V. Nazari, and G. Rupp, *Phys. Rev. D* 102 (2020) 054029
- [21] N. A. Tornqvist and M. Roos, *Phys. Rev. Lett.* 76 (1996) 1575
- [22] E. van Beveren and G. Rupp, *Eur. Phys. J. C* 10 (1999) 469
- [23] J. R. Pelaez, *Phys. Rep.* 658 (2016) 1
- [24] J. R. Peláez and A. Rodas, preprint 2010.11222
- [25] D. V. Bugg, *Phys. Lett. B* 572 (2003) 1 [*Erratum-ibid* 595 (2004) 556]
- [26] D. Mohler, C. B. Lang, L. Leskovec, S. Prelovsek, and R. M. Woloshyn, *Phys. Rev. Lett.* 111 (2013) 222001
- [27] C. Alexandrou, J. Berlin, J. Finkenrath, T. Leontiou, and M. Wagner, *Phys. Rev. D* 101 (2020) 034502
- [28] A. Le Yaouanc, L. Oliver, S. Ono, O. Pene, and J. C. Raynal, *Phys. Rev. D* 31 (1985) 137
- [29] P. J. d. A. Bicudo and J. E. F. T. Ribeiro, *Phys. Rev. D* 42 (1990) 1611
- [30] J. Beringer *et al.* [Particle Data Group], *Phys. Rev. D* 86 (2012) 010001
- [31] J. Bulava, B. Fahy, J. Foley, Y. C. Jhang, K. J. Juge, D. Lenkner, C. Morningstar, and C. H. Wong, *EPJ Web Conf.* 73 (2014) 03018
- [32] E. van Beveren, G. Rupp, and S. Coito, *Acta Phys. Pol. B Proc. Suppl.* 8 (2015) 145
- [33] E. van Beveren and G. Rupp, *Phys. Rev. Lett.* 91 (2003) 012003
- [34] K. Hagiwara *et al.* [Particle Data Group], *Phys. Rev. D* 66 (2002) 010001
- [35] S. K. Choi *et al.* [Belle Collaboration], *Phys. Rev. Lett.* 91 (2003) 262001

- [36] S. Coito, G. Rupp, and E. van Beveren, *Eur. Phys. J. C* 71 (2011) 1762
- [37] S. Coito, G. Rupp, and E. van Beveren, *Eur. Phys. J. C* 73 (2013) 2351
- [38] M. Cardoso, G. Rupp, and E. van Beveren, *Eur. Phys. J. C* 75 (2015) 26
- [39] E. van Beveren, G. Rupp, and J. Segovia, *Phys. Rev. Lett.* 105 (2010) 102001
- [40] G. Rupp and E. van Beveren, *J. Phys. Conf. Ser.* 1137 (2019) 012021
- [41] P. C. Tiemeijer and J. A. Tjon, *Phys. Rev. C* 49 (1994) 494
- [42] E. E. Salpeter and H. A. Bethe, *Phys. Rev.* 84 (1951) 1232
- [43] P. C. Tiemeijer, “Relativistic Analysis of the Constituent Quark Model for Mesons”, PhD Thesis, University of Utrecht, September 1993, ISBN 90-393-0427-0, <https://dspace.library.uu.nl/handle/1874/13400>
- [44] A. A. Logunov and A. N. Tavkhelidze, *Nuovo Cimento* 29 (1963) 380; R. Blankenbecler and R. Sugar, *Phys. Rev.* 142 (1966) 1051
- [45] E. D. Cooper and B. K. Jennings, *Nucl. Phys. A* 500 (1989) 553
- [46] V. B. Mandelzweig and S. J. Wallace, *Phys. Lett. B* 197 (1987) 469
- [47] H. Hersbach, *Phys. Rev. C* 50 (1994) 2562
- [48] H. Hersbach, *Phys. Rev. A* 46 (1992) 3657
- [49] N. A. Tornqvist, *Ann. Phys. (N.Y.)* 123 (1979) 1
- [50] M. Roos and N. Tornqvist, *Z. Phys. C* 5 (1980) 205
- [51] M. Boglione and M. R. Pennington, *Phys. Rev. Lett.* 79 (1997) 1998
- [52] E. S. Swanson, *J. Phys. G* 31 (2005) 845
- [53] R. Bijker and E. Santopinto, *AIP Conf. Proc.* 947 (2007) 168
- [54] P. Gonzalez, *Int. J. Mod. Phys. Conf. Ser.* 02 (2011) 178
- [55] T. J. Burns, *Phys. Rev. D* 90 (2014) 034009
- [56] R. Bijker and E. Santopinto, *Phys. Rev. C* 80 (2009) 065210
- [57] P. Geiger and N. Isgur, *Phys. Rev. Lett.* 67 (1991) 1066
- [58] J. Ferretti, G. Galatà, and E. Santopinto, *Phys. Rev. C* 88 (2013) 015207
- [59] J. Ferretti and E. Santopinto, *Phys. Rev. D* 90 (2014) 094022
- [60] J. Segovia, D. R. Entem, and F. Fernandez, *J. Phys. G* 37 (2010) 075010
- [61] G. Rupp, S. Coito, and E. van Beveren, *Acta Phys. Pol. B Proc. Suppl.* 9 (2016) 653
- [62] G. Rupp and E. van Beveren, *Chin. Phys. C* 41 (2017) 053104
- [63] E. van Beveren, T. A. Rijken, K. Metzger, C. Dullemond, G. Rupp, and J. E. Ribeiro, *Z. Phys. C* 30 (1986) 615, preprint 0710.4067
- [64] S. Coito, G. Rupp, and E. van Beveren, *Phys. Rev. D* 84 (2011) 094020
- [65] K. Heikkilä, S. Ono, and N. A. Tornqvist, *Phys. Rev. D* 29 (1984) 110 [Erratum-ibid 29 (1984) 2136].
- [66] P. J. d. A. Bicudo and J. E. F. T. Ribeiro, *Phys. Rev. D* 42 (1990) 1635
- [67] Y. A. Simonov and J. A. Tjon, *Phys. Rev. D* 70 (2004) 114013
- [68] Y. S. Kalashnikova, *Phys. Rev. D* 72 (2005) 034010
- [69] T. Barnes and E. S. Swanson, *Phys. Rev. C* 77 (2008) 055206
- [70] L. Micu, *Nucl. Phys. B* 10 (1969) 521 *Nucl. Phys. B* 10 (1969) 521.
- [71] R. D. Carlitz and M. Kislinger, *Phys. Rev. D* 2 (1970) 336
- [72] G. S. Bali *et al.* [SESAM Collaboration], *Phys. Rev. D* 71 (2005) 114513

- [73] R. L. Jaffe, *Phys. Rev. D* 15 (1977) 267
- [74] P. J. d. A. Bicudo and J. E. F. T. Ribeiro, *Phys. Rev. D* 42 (1990) 1625
- [75] M. R. Pennington, *Acta Phys. Pol. B Proc. Suppl.* 8 (2015) 9
- [76] E. van Beveren, *Z. Phys. C* 21 (1984) 291
- [77] C. Dullemond, T. A. Rijken, E. van Beveren, and G. Rupp, in Proc. of 6th Warsaw Symposium on Elementary Particle Physics, Kazimierz, Poland, 1983, pp. 257–262
- [78] G. Rupp, E. van Beveren, and M. D. Scadron, *Phys. Rev. D* 65 (2002) 078501
- [79] N. A. Tornqvist, *Phys. Rev. Lett.* 49 (1982) 624
- [80] G. Rupp, F. Kleefeld, and E. van Beveren, *AIP Conf. Proc.* 756 (2005) 360
- [81] T. Wolkanowski, F. Giacosa, and D. H. Rischke, *Phys. Rev. D* 93 (2016) 014002
- [82] T. Wolkanowski, M. Soltysiak, and F. Giacosa, *Nucl. Phys. B* 909 (2016) 418
- [83] Jeffrey A. Appel, private communications, May–June 2001.
- [84] C. Gobel [E791 Collaboration], *Frascati Phys. Ser.* 20 (2001) 373, preprint hep-ex/0012009
- [85] E. M. Aitala *et al.* [E791 Collaboration], *Phys. Rev. Lett.* 89 (2002) 121801
- [86] E. van Beveren and G. Rupp, *Eur. Phys. J. C* 22 (2001) 493
- [87] E. van Beveren and G. Rupp, *Int. J. Theor. Phys. Group Theor. Nonlin. Opt.* 11 (2006) 179, preprint hep-ph/0304105
- [88] E. van Beveren and G. Rupp, *eConf C* 070910 (2007) 130, preprint 0710.3056
- [89] B. Aubert *et al.* [BaBar Collaboration], *Phys. Rev. Lett.* 90 (2003) 242001
- [90] P. Krokovny [Belle Collaboration], *Nucl. Phys. Proc. Suppl.* 117 (2003) 582
- [91] K. Abe *et al.* [Belle Collaboration], *Phys. Rev. D* 69 (2004) 112002
- [92] E. van Beveren and G. Rupp, *Eur. Phys. J. C* 11 (1999) 717
- [93] E. van Beveren and G. Rupp, *Mod. Phys. Lett. A* 19 (2004) 1949
- [94] E. van Beveren and G. Rupp, *Phys. Rev. Lett.* 97 (2006) 202001
- [95] E. van Beveren, D. V. Bugg, F. Kleefeld, and G. Rupp, *Phys. Lett. B* 641 (2006) 265
- [96] E. van Beveren, F. Kleefeld and G. Rupp, *AIP Conf. Proc.* 814 (2006) 143
- [97] P. Krokovny *et al.* [Belle Collaboration], *Phys. Rev. Lett.* 91 (2003) 262002
- [98] E. van Beveren and G. Rupp, *Eur. Phys. J. C* 32 (2004) 493
- [99] G. Rupp and E. van Beveren, *Eur. Phys. J. A* 31 (2007) 698
- [100] B. Aubert *et al.* [BaBar Collaboration], *Phys. Rev. Lett.* 97 (2006) 222001
- [101] B. Aubert *et al.* [BaBar Collaboration], *Phys. Rev. D* 80 (2009) 092003
- [102] E. van Beveren and G. Rupp, *Phys. Rev. D* 81 (2010) 118101
- [103] R. Aaij *et al.* [LHCb Collaboration], *J. High Energy Phys.* 1210 (2012) 151
- [104] R. Aaij *et al.* [LHCb Collaboration], *Phys. Rev. Lett.* 113 (2014) 162001, *Phys. Rev. D* 90 (2014) 072003
- [105] E. van Beveren, S. Coito, and G. Rupp, *EPJ Web Conf.* 95 (2015) 02007
- [106] E. van Beveren and G. Rupp, *Ann. Phys. (N.Y.)* 324 (2009) 1620
- [107] S. Coito, G. Rupp, and E. van Beveren, *Phys. Rev. D* 80 (2009) 094011
- [108] E. van Beveren, C. Dullemond, and T. A. Rijken, *Z. Phys. C* 19 (1983) 275
- [109] E. van Beveren and G. Rupp, *Phys. Rev. Lett.* 93 (2004) 202001
- [110] A. G. M. Verschuren, C. Dullemond, and E. van Beveren, *Phys. Rev. D* 44 (1991) 2803

- [111] I. V. Danilkin and Y. A. Simonov, *Phys. Rev. Lett.* 105 (2010) 102002
- [112] I. W. Lee, A. Faessler, T. Gutsche, and V. E. Lyubovitskij, *Phys. Rev. D* 80 (2009) 094005
- [113] P. Wang and X. G. Wang, *Phys. Rev. Lett.* 111 (2013) 042002
- [114] V. Baru, E. Epelbaum, A. A. Filin, F. K. Guo, H. W. Hammer, C. Hanhart, U. G. Meißner, and A. V. Nefediev, *Phys. Rev. D* 91 (2015) 034002
- [115] M. Lüscher, *Nucl. Phys. B* 354 (1991) 531
- [116] R. A. Briceno, J. J. Dudek, and R. D. Young, *Rev. Mod. Phys.* 90 (2018) 025001
- [117] R. A. Briceno, J. J. Dudek, R. G. Edwards, and D. J. Wilson, *Phys. Rev. D* 97 (2018) 054513
- [118] M. Padmanath, C. B. Lang, and S. Prelovsek, *Phys. Rev. D* 92 (2015) 034501
- [119] S. Weinberg, *Phys. Rev. Lett.* 110 (2013) 261601
- [120] C. B. Lang, L. Leskovec, D. Mohler, S. Prelovsek, and R. M. Woloshyn, *Phys. Rev. D* 90 (2014) 034510
- [121] D. Mohler, S. Prelovsek, and R. M. Woloshyn, *Phys. Rev. D* 87 (2013) 034501
- [122] R. A. Briceno, J. J. Dudek, R. G. Edwards, and D. J. Wilson, *Phys. Rev. Lett.* 118 (2017) 022002
- [123] D. J. Wilson, J. J. Dudek, R. G. Edwards, and C. E. Thomas, *Phys. Rev. D* 91 (2015) 054008
- [124] J. J. Dudek *et al.* [Hadron Spectrum Collaboration], *Phys. Rev. D* 93 (2016) 094506
- [125] C. Alexandrou, J. O. Daldrop, M. Dalla Brida, M. Gravina, L. Scorzato, C. Urbach, and M. Wagner, *J. High Energy Phys.* 1304 (2013) 137
- [126] G. P. Engel, C. B. Lang, M. Limmer, D. Mohler, and A. Schafer, *Phys. Rev. D* 85 (2012) 034508
- [127] G. P. Engel, C. B. Lang, D. Mohler, and A. Schäfer, *PoS Hadron 2013* (2013) 118, preprint 1311.6579
- [128] S. Prelovsek, L. Leskovec, C. B. Lang, and D. Mohler, *Phys. Rev. D* 88 (2013) 054508
- [129] C. B. Lang, L. Leskovec, D. Mohler, and S. Prelovsek, *PoS LATTICE 2013* (2014) 260, preprint 1310.4958
- [130] D. Aston *et al.*, *Nucl. Phys. B* 296 (1988) 493
- [131] E. van Beveren and G. Rupp, *Ann. Phys. (N.Y.)* 323 (2008) 1215
- [132] E. van Beveren and G. Rupp, *Europhys. Lett.* 81 (2008) 61002
- [133] E. van Beveren and G. Rupp, *Europhys. Lett.* 84 (2008) 51002
- [134] M. R. Pennington and D. J. Wilson, *Europhys. Lett.* 84 (2008) 51001
- [135] E. van Beveren and G. Rupp, *Phys. Rev. D* 80 (2009) 074001
- [136] B. Aubert *et al.* [BaBar Collaboration], *Phys. Rev. Lett.* 95 (2005) 142001
- [137] S. Coito and F. Giacosa, *Acta Phys. Pol. B* 51 (2020) 1713
- [138] E. van Beveren, X. Liu, R. Coimbra, and G. Rupp, *Europhys. Lett.* 85 (2009) 61002
- [139] G. Pakhlova *et al.* [Belle Collaboration], *Phys. Rev. Lett.* 101 (2008) 172001
- [140] E. van Beveren and G. Rupp preprint 1010.1401
- [141] E. van Beveren and G. Rupp, preprint 0910.0967
- [142] B. Aubert *et al.* [BaBar Collaboration], *Phys. Rev. Lett.* 102 (2009) 012001
- [143] R. Mizuk *et al.* [Belle Collaboration], *J. High Energy Phys.* 1910 (2019) 220
- [144] W. H. Liang, N. Ikeno, and E. Oset, *Phys. Lett. B* 803 (2020) 135340
- [145] E. van Beveren and G. Rupp, preprint 1009.4097
- [146] J. A. Oller, E. Oset, and A. Ramos, *Prog. Part. Nucl. Phys.* 45 (2000) 157
- [147] E. Oset *et al.*, *Prog. Theor. Phys. Suppl.* 186 (2010) 124

- [148] A. A. Osipov, B. Hiller, A. H. Blin, and J. da Providencia, *Ann. Phys. (N.Y.)* 322 (2007) 2021
- [149] M. D. Scadron, G. Rupp, and R. Delbourgo, *Fortsch. Phys.* 61 (2013) 994
- [150] M. G. Alexeev *et al.* [COMPASS Collaboration], preprint 2006.05342
- [151] C. Adolph *et al.* [COMPASS Collaboration], *Phys. Rev. Lett.* 115 (2015) 082001
- [152] J. H. Alvarenga Nogueira *et al.*, “Summary of the 2015 LHCb workshop on multi-body decays of D and B mesons,” preprint 1605.03889